Aus dem Max-Planck-Institut für Kolloid- und Grenzflächenforschung in Golm

Self-Structuring of Functionalized Micro- and Mesoporous Organosilicas Using Boron-Silane-Precursors

Dissertation

zur Erlangung des akademischen Grades

Doktor der Naturwissenschaften

(Dr. rer. nat.)

in der Wissenschaftsdisziplin Kolloidchemie

eingereicht an der Mathematisch-Naturwissenschaftlichen Fakultät

der Universität Potsdam

von

Andreas Hans Peter Ide

aus Berlin

Potsdam, im September 2008

„Halte ein auf dem beschwerlichen Weg
und blicke um dich!
Wer immer auf den Boden schaut
kann nicht die Sterne sehen!“

Abstract

The structuring of porous silica materials at the nanometer scale and their surface functionalization are important issues of current materials research. Many innovations in chromatography, catalysis and electronic devices benefit from this knowledge.

The work at hand is dedicated to the targeted design of functional organosilica materials. In this context a new precursor concept based on boron-silanes is presented. These precursors combine the properties of a structure directing group and a silica source by covalent borane linkage. Formation of the precursor is easily realized by a sequential two-step hydroboration, firstly on bis(triethoxysilyl)ethene, and secondly on an unsaturated structure directing moiety such as alkenes or polymers. The so prepared precursors self-organize when hydrolysis of their inorganic moiety takes place via an aggregation of their organic side chains into hydrophobic domains. In this way, the additional use of a surfactant as a template is not necessary. Chemical cleavage of these moieties (e.g. by ammonolysis or oxidative saponification) yields an organosilica where all functionalities are exclusively located at the pore wall and therefore accessible. The accessibility of the functionalities is a vital point for applications and is not necessarily granted for common silica functionalization approaches. Further advantages of the boron-silane concept are the possibility to introduce a variety of surface functionalities by heterolytic cleavage of the boron linker and the control of the pore morphology. For that purpose the covalent linkage of different alkyl groups and polymers was studied. Another aspect is the access to chiral boron silane precursors yielding functionalized mesoporous organosilica with chiral functionalities exclusively located at the pore walls after condensation and removal of the structure directing moiety. These materials possess great potential for applications documented by preliminary investigations on chiral resolution of a racemic mixture by HPLC and asymmetric catalysis.

In the course of this work valuable insights into the targeted structuring and surface functionalization of organosilicas were gained. A promising outlook for further investigations is the extension of this concept by altering the structure directing moieties of the precursor. That way the morphology of the final organosilica might be controlled by for example mesogens. Furthermore, the use of the boron linker enables the introduction of multiple functionalities into organosilicas, making the obtained material unique in its performance.

Abstract

Die Nanostrukturierung von funktionalisierten porösen Materialien auf Silikatbasis steht im Brennpunkt der aktuellen Forschung. Anwendungen wie Chromatographie, Katalyse oder die Herstellung elektronischer Bauteile profitieren von den Erkenntnissen, die auf diesem Gebiet gewonnen werden.

Die vorliegende Arbeit soll einen Beitrag zur gezielten Herstellung dieser Funktionsmaterialien leisten. Hierfür wurde ein neues Precursor-Konzept auf der Basis von Borsilanen vorgestellt. Diese Precursoren werden über eine sequentielle zweistufige Hydroborierung an Bis(triethoxysilyl)ethene und ein Alken oder ein ungesättigtes Polymer erhalten. Über den zweiten Schritt wird hierbei die so genannte strukturgebende Gruppe eingeführt und damit das Template kovalent gebunden. Dadurch entfällt im Vergleich zum bekannten Nanocasting-Mechanismus zum einen die Verwendung des herkömmlichen Templates für die Bildung der Porenstruktur und zusätzlich führt die Mikrophasenseparation während der Kondensation zu einer Anordnung der strukturgebenden Gruppen des Precursors an der Silikatphasengrenze. Nach der chemischen Abspaltung dieser Gruppen, die gleichzeitig zur Einführung funktioneller Gruppen führt, werden somit hochporöse Organosilikate erhalten, in denen sich die funktionellen Gruppen ausschließlich an der Porenoberfläche befinden. Ein Vorteil der Verwendung der Hydroborieung wird in der Vielfalt der funktionellen Gruppen deutlich, die eingeführt werden können. Die Zugänglichkeit der funktionellen Gruppen ist entscheidend für potentielle Anwendungen und bei herkömmlichen Organosilikaten nicht zwangsläufig gegeben. Ein herausragender Aspekt dieses Konzepts besteht in der Möglichkeit, sehr einfach chirale Precursoren und damit Organosilikate mit hoch funktionalisierten, chiralen Oberflächen herzustellen. Es konnte gezeigt werden, dass sich diese Materialien sowohl für die chromatographische Trennung von Racematen mittels HPLC als auch für die asymmetrische Katalyse eignen.

Durch die in dieser Arbeit erhaltenen Ergebnisse konnten wertvolle Erkenntnisse zur Oberflächenfunktionalisierung und Strukturierung von mesoporösen Silikaten gewonnen werden. Die Möglichkeit, das vorgestellte Konzept auf andere strukturgebende Gruppen wie zum Beispiel Mesogene zu übertragen und damit die Porenmorphologie gezielt zu steuern, eröffnet viele weitere interessante Materialeigenschaften.

Table of Contents

1. Introduction

1.1 Motivation and Objective

„*Nanotechnology*“ is undoubtedly one of the most prominent catchwords of today, but scarcely anybody associates therewith all the different contributions to our everyday live. Many of the associated inventions in chemistry, pharmacy (drug delivery), electronics (as seen in the downscaling of computers, cell phones etc.), food technology, cosmetics but also adhesive and pigments (carbon black and highly disperse silica gels) are omnipresent. The term “nano” originates from the Greek word for “dwarf” and describes the size scale of 10^{-9} m. For comparison sake, an average hair is about 60 µm in diameter. There are several reasons for the boom in nanotechnology: First of all, rational design of materials in the nanometer range grants access to materials having new properties which would be inaccessible by macroscopic manipulation (e.g. hydrogen fuel cell, membrane technology, hydrogen storage). In addition, acquirements in surface processes result in a better understanding of catalytic processes. In this context, G. ERTL has been awarded the 2007 Nobel Prize in Chemistry for his research on surface chemistry of catalytic processes this year. Of course, these inventions are not only limited to technological applications, they also improve diagnosis and therapy methods. Appropriate nanoparticles applied as contrast agents in living organisms allow gaining valuable perceptions on complex biological processes. Further interesting recent examples include the exceptional electronic and optical properties of carbon nanostructures, among them the very famous Buckminsterfullerene[1] and carbon nanotubes[2] (Figure 1.1). Prototypes of flat panel displays made from carbon nanotubes have several advantages over commercial liquid crystal displays, such as low power consumption,

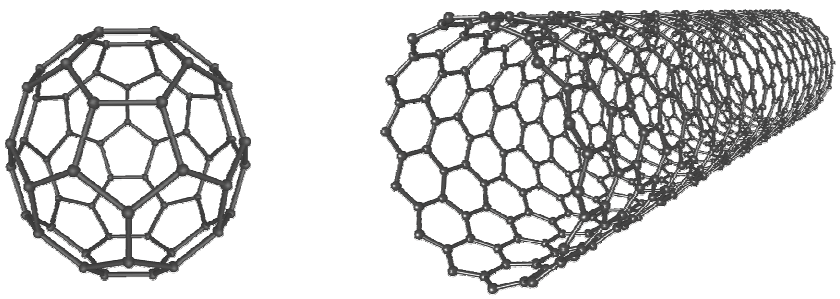

Figure 1.1: Scheme of C_{60}-Buckminsterfullerene and single layer carbon nanotube

higher brightness, wider viewing angles, faster response rates, and a wider operating temperature range. [3,4]

This variety of contributions to modern technological development and to the understanding of complex processes illustrates the importance of structuring materials at the nanometer scale. The present work will focus upon the theme and will specifically deal with the targeted structuring of organosilica materials. This includes the design of different morphologies and the synthesis of organically functionalized surfaces. Therefore, the concept of a new organosilica precursor, namely boron silanes, will be presented and its scopes outlined. The employment of the synthesized organosilicas in current applications of interest, especially asymmetric catalysis and chiral resolution by High Performance Liquid Chromatography, will be investigated.

1.2 Introduction

In general, the term „*nanotechnology*“ categorizes all structures and manipulations in dimensions from an atom up to 100 nm. The major source of difference among the materials is the way how they are manufactured. There is a distinction drawn between two methods, the “*top down*” and the “*bottom up*” approach. The „*top down“* approach describes all procedures in which the final structure is obtained by modifying a macroscopic bulk starting material to yield structures at the nanometer scale, e.g. lithography. In contrast to that, according to the „*bottom up“* approach nanostructures are formed via a smaller precursor system which assembles to generate larger structures. The next smaller dimension beyond the nanometer scale is the molecular scale which is of great interest for chemists. The crucial difference between both approaches is getting more transparent when looking at an example, the morphogenesis of diatoms or radiolarians.[5,6] Although diatoms are assigned to the phytoplankton and radiolarians are zooplankton, they both possess a similar structural complexity. The characteristic feature of both cell Types is that they are encased within a unique cell wall made of silica called a frustule (diatom). These skeletons show a wide diversity in form that arises from a filigree construction (Figure 1.2). It is obvious that the formation of these fine structures is almost impossible to be realized by modifying (by e.g. leaching) a compact silica shell as it has to be done according to the “*top down*” approach. Although there is little known about the precise pathway for the structural formation, it is

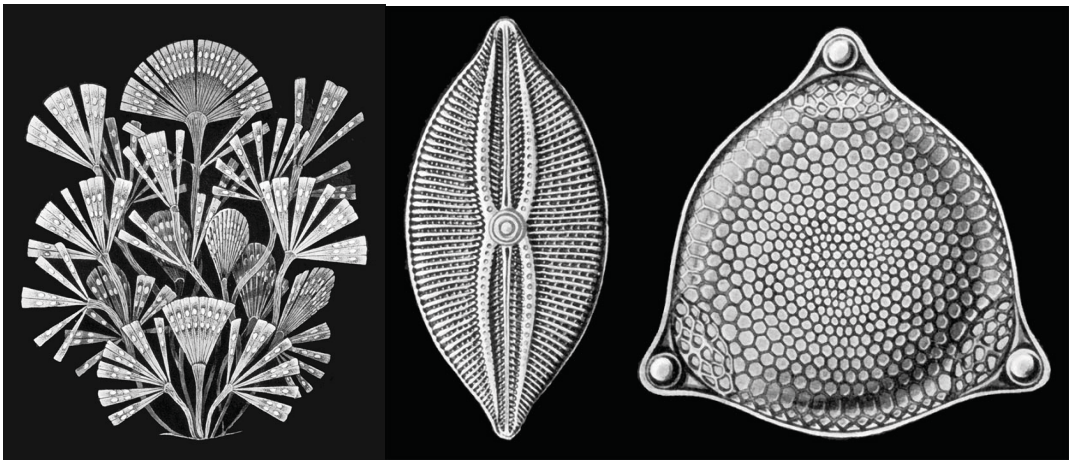

Figure 1.2: Silica skeleton of diatoms (left: licmophora flabellata, centre: navicula bullata, right: triceratium robertsianum)[7]

certain that carbohydrates and proteins in these skeletal elements act as nucleators and structure directing agents for the condensation of silicic acid. Thus, the construction of all features is directed from the molecular scale, and the growth can be regarded as a single-step process. This build-up process which is essentially the "*bottom up*" approach, enables a very efficient and highly specific growth of the structure.

Scientists recognized from nature very quickly the superiority of this approach and have attempted to utilize these principles to create artificial nano-structured materials. The development was especially accelerated by the potential of these silica based skeletons for specific industrial applications. However, the transfer of the synthetic concept from nature to man-made porous silica, although simplified, is rapidly being realized.

1.3 Porous Materials

In general, synthetic porous materials are commonly obtained by the sol-gel process which will be described in detail later. The materials can be classified into aero- and xerogels with respect to the conditions of solvent removal step of the wet gel and the therefore resulting different material properties. Simple drying of the gel leads to xerogels with high surface areas (150-900 m^2/g). In contrast when solvent removal occurs under supercritical conditions the network does not shrink and a highly porous, low-density (up to 95 % porosity) material denoted as aerogel is produced (Figure 1.3). Although having a transparent appearance like a hologram, aerogels are solid and exhibit extraordinary properties. The very high surface area

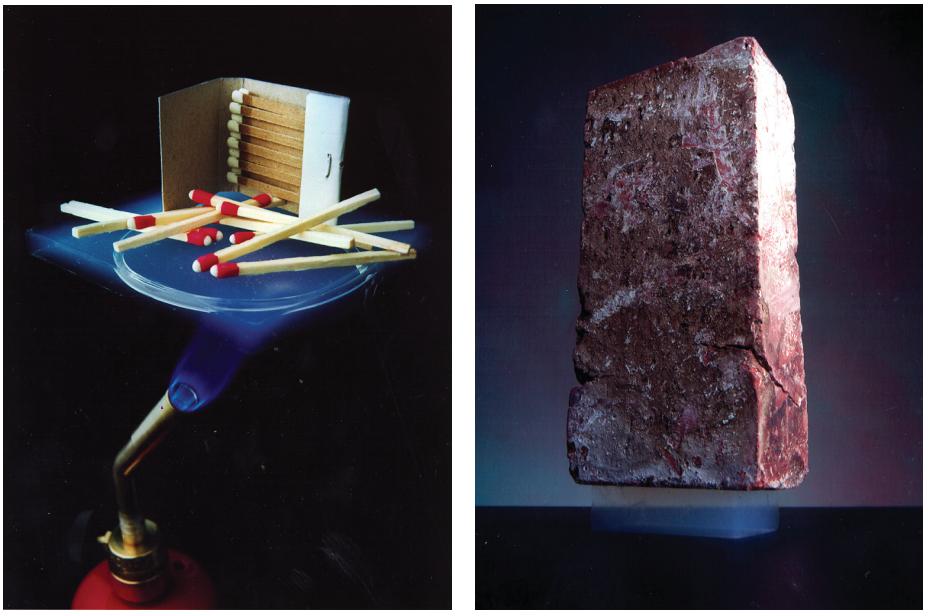

Figure 1.3: left: matches on top of an aerogel are protected from ignition by the flames underneath; right: extreme rigidity – 2 g aerogel carries 1000-fold heavier brick[8]

and good accessibility of pores in the material makes these materials very interesting for potential applications in catalysis, sensing, microelectronics and separation.

The synthesis of porous materials following the "bottom up" approach is realized based on the "nanocasting approach". This process can be subdivided into three steps (Figure 1.4):

1st - a template which serves as a spacer, is homogeneously imbedded in a dispersion or solution of a precursor molecule

2nd - after formation of the network from the precursor, a composite is obtained which is a direct cast of the metastable template system

3rd - removal of the template then yield the porous structure

Most common is the removal of the template by heat treatment, but also extractions are feasible. The Type of template used is either "soft templating" or "hard templating" must be distinguished. Soft templates are typically organic molecules, supramolecules and molecular associates, such as organic ammonium or sulfonic acid salts and amphiphile copolymers. These soft templates have been employed in synthesizing microporous zeolites and ordered mesoporous molecular sieves. Additionally, vesicles,[9] ionic liquids,[10,11] self-assembled colloidal crystals,[12,13] biomolecules[14,15] and air bubbles[16] can be considered as soft templates.

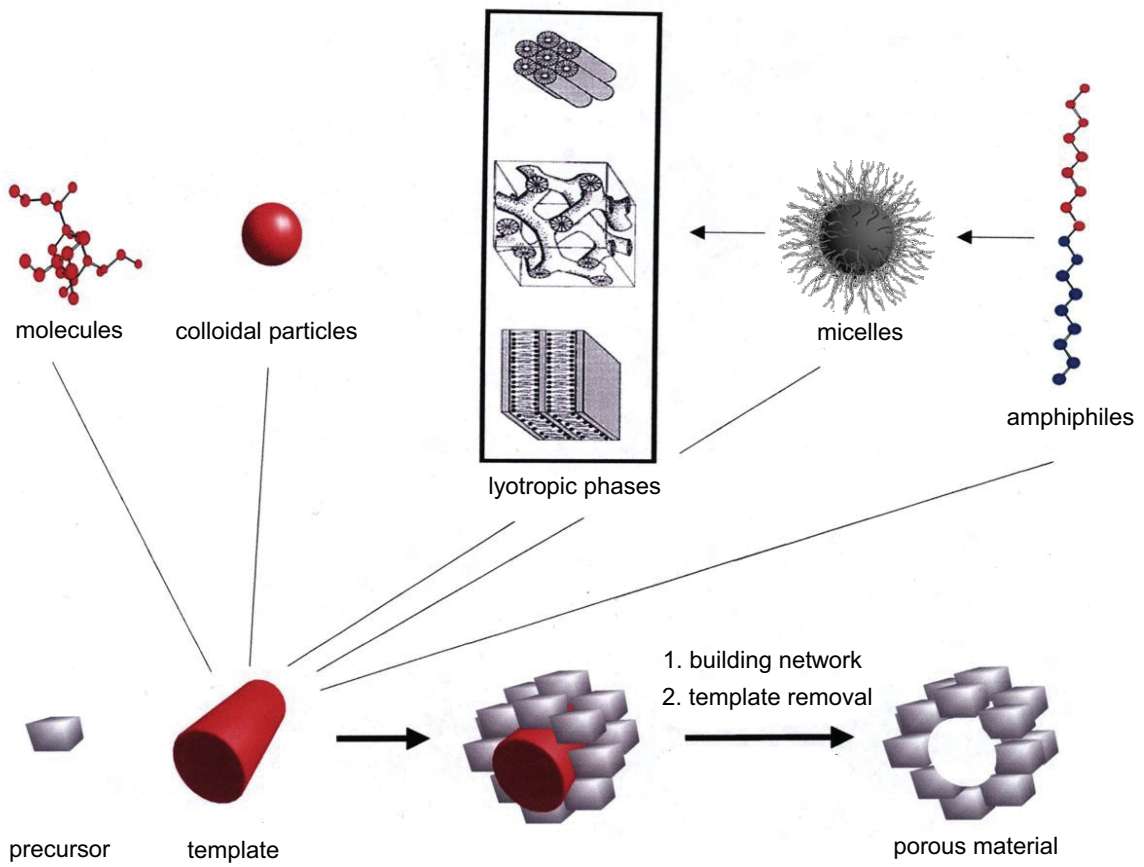

Figure 1.4: Nanocasting approach for synthesis of porous materials

Removal of these templates is achieved by solvent extraction or heat treatment. Hard templates[17] are composed of inorganic materials (e.g. silica,[18,19] alumina[20]) can be leached away by using acid or alkali solution. In general hard templates are used for the synthesis of soft materials and vice versa. While lyotropic phases of e.g. tertiary ammonium salts and block-copolymers are used for the synthesis of porous silica,[21] silica templates can be used for polymer casts.[22]

The nanocasting approach for the formation of a network requires a chemical procedure that is reproducible, controllable and do not disturb the formation of the lyotropic phase. Those rather mild conditions can be realized at its best by sol-gel chemistry. Therefore, a reactive multivalent metal complex serves as a reactant which is usually an alkoxide, hydroxide or halide. Many precursors yielding porous silica,[23,24] titania,[23,25] zirkonia,[23,26] alumina,[27,28,29] tungsten oxide[30] or iron oxide[31] are known. Most developments for the synthesis of porous silicas base on the strategy that utilizes tetramethoxysilane (TMOS) or tetraethoxysilane (TEOS). The condensation of these precursors is carried out by acidic, basic or fluoride ion

catalysis. The process for the formation of the network can be subdivided into two steps, first hydrolysis, where the substitution of alkoxy groups to hydroxyl groups takes place and second, the condensation (Figure 1.5). The latter step is responsible for the cross-linking of the precursor in the liquid phase (sol) to form a 3D network (gel). Depending on the proton concentration, the reaction rate of the solid material formation starting from the precursor can be controlled. While pH values > 5 lead to a fast condensation and slow hydrolysis, for

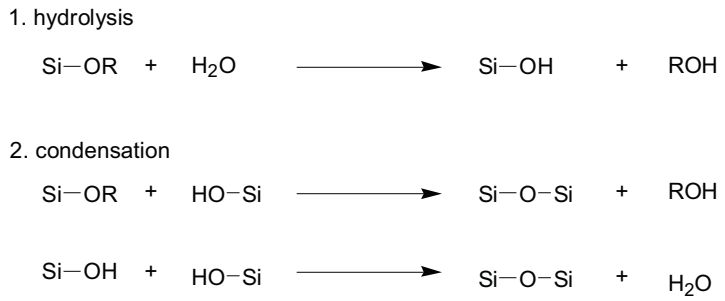

Figure 1.5: Hydrolysis condensation mechanism for formation of SiO_2

pH values between 2 and 5 this effect is reversed.[32] The result of a fast hydrolysis, as occurring when applying pH 2 – 5, is the formation of a high concentration of orthosilicic acid $Si(OH)_4$ or small oligomers with reactive silanol groups. Under these conditions, reactions at terminal silicon atoms are favored for electronic reasons, yielding polymer-like gels with only a few branches. This mechanism is denoted as RLCA (Reaction Limited Cluster Aggregation).[33,34] In contrast, hydrolysis is the rate-determining step under basic conditions resulting in a preferred condensation of the silica monomer at highly substituted silicon centers. Hence, the resulting network is characterized by larger particles. This model is called reaction limited monomer cluster growth (RLMC) or Eden growth.[35] Further parameters that play an important role on the outcome of the network formation are the temperature, aging conditions, solvent and the substitution of the precursor.[33,36] For example, alkyl substituted (e.g. MTMS (methyltrimethoxysilane)) and sterical demanding alkoxy groups substituted silanes possess lower reactions rates under basic conditions (e.g. TEOS << TMOS > MTMS).[37] In contrast the condensation rate of TEOS and TMOS under acidic conditions is similar.

Beside the possibility of adjusting the reaction conditions the template has a decisive effect especially on the structure and the size of the pores in the final material. Depending on the envisaged application the pore size in the material is of interest. A distinction is drawn between microporous (< 2 nm), mesoporous (2 – 50 nm) and macroporous (> 50 nm)

materials. The tuning of pore sizes was first considered in order to tailor the accessibility of zeolite based catalysts with respect to the involved substrates. This was particularly accelerated by the known catalytic activity of zeolites.[38] Limited by the pore size of only a few Ångström, zeolites are not suitable for conversion of large molecules. This was expected to be overcome with mesoporous materials, but failed due to the significant change in the chemical material properties. In 1992 BECK, KRESGE and VARTULLI reported on MCM-41 (Mobile Composition of Matter 41) the first ordered material with a uniform pore size of more than 1.5 nm (Figure 1.6).[21] This was the breakthrough beyond the pore size limitation of zeolites.[39] However, the hexagonal ordered MCM 41 obtained using cetyltrimethyl-ammoniumbromide (CTAB) as template was not, as first assumed, an imprint of the micellar structure. The CTAB concentration applied was far beyond the critical micelle concentration (CMC) and therefore the obtained structure could not have been caused by a micellar structure. The exact mechanism which leads to the formation of the hexagonal phase in this system is supposed to origin from synergetic effects of the hydrophilic head group and the silica cluster leading to the final structure. By the change of reaction conditions and the surfactant also other member of the M41S family e.g. MCM-41 (2d hexagonal, *p6m*), MCM-48 (cubic *Ia3d*), MCM-50 (lamellar) were accessible.[40] In contrast to the synergetic templating mechanism, block-copolymers used as templates with concentration above the CMC exhibit a casting of the real liquid crystalline phase and is thus denoted as “true liquid crystal approach” or “nanocasting”.[42,41] The one-to-one transfer of the lyotropic phase was

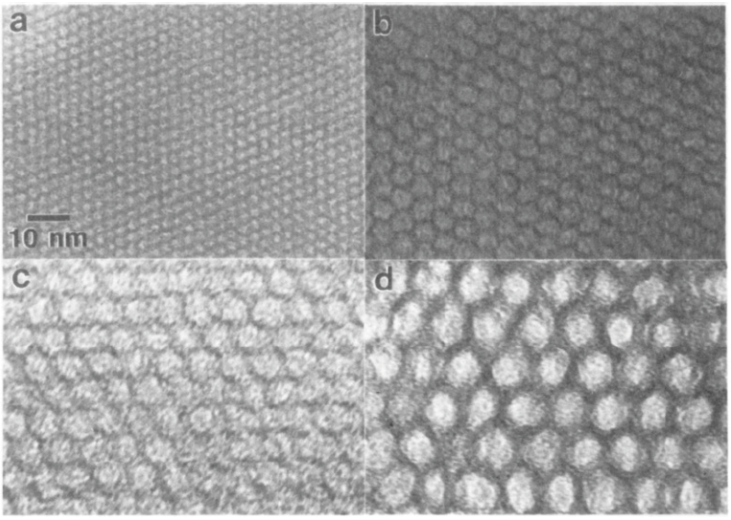

Figure 1.6: Transmission electron micrographs of several hexagonal MCM-41 materials having pore sizes of (a) 2 nm, (b) 4 nm, (c) 6.5 nm, and (d) 10 nm

proved by XRD measurements.[42,43] Hence, this method can be used as a powerful tool for the characterization of liquid crystalline phases.[44]

1.4 Functionalized silicas

Porous silicas consist of an exclusively inorganic network featuring only silanol and oxide functionalities on the surface. This unfortunately limits the range of applications. To further optimize the properties it was obvious to combine the characteristics of these porous glasses, such as high surface area, defined pore structure and rigidity with chemical and physical properties of organic molecules, leading to various potential applications in catalysis, sensing, microelectronics and separation.[45,46,47,48] The research was particularly accelerated by the need of heterogeneous catalysts which grant easier catalyst recovery and product purification. For that purpose silica material are promising candidates. Three different approaches can be distinguished for the incorporation of organic functionalities into an inorganic silica matrix, namely (i) co-condensation, (ii) post condensation functionalization (grafting), and a special case of the co-condensation, namely the condensation of bridged silanes(iii). These methods differ significantly in the distribution, accessibility and density of the functionalities.

(i) Silsequioxanes[49], having the general molecular formula $RSi(OR')_3$ offer a good opportunity to add various organic functionalities into a silica network. Using the appropriate monoalkylsilane various organic functionalities, such as alkyl,[50,51] thiol,[51,52,53,54] amino,[55,56,57,58,59,60] cyano/isocyano,[58,61,62] vinyl / allyl,[51,52,58,63,64,65] organophosphine,[62,66] alkoxy[52] or aromatic groups[50,52,62,67,68] can be incorporated into the pore walls of the silica network. Co-condensation of mono-functionalized trialkoxysilanes $R\text{-}Si(OR')_3$ towards porous organosilicas is usually done in the presence of a structure directing agent and a network former like TEOS or TMOS. This reaction pathway enables a simple, one step modification of the silica material. However, the distribution of the functionalities is usually uneven due to the possibility of domain formation (macrophase separation). Furthermore the structural collapse tendency, especially when using high amounts of the polysilsesquioxane was reported.[69] By using the here described method control of the location of the functionalities is difficult, but this is a crucial point for potential applications. Procedures that enable the incorporation of accessible functionalities are often denoted as “writing on the

wall".[70] However, the lack of control is often overcome by the aid of so called "grafting" procedures.

(ii) Grafting is a two step process, starting with the synthesis of a porous material followed by subsequent surface modification. Thus, all functional groups are exclusively located on the pore surface which makes these materials especially interesting for applications in chromatography. Most common reagents for the modification are monoorganyl-trialkoxy, -trichlorides, -amides etc. The structure of the initial porous silica material remains unaffected during the modification and determines the structure of the resulting material. Organic loadings depend on the organosilane and number of surface silanol groups and are usually about 0.3-2 mmol/g.[71] A drawback of this approach arises from the narrowing of pores caused by the surface coverage with the organic modifier. This effect is especially dramatic in the somewhat smaller interconnections of the pores. This might result in a diminished or fully hindered accessibility of the pores. Furthermore, kinetic studies revealed an inhomogeneous distribution of functionalities which are preferably located at the pore openings.[65]

(iii) The condensation of bridged polysilsesquioxanes enables the incorporation of the organic functionality into the silica wall and represents a new class of materials (Figure 1.7).[72,73,74] The organic functionalities possess a higher stability compared to simple condensed non-bridged silanes since they are anchored via two or more silane functionalities. However, this approach is based on the co-condensation (i) but will be focused upon because of the boron-silane precursor concept that involves bridged polysilsesquioxanes. The use of bridged polysilsesquioxanes combines high chemical stability, high loading and homogeneous distribution of the functionalities. Furthermore, these precursors can yield organosilicas with periodically ordered pore systems denoted as periodic mesoporous organosilica (PMO).[75,76] Various defined pore morphologies like hexagonal, lamellar etc. are achieved by changing the condensation conditions, the precursor or the surfactant for the templating route. Also crystalline structures are observed. Considering the condensation of *para*-bis(triethoxysilyl)benzene, this material shows a crystal-like orientation of the benzene ring in its pore wall.[77] The high density of organic functionalities does not necessarily result in their accessibility. It was reported by STEIN and OZIN that the ethylene bridge in PMOs are not fully accessible for either bromination or hydroboration.[78,79] In contrast, terminal

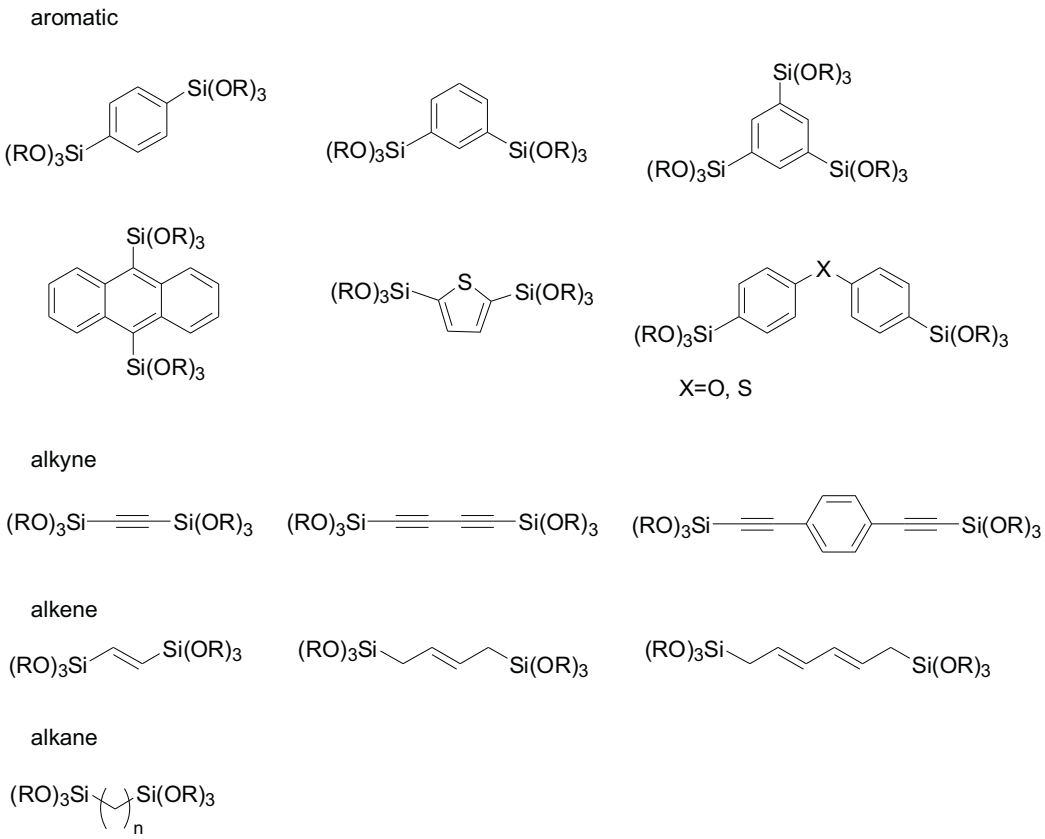

Figure 1.7: Bridge polysilsesquioxane precursor for PMO synthesis

alkenes undergo these reactions, indicating that the bridged unsaturated bonds presumably are buried within the pore wall.

From the above presented methods various functionalities can be introduced in silica based materials. Since the focus of this work is on amine-functionalized organosilicas only a brief introduction of these materials reported so far will be given. For a more detailed review see the following publications.[80,81,82] Most materials are based on grafted or cocondensed 3-aminopropylsilane (APTS) in which APTS serves as a linker to anchor further organic moieties. CHISEM et al. reported on a very active catalyst for the oxidation of ethylbenzene that is based on this principle where a SCHIFF base (or azomethine) chromium complex is immobilized on silica by an APTS linkage (Figure 1.8).[83] Due to the high chemical resistance of the amide bond many chiral stationary phases based on the amine linkage are known which are also used in industrial scale.[84] Beside the approaches where APTS is exploited as a linker, organosilicas with the free amine group have been shown to be effective catalysts for the KNOEVENAGEL reaction.[85,86] The catalytic effects of grafted primary, secondary, and

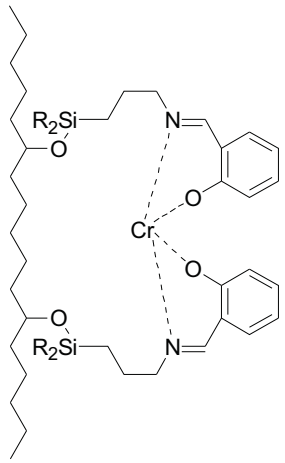

Figure 1.8: Chromium complex immobilized on silica via SCHIFF base

tertiary amines on silica have been investigated using base-catalyzed reactions such as the nitroaldol condensation and MICHAEL addition reactions.[87] UTTING and MACQUARRIE investigated the use of the imine-based active sites for catalyzing the KNOEVENAGEL condensation and MICHAEL addition reactions.[88] Various examples of higher substituted amines for catalytic applications are known (e.g. guanidine derivatives for MICHAEL addition) which will not be discussed here in detail.[89] These examples give an insight into the importance of amine-functionalized silica materials. Therefore this work will explore a concept which enables the introduction of accessible amines functionalities and allow a simple tailoring of the porosity.

1.5 Hydroboration of alkenes

A central part of this work is the hydroboration reaction and a brief summary of the reaction mechanism as well as the scope of the reaction will be given. The first report and the major developments on this reaction were done by H.C. BROWN.[90,91] In general the hydroboration describes the addition of boranes (RR'BH) on alkenes usually followed by substitution of the boron moiety. The borane addition on alkenes is usually very quick, highly regioselective and stereospecific, caused by the reaction mechanism.[92] Hydroboration on alkenes follows a concerted reaction mechanism, with multiple bond formation and breaking occurring simultaneously, thus a *syn* addition occurs (Figure 1.9).[93,94] The four centre transition state is formed by the occupied π–orbitals of the alkene, the empty boron p-orbital and the s-orbital of hydrogen. The coupling between boron-carbon occurs at the less substituted carbon (anti-

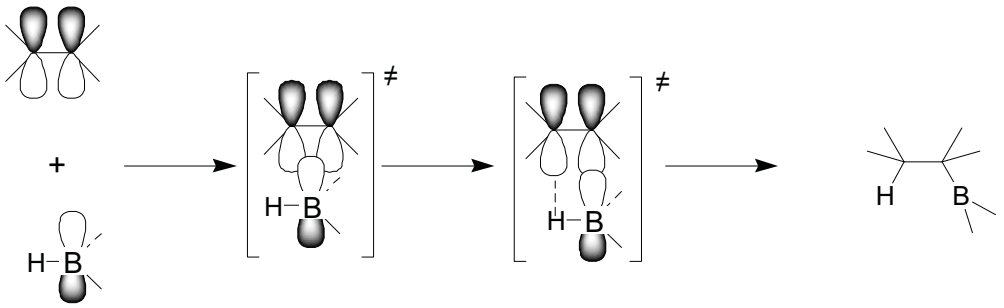

Figure 1.9: Orbital model for the hydroboration reaction

Markovnikov) which is caused by sterical and electronic interactions. According to the three BH bonds the addition of three and even different alkenes can be realized. Most common is the oxidative cleavage of the boron-carbon bond yielding alcohols, but functionalization to aldehydes, ketones, amines, halides and the cross coupling is feasible (Figure 1.10).[95]

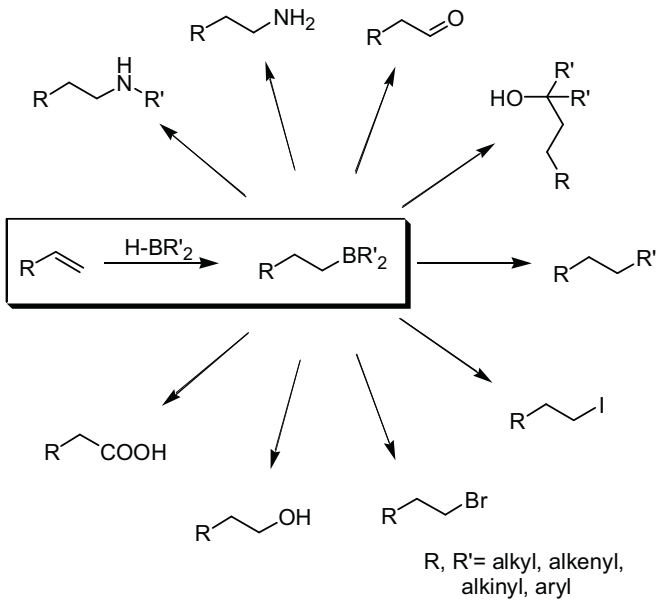

Figure 1.10: Versatility of organoboranes – functional groups derived from boranes

Another very interesting benefit of the hydroboration is the accessibility of chiral, terpene derived boranes (Figure 1.11) which enable a highly enantioselective addition on double bonds. The use of monoisopinocampheylborane offers very high enantioselectivities for the conversion of pro-chiral alkenes and is often applied for the synthesis of chiral alcohols via oxidative cleavage of the CB bond.[96]

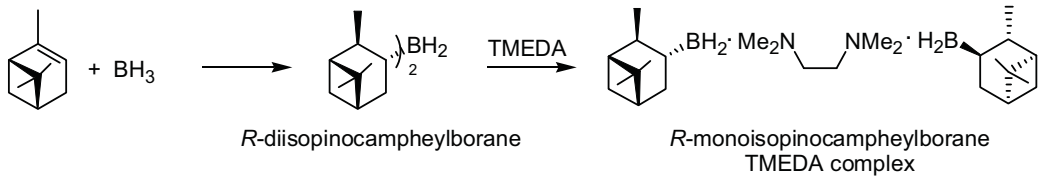

Figure 1.11: Synthesis of enantiomerically pure mono-isopinocampheylborane

The interesting opportunities which are offered by the hydroboration were exploited for the development of a new organosilica precursors. This innovative concept will be presented in the following sections.

1.6 Hydroboration approach for organosilica precursors

The focus of this work is set on the rational design of a new precursor for highly functionalized mesoporous organosilicas. This precursor should enable a simple modification of the functionalities and, more important, a predefinition of the functionalities on the pore surface. In general, accessibility of functionalities is a vital point for application and common functionalization methods (e.g. grafting, co-condensation, PMO materials) do not necessarily offer homogeneously distributed and accessible functionalities. For that reason, hydroboration was recognized as a tool for the synthesis of a suitable precursor. By a double addition of borane a linkage between an ethylene bridged organosilica precursor and a terminal alkene is formed (Figure 1.12). This concept was envisaged to some extent by VOSS et al. and will be further studied and extended in this work.[97,98] The anchoring of the structure directing moiety is the crucial dodge to obtain all described features in one precursor. As a

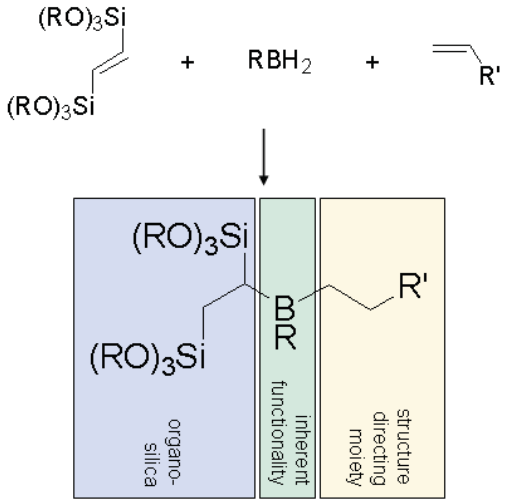

Figure 1.12: Hydroboration for the design of organosilica precursor

result of this group, self-organization of the precursor during the condensation is comparable to amphiphilic molecules where organic moieties are aggregating into hydrophobic domains. After the chemical cleavage of the organic functionalities, a porous material with activated amine sites accessible at the pore interface results. This approach differs significantly from other strategies, where the organic group of the precursor was used as a template for porosity. There the organic bridging group is removed e.g. via calcination creating porosity[99,100,101,102] which is accompanied with a structural weakening of the organosilica framework. In contrast, in the presented approach only the appending parts of the organic moieties are selectively cleaved. This maintains the bridging organic group, while introducing a viable functionality on the pore wall. The advantage of this approach is the introduction of various porogenes by linking the silica source and terminal alkenes (e.g. long alkyl chain olefins, unsaturated polymers, and mesogens). Beside the broad spectrum of substrates for the hydroboration this reaction allows the synthesis of chiral organosilica precursors which is an approach to organosilicas with an accessible chiral surface. In this work, the focus of the functionalization of the organosilicas is kept on primary amines. This can be explained by the great potential which arises from this functional group. First, primary amines themselves possess due to their high polarity and ability to form hydrogen bonds, strong interactions with secondary molecules or metal centers. This property makes them interesting for adsorption applications and catalysis. Second, various C-N coupling reactions yielding thermodynamically stable compounds like SCHIFF bases, amides and carbamates enable unrestricted further functionalization. While the functionalization of mesoporous silicas with grafted amines was frequently described,[103] only a few examples of porous bridged organosilicas with directly incorporated functional groups such as amines are reported.[104,105,106]

Based on the presented precursor system the versatility of boron silanes for the synthesis of highly functionalized mesoporous organosilicas will be discussed in this work. The focus is set on the tailoring of porosity in organosilicas by the incorporation of various porogenes and the synthesis of chiral mesoporous organosilicas.

2. Analytical Methods

2.1 X-ray analysis

Interactions of electromagnetic radiation with matter provide a multitude of information on the material structure. X-ray scattering is used for mainly two species of characterization, namely Wide Angle X-ray Scattering (WAXS) which provides information about crystallinity, phase, crystallite size, purity and Small Angle X-ray Scattering (SAXS) which allows for gaining information about order, size, and Type of order for the characterization of colloidal systems. As already implied by the denotation, SAXS is applied for 2Θ smaller than 10° which means for structures larger than 0.9 nm (Cu K_α). Since, this work is exclusively dealing with colloidal systems the focus in this section will be kept on SAXS analysis.

Both methods require the existence of a scattering contrast of the matter, with the origin of the contrast depending on the specific method in use. Scattering experiments are carried out by exposing the sample to a coherent x-ray beam, where interactions of this incident beam with the electrons of the atom cause diffraction of the beam. The intensity of the scattered beam is then measured as a function of the angle between the incident and exiting beam. All atoms in the material serving as scattering centers with the electron density distribution $\rho(\vec{x})$ and leading by superposition of the secondary x-ray waves to a final complex amplitude $A(\vec{s})$ with $\vec{s}$ the scattering vector.

$$A(\vec{s}) = \int \rho(\vec{x}) \exp(2\pi i \vec{s}\vec{r}) dV = \Im(\rho(\vec{x})) \qquad \textbf{2.1}$$

This complex amplitude is equal to the Fourier transformed electron density distribution $\Im(\rho(\vec{x}))$. However, scattering experiments allow access only to the intensity distribution I($\vec{s}$) which is the square of the complex amplitude A($\vec{s}$).

$$I(\vec{s}) = \left|A(\vec{s})\right|^2 \qquad \textbf{2.2}$$

This equation lacks a one-to-one relation caused by the loss of the sign and the phase angle of the complex amplitude A($\vec{s}$) when measuring the intensity distribution I($\vec{s}$). Therefore, it is not possible to determine the electron density distribution $\rho(\vec{x})$ in real space which is

referred as a "*phase problem*". Thus, all analysis from the scattering curve can only be used as supposition and has to be verified by use of additional methods or simulations.

The Fourier transformation of the intensity distribution $I(\vec{s})$ gives the "PATTERSON function" $P(\vec{r})$ also denoted as the autocorrelation-function of density.

$$I(\vec{s}) = \int P(\vec{r}) \exp(2\pi i \vec{s}\vec{r}) dV = \Im(P(\vec{r})) \qquad \textbf{2.3}$$

Since a convolution of the electron density distribution gives $P(\vec{r})$, it is also not possible to determine the real electron density distribution $\rho(\vec{r})$ via the PATTERSON function. However, $P(\vec{r})$ gives the distribution of distances between the scattering centers in real space. The relations between all these parameters are illustrated in Figure 2.1.

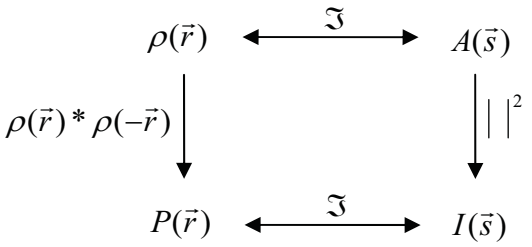

Figure 2.1: Relations between real and reciprocal space

In a typical X-ray scattering experiment with BRAGG-BRENTANO geometry, the scattering intensity is measured with varying scattering angle 2Θ. For scattering in crystalline systems the "BRAGG"-equation is applied (Figure 2.2).

$$\frac{1}{d} = \frac{2\sin\Theta}{\lambda} = |\vec{s}| = s \qquad \textbf{2.4}$$

Here, d is the lattice plane distance, and λ the wave length of the incoming x-ray beam (commonly 0.154 nm for copper K_α-radiation).

In Equation 2.4 the scattering vector *s* and the lattice plane distance *d* behave reciprocally. Therefore, large structures can be assigned to small scattering angles in general (SAXS) and vice versa.

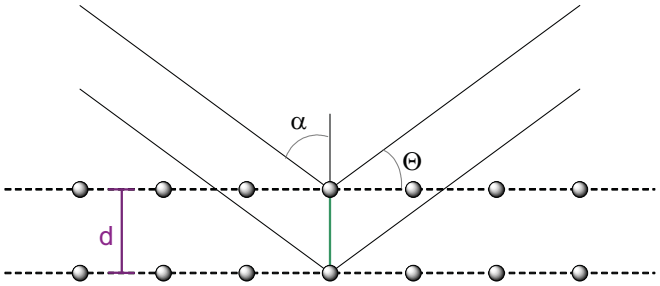

Figure 2.2: Diffraction on lattice planes, illustration of Bragg's law

2.1.1 SAXS

As already mentioned, SAXS is a useful tool for the characterization of systems in the range of colloidal sizes, such as diluted systems, lyotropic phases, polymers and mesoporous materials. An important method for the evaluation of the obtained scattering curve was established by POROD. The corresponding law of the same name gives a relation between the measured intensity distribution and the so-called "characteristic function" $\gamma(\vec{r})$. Both quantities are correlated by the use of the POROD constant k.

$$I(\vec{s}) = k\Im\left(\gamma(\vec{r})\right) \qquad k = \int I(\vec{s})dV = \left(\Delta\rho(\vec{r})\right)^2 V\Phi_\alpha\Phi_\beta \qquad \textbf{2.5}$$

This equation enables the determination of the volume ratio Φ of the phases α and β, thus consequently the calculation of the POROD length l_P. The POROD length is a measure for the cord length. Rearrangement of this equation gives the relation of the POROD length to the ratio of the interfacial area S and the corresponding sample volume. Thus, the surface area S of a porous material can be obtained by SAXS measurements.

$$\gamma(r) = 1 - \frac{|\vec{r}|S}{4\Phi_\alpha\Phi_\beta V} + \ldots = 1 - \frac{r}{l_P} + \ldots \quad \Rightarrow \quad l_P = \frac{4\Phi(1-\Phi)V}{S} \qquad \textbf{2.6}$$

In the case of porous systems, the volume ratio Φ corresponds to the porosity of the material. Since the POROD length describes the cord length, the following equation facilitates the determination of the respective phase length of each phase for a two phase system (Figure 2.3).

$$\frac{1}{l_P} = \frac{1}{\langle l_\alpha \rangle} + \frac{1}{\langle l_\beta \rangle} = \frac{1}{\langle l_\alpha \rangle\Theta_\beta} = \frac{1}{\langle l_\beta \rangle\Theta_\alpha} \qquad \textbf{2.7}$$

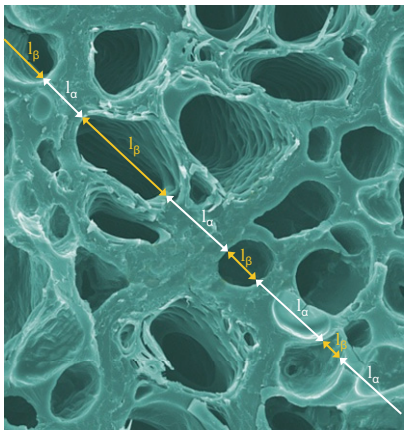

Figure 2.3: Schematic illustration of the phase length as measure for the POROD length

However, this relation allows a conclusion on the pore size independently from the pore shape.

The experimental access to the POROD length is given by the POROD asymptote. For a point collimation the asymptote is defined as:

$$\lim_{s\to\infty} s^4 I(s) = \frac{k}{2\pi l_P} \qquad \textbf{2.8}$$

It should be noted that in the strictest sense the POROD law is only valid for a two phase system with sharp interfaces. With this relation it is possible to determine the POROD length by measuring the scattering intensity I as a function of s, in a numerical manner.

$$l_P = \frac{4\pi \int s^2 I(s) ds}{2\pi^3 \lim_{s\to\infty} s^4 I(s)} \qquad \textbf{2.9}$$

2.2 Electron Microscopy (EM)

The question “What is the purpose of EM when apparently light microscopy is highly developed?” is very simple to answer. There is a certain size limit for observing objects that is related to the wavelength of the electromagnetic beam. In 1900, E. ABBE showed that the wavelength of electromagnetic radiation λ, the angle of the incident beam with the objective α and the refractive index n of the medium between the objective and the sample are related to the resolution limit as shown in Equation 2.10.

$$\Delta x = \frac{\lambda}{n \sin\alpha} \qquad \textbf{2.10}$$

Hence, the minimum resolution that can be achieved when observing objects under visible light (λ_{vis} > 400 nm) is about 200 nm. In order to overcome these limits, electromagnetic radiation with a smaller wavelength, like highly energetic electrons must be applied. However, the theoretical background of the interactions of visible light and electrons with matter are equal. The wavelength of electrons is given by the de Broglie equation, with h the Planck's constant and the product of the mass m and the electron velocity υ.

$$\lambda = \frac{h}{m\upsilon} \qquad \textbf{2.11}$$

The kinetic energy of electrons accelerated in an electric field is related to the quotient of the acceleration voltage U divided by the electron mass m.

$$\upsilon = \sqrt{\frac{2Ue}{m}} \qquad \textbf{2.12}$$

Applying this equation for a common acceleration voltage of 120 kV, a wavelength of 3.5 picometre is obtained for electrons which results in a maximum resolution of about 1.8 picometre. This is 5 orders of magnitude higher resolved compared to light microscopy and proves the exceptional performance of EM. In the following the working principles behind Transmission and Scanning Electron Microscopy are described.

2.2.1 Scanning Electron Microscopy (SEM)

A monochromatic electron beam (produced by e.g. thermoionic emission) is needed for all Types of EM's. The primary beam is collimated by electromagnetic condenser lenses, focused by an objective lens and scanned across the surface by electromagnetic deflection coils (Figure 2.4). Surface electrons, excited by the high energetic electrons of the incident beam are emitted as result of the collision. These secondary electrons are selectively attracted towards the detector through a grid held at low positive potential with respect to the

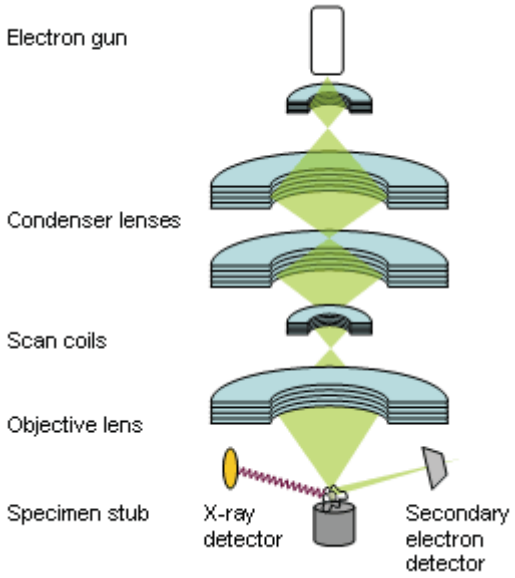

Figure 2.4: Model of a scanning electron microscope (SEM)

specimen. By counting the emitted electrons and considering geometric dependence of the electron flux a magnified image of the sample with topological detail is obtained. The contrast of the image is determined by the number of emitted electrons. A large number of secondary electrons lead to a brighter image, while areas with a low secondary electron output are shown as darker parts in the image. During the electron bombardment of the sample the surface is charged with electrons. In case of a non-conducting sample, domains with a high charge density are built up, resulting in an increased brightness throughout the sample image. To avoid this charging effect in the case of a non-conducting sample, the surface is sputtered with a thin conducting layer of metal like gold / palladium alloys.

2.2.2 Transmission electron Microscope (TEM)

The source of monochromatic high energy electron beam is similar to that of the SEM mentioned in the previous section. The setup for the electron gun consists either of thermoionic emission using a heated filament (e.g. $LaBa_6$) or a field emission gun using a tungsten tip. After acceleration towards the anode, the resulting beam is focused to a small coherent beam using several condenser lenses (Figure 2.5). When the beam hits the specimen, the electrons undergo several interactions, namely absorption, diffraction and elastic or inelastic scattering. Scattering results from interactions with the nuclei of the

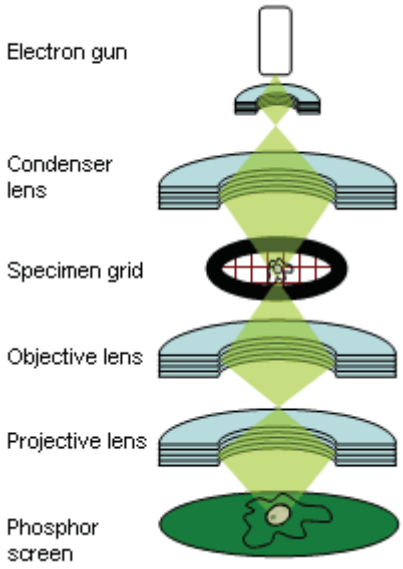

Figure 2.5: Model of a transmission electron microscope (TEM)

sample. The scattering intensity is proportional to the electric field of the nuclei. Thus, the heavier elements possess more intense scattering. After transmitting through the specimen, the beam is focused and passes several lenses for magnification, finally hitting a fluorescent screen coated with cadmium sulphide and tin sulphide, resulting in an illumination of the screen. The resulting image is then recorded with a CCD camera.

2.3 Nitrogen Adsorption

Porous systems are characterized by their surface area, pore volume and pore size distribution. Thus, these parameters are of great interest. The adsorption of gases, specifically nitrogen adsorption at liquid nitrogen temperature (77.35 K) onto the surface is the most common method to gain this information. Examples of materials that can be characterized by nitrogen adsorption include porous silica gel, glasses / carbon materials, aerogels, titania and alumina.

To classify the kind of adsorption, one distinguishes between weak (physical) or strong (chemical) interactions. Physical adsorption takes place due to the presence of attractive "*Van der Waals*" interactions of gas molecules (adsorbate) on a surface (adsobent). In contrast, chemical adsorption is derived from strong chemical interactions. A good approximation for the interaction energy E(r) of a gas molecule at a distance r from a solid surface is:

$$E(r) = -\left(\frac{\pi}{6}\right) C_{sf} \frac{\rho_S}{r^3} \qquad \textbf{2.13}$$

Here, C_{sf} represents a constant for the strength of attractive fluid-wall interactions and ρ_s is the density of the solid.

Usually the sorption isotherm is obtained by measuring the adsorbed volume of the appropriate gas in relation to the corresponding relative pressure p/p^0 at a constant temperature with p^0 being the saturation pressure of the adsorbate and p is the existing pressure of the vapor above the adsorbent. In general, the adsorption isotherms are classified into five categories (Types I-V) according to the IUPAC[107] (Figure 2.6). It should be noted that on the basis of IUPAC notation, pores are classified into micropores with a diameter smaller than 2 nm, mesopores are in the 2 - 50 nm range and macropores are larger than 50 nm. The Type I isotherm shows considerable adsorption at low relative pressures and is typical for microporous solids and chemisorption isotherms. For a leveling off at relative pressures below 0.1 it has been shown that siliceous materials exclusively consists of micropores.[108,109] Type II and III isotherms are indicative for an unrestricted multilayer build-up usually appearing in many macroporous solids. In this case, the adsorption and desorption branches of the isotherm coincide (i.e. there is no adsorption-desorption hysteresis).

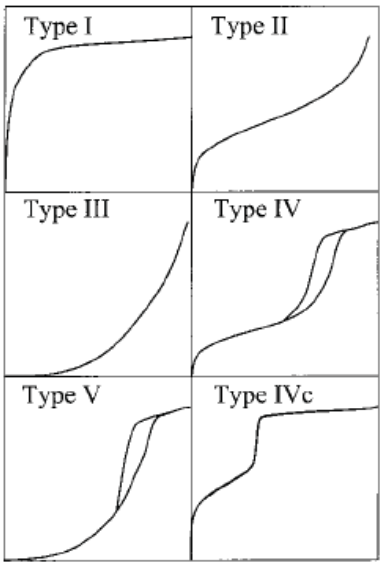

Figure 2.6: IUPAC classification of nitrogen adsorption isotherms

However, Type II has a pronounced stage of monolayer formation can be observed for adsorbates which interact rather weak with the adsorbent (e.g. non-polar gases like nitrogen on silica). In contrast, Type III isotherms shows convex behavior in the whole pressure range which is typical for strong interactions. The latter case can be observed for e.g. water adsorption on hydrophilic solids. Type IV and V isotherm slopes are observed for mesoporous materials on which the adsorption leads to capillary condensation via a multilayer formation. While macroporous solids and materials with Type IV/V show initial similarities in adsorption behavior, the adsorption at higher pressures rises step-like due to the capillary condensation in the mesopores. Therefore, capillary condensation features a hysteresis loop and is a direct hint for mesoporous materials which are especially of interest in this work. The typical hysteresis is closed at a relative pressure of 0.42-0.48.[110] After complete filling of the pores the adsorption isotherm levels off. The desorption of an adsorbate from a mesoporous adsorbent is indicated by the Type IVc isotherm. Finally, it should be noted that some adsorbents may possess adsorption isotherms that are regarded as a combination of the aforementioned five Types of isotherms, as a result of the presence of different pores Types in the structure.

The following scheme represents the sorption characteristics of an adsorbate on an adsorbent with single size cylindrical pores (Figure 2.7) and the resulting isotherm. Starting with the formation of an adsorbate monolayer (**A**). Further condensation leads via adsorbate multilayer (**B**) then to a critical film thickness (**C**) when reached capillary condensation

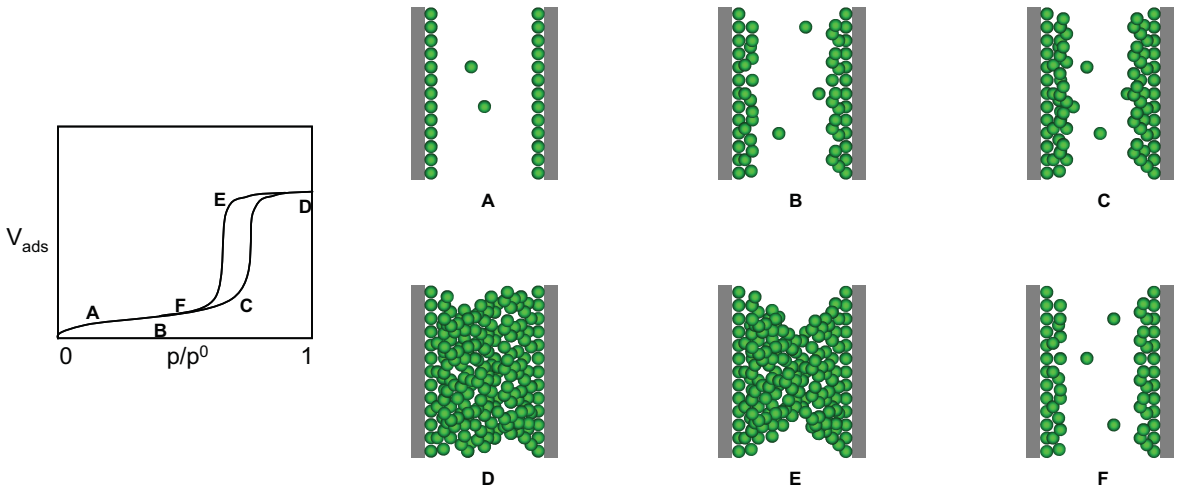

Figure 2.7: Schematic illustration of nitrogen adsorption in pores

occurs and is indicated by a strong slope of the isotherm followed by a complete filling of the pore (**D**) at relative pressures close to 1. Since evaporation from mesopores is strongly affected by capillary pressure, the desorption takes place at smaller pressures than the adsorption. This effect can be depicted as receding meniscus (**E**). The pressure at which the hysteresis loop closes (**F**) coincides again with the situation of a multilayer film, as already indicated by (**B**). Between the limits of (**A**) and (**F**) the adsorption and desorption are reversible. The aforementioned mechanism is essential for the BROECKHOFF and de BOER[111] and as well as for the SAAM-COOLE[112], both theories in adsorption. Both of the latter theories recognize first the influence of the adsorption potential on the chemical potential and secondly the effect of curvature on the thickness of the adsorbed multilayer film. In agreement with experimental observations, these theories predict that an increase in the strength of the attractive fluid-wall interactions, or a lowering of the experimental temperatures and as well as decreasing the pore size will shift the pore condensation transition to lower relative pressures. However, all these thermodynamic and macroscopic theories do not account the particularities of the critical region. The most common applied KELVIN approach emanates from pore condensation as a gas-liquid transition in the core of the pore between the two homogenous phases. In contrast, microscopic approaches such as DFT[113] and various further computer simulation[114] studies suggest that a fluid confined in a single pore can exist with two possible density profiles according to the gaseous and liquid state on the surface.

The specific surface area is determined by the method introduced by BRUNAUER, EMMETT and TELLER (BET). They assume the formation of an adsorbate multilayer with a specific multilayer capacity N_m at a relative pressure range from 0.05 to 0.3. Determining this capacity, the surface area is defined by the following equation where L is the Avogadro constant and σ the cross sectional area.

$$a_{surf} = N_m L \sigma \qquad \textbf{2.14}$$

The application of the BET equation is in strict sense limited to non-microporous systems with pore sizes usually greater than 4 nm. While in non-microporous systems physisorption of the adsorbate leads to a monolayer, in microporous systems a significant amount of the adsorbate is condensed inside the pores because of the capillary forces. This multilayer

formation causes an overestimation of the monolayer capacity and therefore an over-estimation of the surface area.

As already mentioned above, there are different basic approaches when dealing with adsorption on surfaces. Among those, the most common model for the condensation of an adsorbate in pores with uniform, ideal cylindrical pores is based on the KELVIN equation. This model considers macroscopic values like surface tension γ of the bulk fluid, the densities of the coexisting phases ρ_l and ρ_g and the contact angle Θ of the liquid meniscus against the pore wall for the determination of the gas-liquid phase transition. For cylindrical pores the modified KELVIN equation is,

$$\ln\left(\frac{p}{p^0}\right) = \frac{-2\gamma\cos\Theta}{RT\Delta\rho(r_p - t_c)} \qquad \Delta\rho = \rho_l - \rho_g \qquad \textbf{2.15}$$

with R being the universal gas constant, r_p the pore radius and t_c the thickness of an adsorbed multilayer film which is formed prior to condensation. Pore condensation can only be expected unless the contact angle Θ is 90 degrees or more. For nitrogen adsorption a contact angle of 0 degree is usually assumed for adsorption at 77 K. The KELVIN equation gives the relation between pore diameter and pore condensation pressure and predicts the adsorption characteristics of mesoporous systems. With an increase in either pore diameter or temperature an increase in relative pressure is expected. This modified KELVIN equation is the basis for many methods applied for the determination of the pore size distribution in a porous material, e.g. the most common BARETT-JOYNER-HALENDER method (BJH).[115] Unfortunately, this method and all related methods which are based on the KELVIN equation face a drawback, i.e. inaccurate predictions of the pore size of microporous materials. Fluid-wall interactions are dominant in systems with narrow pores, whereas the strict two-phase system with no phase transition given by the KELVIN Equation leads to unrealistic results. In a nutshell, the KELVIN equation does not consider the influence of adsorption potential on the position of pore condensation transition and the differences of physical properties like the surface tension which depends on the radius of curvature. Therefore, a precise pore size analysis covering the complete micro-mesopore range must be involved. Non-Local-Density-Functional-Theory (NLDFT)[116] or computer simulation methods like Grand Canonical Monte Carlo (GCMC)[117] and Molecular Dynamics (MD)[118] allow a description of the configuration of adsorbate molecules on a molecular scale. Pore size distributions obtained with these

methods match very well with results obtained from independent methods (e.g. XRD and TEM).

2.4 Circular Dichroism Spectroscopy (CD)

Circular dichroism spectroscopy (CD) is based on the differential absorption of left- and right-handed circularly polarized light when interacting with optically active compounds. In general, polarized light is classified into two categories, these being linear and circular polarized light. While the electric field vector in the first case oscillates only in one plane, the electric field vector for circular polarized light has a constant length, but rotates about its propagation direction. Since circularly polarized light itself is "chiral", it interacts differently with chiral molecules. In a typical CD experiment, equal amounts of left- and right-circularly polarized light are radiated through the chiral analyte solution. One of the two Types is absorbed more and the wavelength dependent difference of absorption is measured yielding the CD spectrum of the sample. This method can be used to distinguish between two enantiomers or to determine the structure of macromolecules (including the secondary structure of proteins and the handedness of DNA).

CD is closely related to the optical rotary dispersion (ORD) technique, and is commonly considered to be more advanced. An ORD measures the variation in the optical rotation of a substance with a change in the wavelength of light. In spectroscopic applications the difference of the refractive index for the interaction of either right- or left-handed circularly polarized light with an analyte is determined.

2.5 High Performance Liquid Chromatography (HPLC)

High performance liquid chromatography (HPLC) is a form of column chromatography used frequently in biochemistry and analytical chemistry. The analytical principle of the separation of two or more analytes is based on the different interactions of the dissolved analytes with a stationary phase. The solvent (mobile phase) passes through the stationary phase and depending on the nature of the analyte, the stationary phase and the mobile phase composition the analyte is more or less retained. This results in different velocities on the column which can be detected by e.g. flame ionization detector (FID) or mass spectrometer (MS). The time at which a specific analyte elutes (leaves the column) is called the retention time and is considered a reasonably unique characteristic for a given analyte. The use of

pressure increases the linear velocity (speed), giving the components less time to diffuse within the column, leading to improved resolution in the resulting chromatogram.

An illustrative concept for understanding the chiral separation is the so called *three point rule*. For chromatographic separation at least three simultaneous interactions must be present with a of one of these interactions being stereochemically dependent (Figure 2.8). However, these interactions are not necessarily attractive forces such as hydrogen bonding, dipole stacking and sterical interactions. Often repulsive forces are involved which result in combination with "bonding" interactions in chiral recognition. As a result of both concepts the chiral resolution can be improved when increasing the number of interactions, no matter attractive or repulsive.

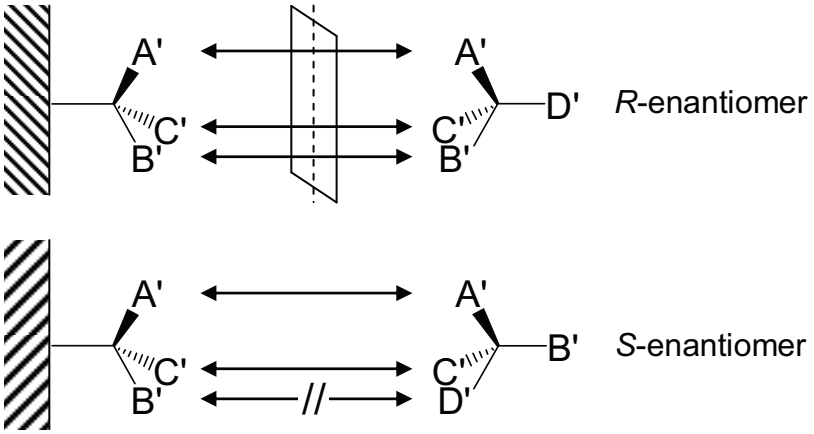

Figure 2.8: The *R*-enantiomer of the analyte is capable of forming three simultaneous interactions with the CSP, whereas the *S*-enantiomer is capable of only two interactions. If all three interactions are free-energy-lowering, the *S*-enantiomer will be less retained by the CSP

The performance of a HPLC and therefore the separation is determined by the column efficiency N, separation factor α, resolution R_S and peak asymmetry A_s which can be obtained from analyzing a chromatogram (Figure 2.9).

In general, the column efficiency is determined by the number of theoretical plates N where commonly the peak width at half peak maximum is used for the determination.

$$N_{W_{1/2}} = a\left(\frac{t_R}{W_{1/2}}\right)^2 \qquad \textbf{2.16}$$

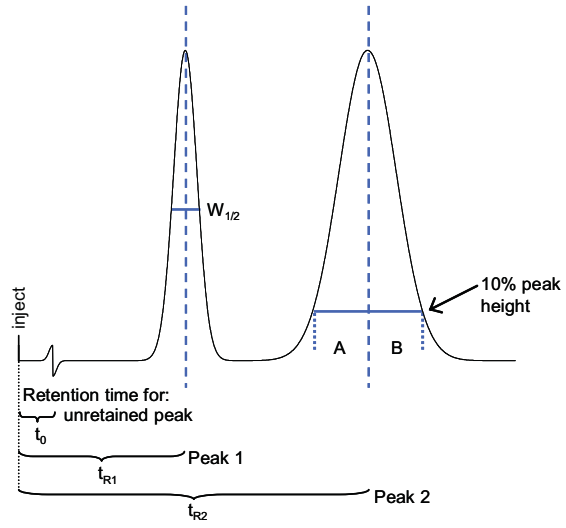

Figure 2.9: Typical HPLC chromatogram with peaks for two analytes

For determination of the separation characteristics, not only the retention time is important, but moreover, how long the interaction of the analyte and stationary takes place. This means that the void which is observed for an unretained analyte t_0 must be subtracted from the retention time of the observed analyte t_{R1}. As a measure the capacity factor or retention factor k was introduced.

$$k = \frac{(t_R - t_0)}{t_0} \qquad \textbf{2.17}$$

The division of two capacity factors of two analytes gives the separation factor α which describes the spacing between two peaks.

$$\alpha = k_2 / k_1 \qquad \textbf{2.18}$$

As the equation already implies, the separation factor α provides neither information on overlapping nor full baseline separation of both analytes. Therefore, the resolution R_S is introduced which is expressed by.

$$R_S = \frac{1}{4}(\alpha - 1)\sqrt{N}\left(\frac{k}{1+k}\right) \qquad \textbf{2.19}$$

The parameter for the characterization of the peak shape is the peak asymmetry A_S which is defined as the ratio between the ratios of the peak integrals A and B (see Figure 2.9).

3. Tailoring organosilicas by boron-silane precursors

3.1 Introduction

Pure MCM 41 silica materials show a hexagonal arrangement of pores which are larger than 20 Å in diameter. In order to increase this pore size, three different techniques are used, namely variation of the template, the utilization of a cosurfactant, or changing the condensation conditions. The size of pores in the above mentioned MCM 41 can be tuned by choosing the appropriate surfactant while maintaining the hexagonal structure. It has been shown that the use of alkyltrimethylammoniumchloride with different alkyl chain lengths as structure directing agent leads to pores increasing from 15 Å to more than 100 Å.[119] Cosurfactant organic molecules, such as 1,3,5-trimethylbenzene, were used to expand the pore size of MCM 41 up to 100 Å.[120,121] Through the addition of cosurfactants like alcohols the pore structure can be significantly changed.[122] OZIN et al. reported on the influence of the reaction conditions on the final pore size. They used extended thermal treatment during synthesis which results in expanded pore size up to 50 Å.[123] However, the breakthrough beyond the upper pore size limit of about 100 Å when using tertiary ammonium salts was realized by the use of block-copolymers, leading to e.g. SBA 15.[124] These well ordered silicas can be readily prepared over a wide range of uniform pore sizes (50 to ~ 300 Å) and pore wall thicknesses at low temperatures (35 to 80 °C) using a variety of poly(alkylene oxide) triblock copolymers which are commercially available and known as Pluronics. Pluronics are in general symmetrical poly(ethylene oxide)-poly(propylene oxide)-poly(ethylene oxide) copolymers. THOMAS et al. showed the concentration dependence of different KLE-Type triblock copolymers used as structure directing agent on the pore size in the resulting silicas.[125]

In the following, the possibility for the tuning of pore sizes according to the change in size of the porogen in boron silanes precursors will be discussed. The general presentation of the synthetic concept by a particular precursor will be followed by the optimization of the condensation conditions and concluded by the study on the influence of different chain length. It has been shown by the different micro- and mesopore distributions that the alkyl chain length of the precursor has an exceptional influence on the average pore size. The dependence of different chain lengths on the porosity in the final material was investigated

by SAXS, BET and TEM measurements. In order to prove the accessibility of surface functionalities and to validate the coverage with amine functionalities, copper adsorption was used. The different interactions of hydroxyl and amine-functionalized silica surfaces resulting in a significant difference of the copper adsorption behavior for both materials.

3.2 Synthesis of Long-Chain-Boron-Silanes (LCBS)

3.2.1 Synthesis of LCBS-C_{10}-NH_2

Boron silane precursors enable the covalent linkage of a porogen (e.g. decyl chain) onto an organosilica precursor. This is realized for LCBS-C_{10} by a sequential double hydroboration on first bis(triethoxysilyl)ethene (BTSE) and second on 1-decene (Figure 3.1). In a third step the vacant BH-site is oxidized with ethanol which can be observed by development of hydrogen gas. In order to realize full conversion and to avoid the formation of side products, all reagents were used in an equimolar ratio. The reaction conditions are easy to handle since the all reagents are liquid and well dissolvable in the reaction solvent tetrahydrofuran. It should be noted that hydroboration of alkenes with borane (BH_3) principally can yield mono-, di- and trisubstituted boranes, and that these products are usually in equilibrium, dependent on the initial molar ratio of the reactants.[126] A similar reaction pathway would form a complex reaction mixture rather than single products as shown in Figure 3.1. However, the products of hydroboration reactions are crucially determined by the bulkiness

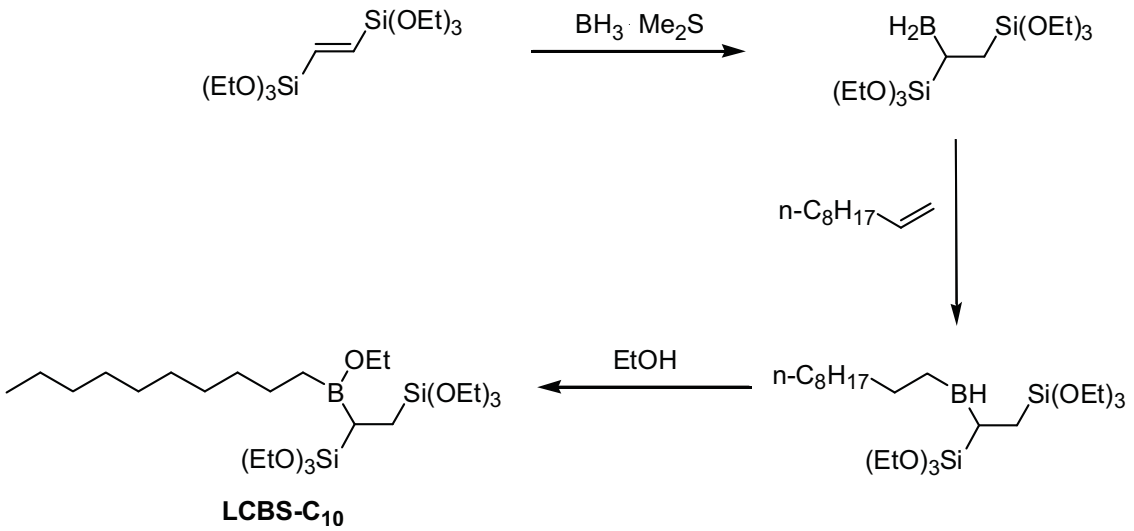

Figure 3.1: Synthesis of the LCBS-C_{10} Precursors with inherent pore size defaults

of the alkene substituents. Thus, given an excess of the alkene, terminal alkenes tend to form tri-substituted alkylboranes, while trans- and cis-alkenes generally form not more than the di-substituted products. Bulky side groups further decrease the rate of substitution. Thus, it was shown that the addition of borane on an excess of 1-methyl-2-tert-butyl-ethylene yields the mono-substituted compound only.[127] Consequently, for alkenes with two triethoxysilyl groups in a vicinal position, only monosubstituted products as shown in Figure 3.1 can be assumed. Indeed control experiments using an excess of bis(triethoxysilyl)ethene over the borane (2:1 molar ratio) left half of the alkene groups unreacted, pointing to mono-substitution of the borane, exclusively.

Even though a second addition of an alkene with bulky substituents is hindered, the remaining active B-H-sites can still react with terminal alkenes which exhibit much lower sterical hindrance. This enables the addition of long chain alkenes to the preformed boron-organosilica precursor (step 2 in Figure 3.1). The remaining reactive BH site is in the last reaction step oxidized by the addition of ethanol (Figure 3.1).

The hydroboration reaction can be monitored using ^{1}H NMR and IR measurements (Figure 3.2). Comparison of the double bond area in the ^{1}H NMR spectra shows no more signals assignable to bis(triethoxysilyl)ethene or the terminal alkene after reaction, proving the successful hydroboration. These results are supported by the IR spectra. The CH-valence vibrational mode at 3076 cm^{-1} and the C=C-valence vibrational mode at 1641 cm^{-1} disappear

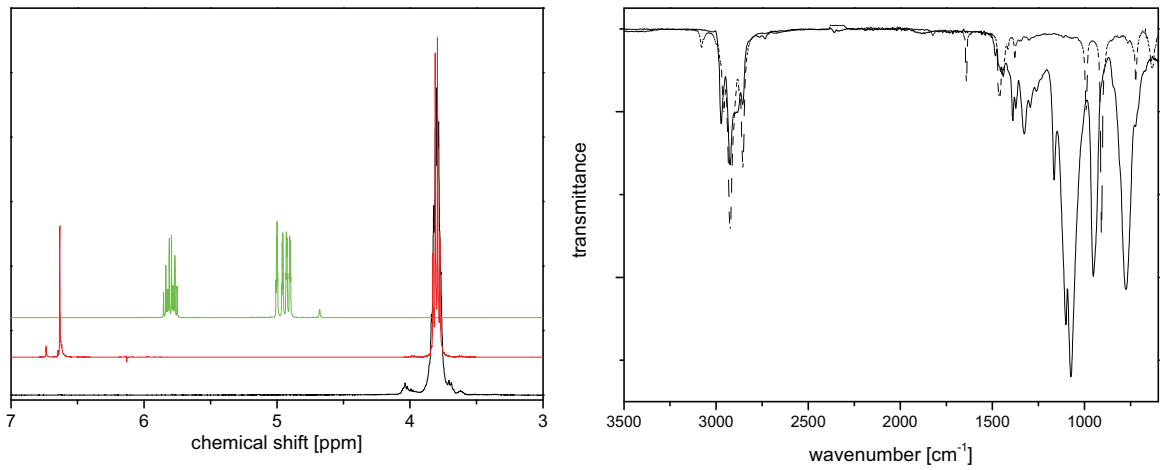

Figure 3.2: Precursor characterization: left ^{1}H NMR of LCBS-C_{10} (-), bis(triethoxysilyl)ethylene (-), 1-decene (-), right infra red spectra of LCBS-C_{10} (solid line) and 1-decene (dashed line)

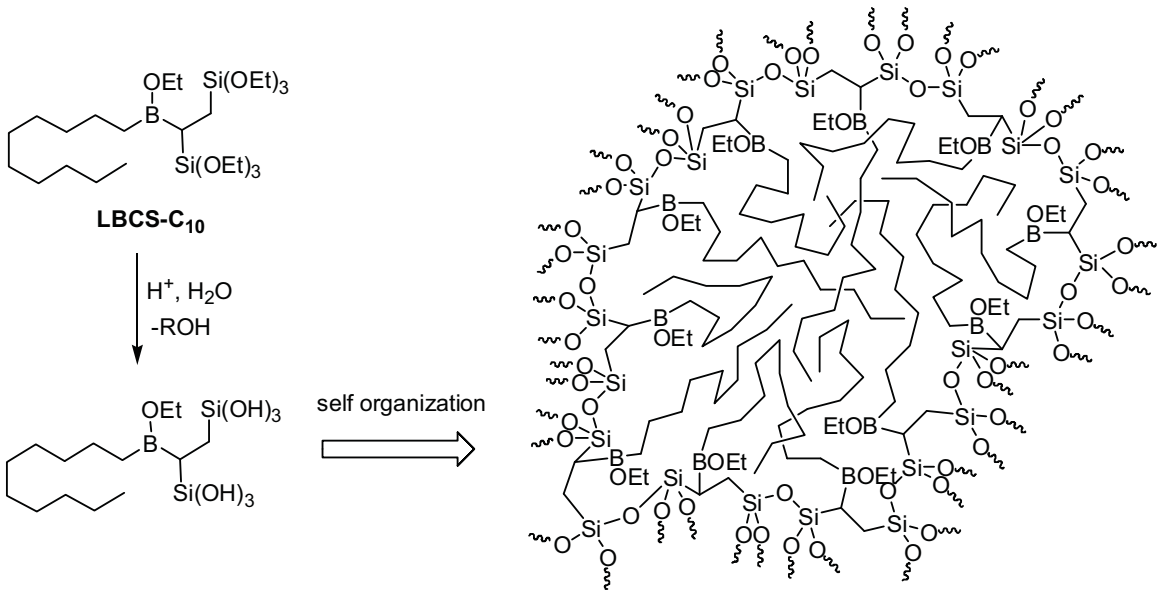

Figure 3.3: Hydrolysis and condensation of LCBS-C_{10} leading to self organization

after successful hydroboration. Furthermore, the CH-wagging modes at 908 cm^{-1} and 910 cm^{-1} are absent after the reaction. C-B and O-B deformation modes appear between 1250 and 1460 cm^{-1} further prove successful synthesis of LCBS-C_{10}. As expected, no signals above 3000 cm^{-1} are observed for LCBS precursors which would be indicative for C=C-H vibrational modes. (However, it should be noted that also in the BTSE precursor the CH double bound vibrational modes are very weak, thus this finding can just be used to monitor the hydroboration of the terminal alkene chains). As this synthesis includes only quantitative reaction steps and LCBS-C_x precursors are formed as single products (fulfilling the criteria of "click-chemistry"[128]), subsequent purification steps can be conceptually avoided.

Condensation of the precursor under aqueous conditions is assumed to lead to a self organization of the hydrophobic alkyl chains resulting in a microphase separation (Figure 3.3). This process is most likely induced by the substitution of ethoxy groups by hydroxyl groups which consequently, change the precursor characteristics from rather hydrophobic (before hydrolysis) to amphiphilic. The condensation conditions have to be set carefully in order to avoid macrophase separation caused by the large hydrophobic organic content in the precursor. This problem can be overcome by addition of ethanol and extensive stirring of the sol before the aging takes place (Figure 3.4). The picture illustrates the transparency of the resulting condensed LCBS-C_{10} organosilica and is therefore a clear evidence for the successful microphase separation.

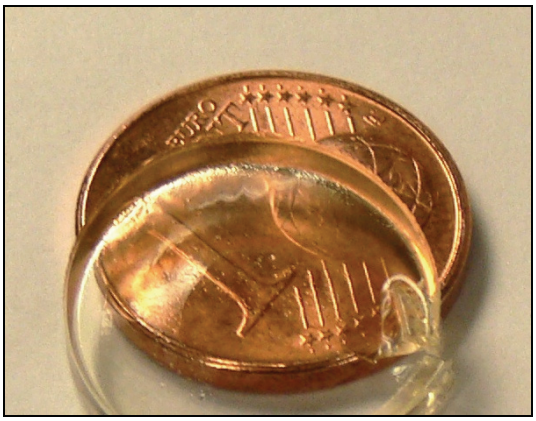

Figure 3.4: Transparency of a LCBS-C_{10} silica gel (20 mol% mixture in TEOS)

A closer insight into the local chemical structure of the LCBS-C_{10} condensate is provided by MAS NMR spectroscopy. To diminish the influence of Q-Type species in ^{29}Si MAS NMR the recorded spectrum is obtained from the pure organosilica without admixing TEOS (Figure 3.5). ^{29}Si resonances appear at -65 ppm and -100 ppm which are assigned to T-Type

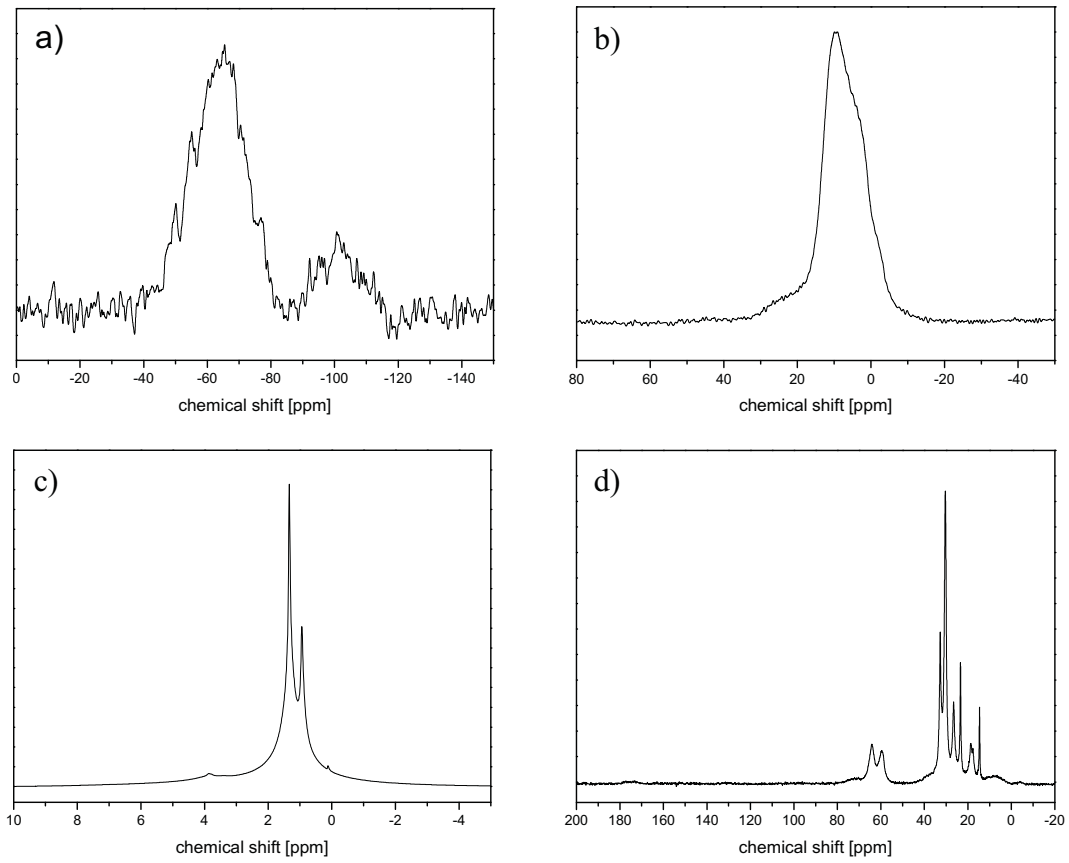

Figure 3.5: MAS NMR results of pure condensed LCBS-C_{10} a) ^{1}H→^{29}Si cp, b) ^{11}B, c) ^{1}H, d) ^{13}C, exemplary for all LCBS organosilica materials

and Q-Type species, respectively. The difference in both integrals reveals only a minor Si-C bond cleavage proving that the ethylene bridges of the polysilsesquioxanes are maintained to a large extent throughout the condensation. However, an exact assignment of the peaks to T^1, T^2 and T^3 is difficult due to an expected overlay of the chemical different silicon nuclei located at the ethylene bridge. ^{11}B MAS NMR for the pure LCBS-C_{10} proves the successful condensation under preservation of the boron species. ^{1}H and ^{13}C MAS NMR show no peaks at the double bond area showing that no unsaturated alkanes originating from incomplete precursor formation are incorporated into the organosilica matrix.

In order to remove the organic moieties and form a highly amine-functionalized organosilica where all functionalities are exclusively located on the surface, ammonolysis was carried out (Figure 3.6). This reaction step involves the heterolytic cleavage of all boron-carbon bonds induced by hydroxylamine-*O*-sulfonic acid under formation of a primary amine functionality.

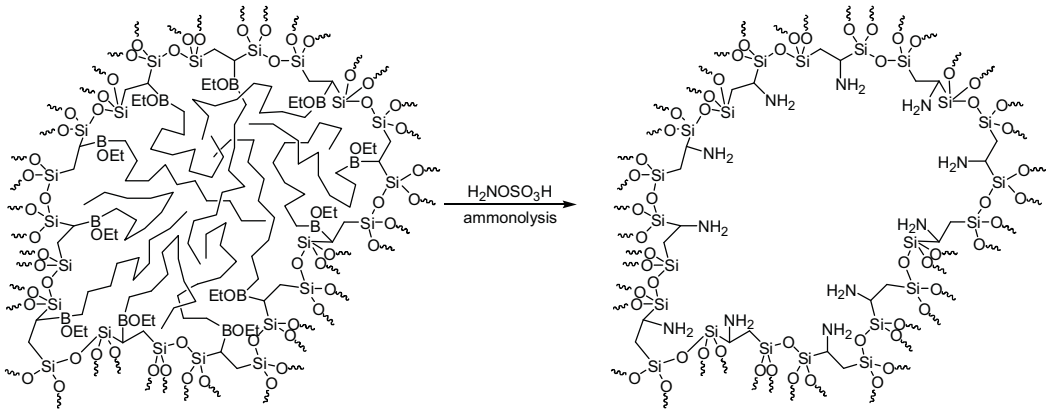

Figure 3.6: Ammonolysis step for the removal of the porogen and amine functionalization of organosilica

The course of the substitution can be monitored by infrared spectroscopy (Figure 3.7). Vibrational modes for C-H at 2840- 2960 cm^{-1} and as well for C-B and B-O at 1320-1470 cm^{-1} can no longer be observed after functionalization. As ammonolysis yields almost complete removal of the hydrocarbons, the remaining CH-groups give only very weak signals. Amine vibrational modes are often rather weak for amine-functionalized organosilicas, as shown by a comparison with an aminopropyltriethoxysilane (APTS) functionalized mesoporous silica, and thus often not suitable for characterization. A small peak at 1635 cm^{-1} can be identified in the product which can be assigned to NH_2-deformation modes. The typically existing NH stretching modes at 3100 cm^{-1} are presumably buried

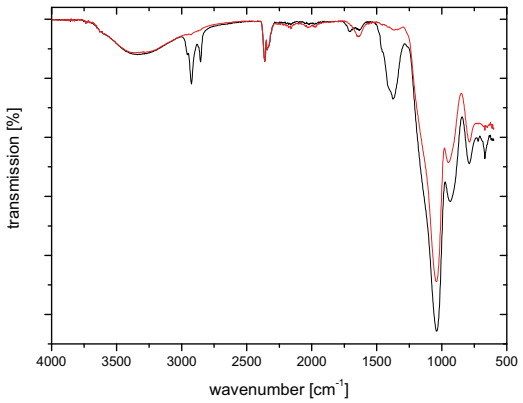

Figure 3.7: IR spectra of LCBS-C_{10} before (-) and after (-) amine functionalization

under the broad vibration band of adsorbed water and therefore not suitable for characterization.

Nitrogen adsorption measurements carried out on the amine-functionalized organosilicas confirm that the LCBS approach yields mesoporous organosilicas with very high surface area of up to 1080 m²/g and pores of 2.8 nm (Figure 3.8). The obtained silica was synthesized from a LCBS-C_{10} TEOS in order to diminish the influence of the flexible LCBS-C_{10} precursor. A detailed study on the TEOS influence will be given in the following chapter. The material shows a wormlike arrangement of pores as can be seen in TEM micrographs (compare Figure 3.14).

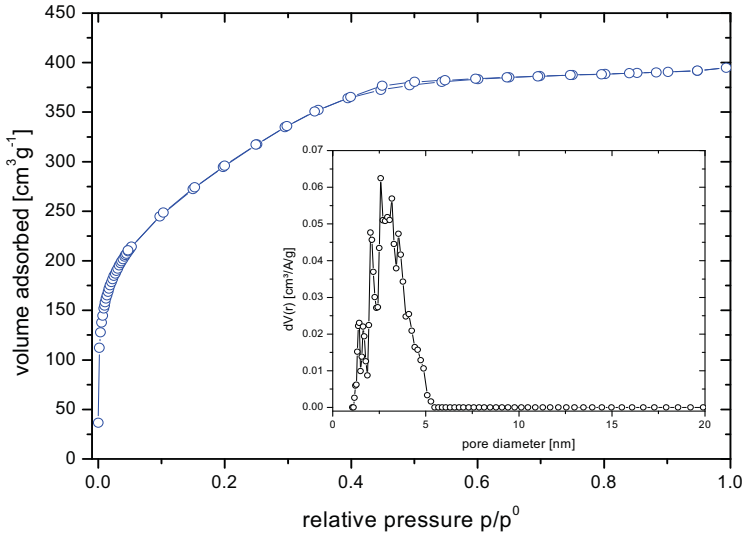

Figure 3.8: Nitrogen adsorption of LCBS-C_{10}-NH_2 (20 mol% mixture in TEOS)

The presented approach for the synthesis of mesoporous amine-functionalized organosilicas via the self organization of boron silanes can be extended to homologous precursors. The difference of the chain length of the alkyl groups leads to a potential control on the pore size. Before this concept will be studied in detail, the reaction conditions leading to the final porous material should be examined. In particular, it is interesting how the material can be stabilized by addition of a network stabilizer like TEOS. Furthermore, a detailed study on the accessibility of the amine functionalities will be provided as well.

3.3 Condensation conditions of LCBS-C_{10} precursor

3.3.1 Stabilizing the LCBS network by admixing TEOS

In the first set of experiments, the LCBS-C_{10}-precursor was condensed under various conditions to study the dependence of the reaction conditions on the porosity. One of the questions to be answered was, "how is the final porosity of the material influenced when increasing the inorganic amount of the precursor mixture". Due to the large organic content in the precursor, a decreased rigidity can be assumed for the final material compared to the pure inorganic SiO_2. This lower rigidity can cause a pore collapse in materials with high surface area because of high capillary pressure.[129] However, the organic content in the pore walls and thus, the rigidity can be easily controlled by admixing TEOS to the described organosilica precursor. For this study, LCBS-C_{10} was mixed with TEOS in different ratios, condensed and amine-functionalized in order to remove the porogen (Table 3.1). Nitrogen adsorption of as synthesized amine-functionalized organosilicas reveals Type I isotherms rather than Type IV because of the huge micropore content (Figure 3.9). However only

Table 3.1: Summary of synthesized LCBS-C_{10} silicas: [a]calculated molar concentration of LCBS-C_{10} in the precursor mixture with TEOS

entry	LCBS-C_{10} [mmol]	:	TEOS [mmol]	Si_{tot} [mmol]	$\zeta_{LCBS\text{-}C10}$ [a] [mol%]	EtOH [µl]	HCl (pH=2) [µl]
LCBS-C_{10}-1	2.00	:	0.00	4.0	**100**	350	175
LCBS-C_{10}-2	1.00	:	2.00	4.0	**33**		
LCBS-C_{10}-3	0.67	:	2.67	4.0	**20**		
LCBS-C_{10}-4	0.50	:	3.00	4.0	**14**		
LCBS-C_{10}-5	0.40	:	3.20	4.0	**11**		
LCBS-C_{10}-6	0.33	:	3.33	4.0	**9**		

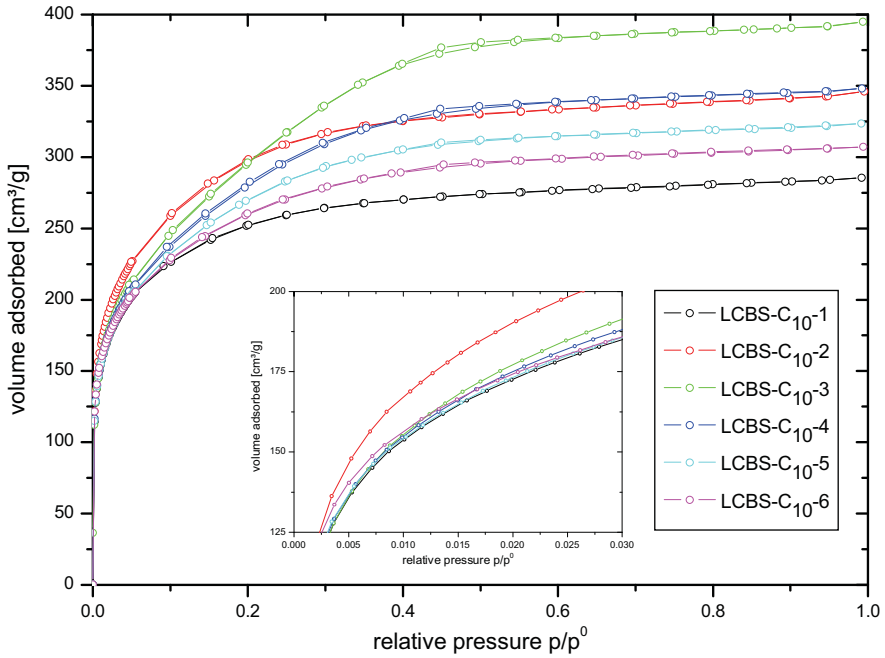

Figure 3.9: Nitrogen adsorption isotherms of aminated LCBS-C_{10}-NH_2 organosilicas silicas, inlay magnification of relative pressure range 0 to 0.3

samples LCBS-C_{10}-3 and 4 show a slightly defined hysteresis, indicating mesopores. While LCBS-C_{10}-1 shows the lowest nitrogen uptake, a stepwise increase up to the maximum at LCBS-C_{10}-3 (20 mol% of LCBS-C_{10}) is observed and then a slight stepwise decrease resulting in somewhat lower adsorption for LCBS-C_{10}-6. This trend already indicates the dependence of inorganic SiO_2 content in the LCBS-C_{10}-NH_2 organosilicas, caused by the admixing of TEOS. Considering the NLDFT pore size analysis and the BET surface area, this result is supported (Figure 3.10). Obviously, self organization of the LCBS-C_{10} takes

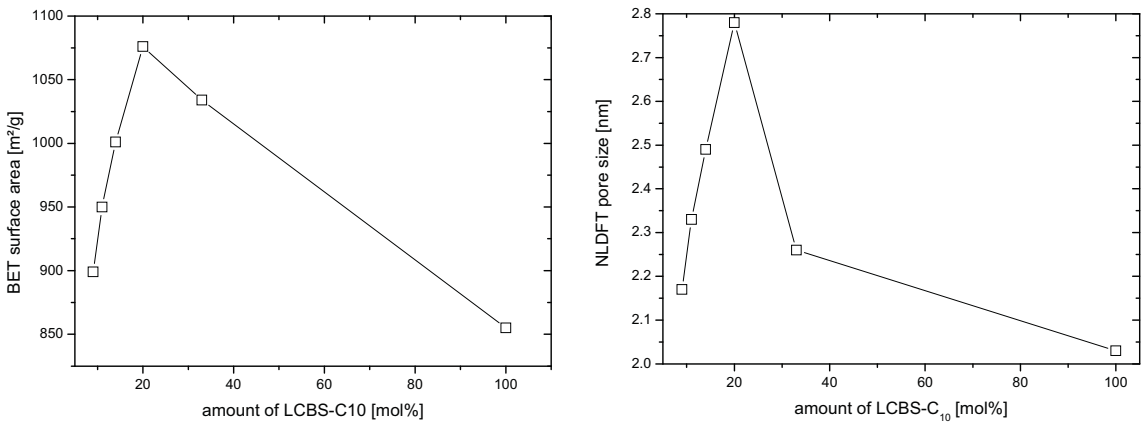

Figure 3.10: Influence of TEOS as at network stabilizer on NLDFT surface area and average pore size

place in all synthesized organosilicas, and consequently pores with an average diameter of 2.0 – 2.8 nm can be observed after ammonolysis. The maximum pore size and the maximum BET surface area are achieved at the same LCBS-C_{10} precursor concentration. All samples show very high surface areas from 850 m²/g up to 1080 m^2/g, proving the good connectivity of the pores and thus, the accessibility of functionalities.

The trend in the nitrogen adsorption results can be explained by the influence of organic moieties, namely the porogen in the silica backbone. The low content of the LCBS-C_{10} precursor results in low porogen concentration which yields after condensation and ammonolysis sequence in a comparable low surface area. By increasing the precursor concentration the porogen concentration increases and thus, a higher surface area should be observed. Barring no side effects on the surface area a further increase of the precursor concentration up to 100 % should result in a proportional increase of the surface area. Since a maximum surface area is observed at a concentration of 20 % LCBS-C_{10} precursor, it is obvious that there is an optimum pore wall stability to withstand the interfacial energies. When adding more precursor, the pore walls are supposed to suffer under the increasing flexibility of organic moieties and consequently, they are less resistant against strain from interfacial energy. Therefore, the porosity and the BET surface area are decreasing after reaching a concentration of more than 20 % precursor.

In this study, it has been shown that the LCBS-C_{10}-NH_2 organosilica made of LCBS-C_{10} precursor and TEOS mixtures providing access to highly porous organosilicas over a wide range of mixture ratios. For a LCBS-C_{10} content of 20 % the obtained material possesses the highest surface area and the maximum porosity, therefore all further investigations were done with this mixture.

3.3.2 Influence of the solvent on the mesophase formation

In this chapter, the influence of ethanol as a phase mediating solvent will be discussed. Based on the LCBS precursor concept several long alkyl chain boron silane precursors will be introduced in the following chapter. All investigated precursors are rather hydrophobic before hydrolysis due to the alkyl groups. This is especially the case of the longer alkyl chains where the addition of ethanol is used to support dissolving of the LCBS precursor. Side experiments on the solubility of the LCBS-C_{12} and the higher homologues in water/ethanol mixtures revealed less solubility shown by intensified turbidity with increasing

chain length. While the mixtures of LCBS-C_{12} and LCBS-C_{16} become clear within several minutes after starting the hydrolysis, LCBS-C_{20} can only be dissolved at elevated temperatures after intense stirring for 15 minutes. Since ethanol is only used to support the initial solubility of the precursor, it should be investigated how a diminished concentration of ethanol affects the final porosity. It is known that ethanol changes the self assembly behavior of e.g. triblock-copolymers[130]. Furthermore studies on the evaporation-induced-self-assembly-process (EISA) using CTAB and ethanol reveal the influence on structure direction[131]. This example illustrates the cosurfactant properties of ethanol.[122] Hence, two systems were investigated, (i) condensation of the precursor was carried out only in hydrochloric acid (pH = 2), (ii) ethanol was used in order to increase to solubility of the precursor.

For the determining of the influence of ethanol, a 20 mol% mixture of the LCBS-C_{10} in TEOS was used because condensation/ammonolysis of this mixture was shown in the previous chapter to result in the highest porosity in the organosilicas. Both experiments for the determination of the influence of ethanol are described here briefly: (i) all substrates and

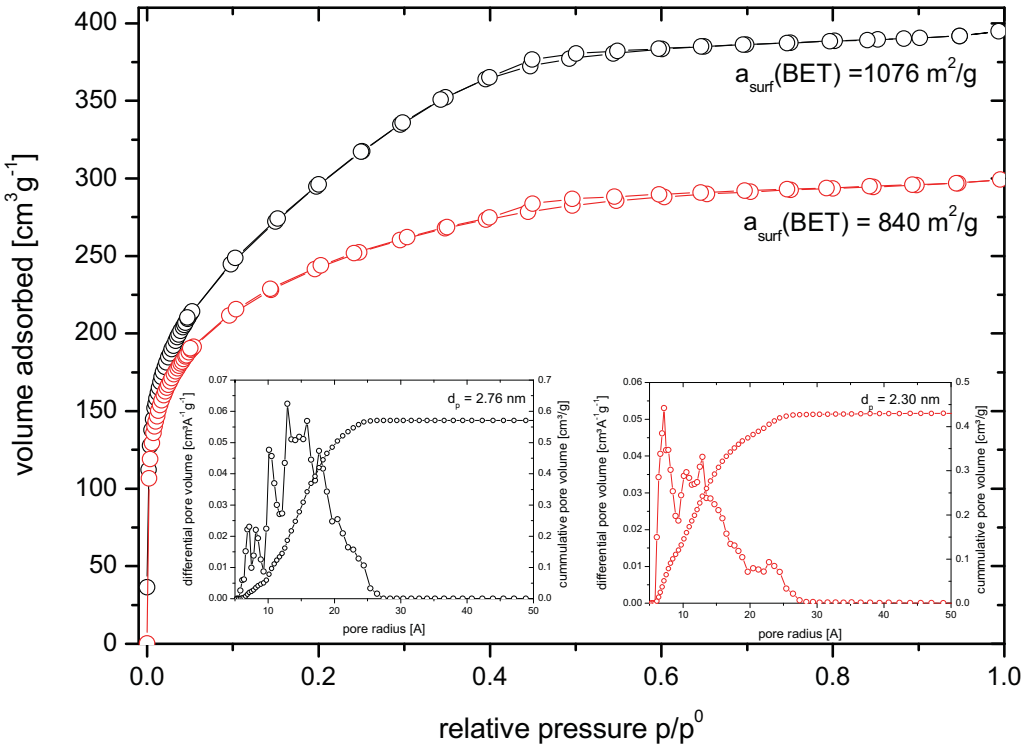

Figure 3.11: Nitrogen isotherms and NLDFT pore size distribution of aminated organosilicas synthesized with ethanol as solvent LCBS-C_{10}-3 (-) and without ethanol LCBS-C_{10}-3a (-)

reagents excluding ethanol were mixed, stirred for 20 min and then aged at 80 °C. (ii) after mixing all substrates including ethanol as co-solvent the mixture was homogenized under intense stirring for 20 minutes and then aged at 80°C. While admixing of ethanol leads to clear sol and thus, a transparent resulting gel, the organosilica obtained without ethanol remains turbid throughout the sol-gel process. The condensed organosilicas were amine-functionalized in order to remove the organic porogen. It was shown that homogenization prior to condensation carried out without the aid of ethanol leads only to a slightly smaller surface area and lower overall porosity (Figure 3.11). Surface areas obtained for both samples are high, from 840 to 1076 m^2/g, proving that the influence of ethanol on the microphase separation is rather negligible. However, without the addition of ethanol, the microporosity of the resulting organosilica is more pronounced.

3.3.3 Calcination versus chemical functionalization – influence of template removal

The general aim of this section is to produce highly functionalized organosilica materials. Although these materials show enhanced properties for applications such as chromatography, the important factor for some other applications (e.g. porous silica support for catalysts) is solely the pore structure of the silica is important. Furthermore, certain porogenes (e.g. polymers) which can be covalently bound to the silica via the boron silane approach cannot be removed by chemical cleavage. Since the expansion of the double hydroboration concept to polymeric porogens will be discussed in Chapter 4, in the following the removal of the porogen by calcination will be shown. This also results in the decomposition of the ethylene bridge in the pore walls yielding pure inorganic silica. The influence on the final porosity and pore morphology by either a thermal treatment or ammonolysis as an extraction step, will be investigated. Again, a 20 mol% mixture of the LCBS-C_{10} in TEOS was used. Nitrogen adsorption of LCBS-C_{10}-3-NH_2 and LCBS-C_{10}-3-calc indicates that the calcined sample exhibit microporosity only (Figure 3.12). While the average pore diameter in aminated organosilicas is 2.78 nm, the calcined sample possesses a pore diameter of 1.62 nm. The BET surface area is decreasing the same way. The change of the porosity reflects an increase in the material density caused by the heat treatment. This process is most likely accompanied by the combustion of the organic bridging group in the silica. Furthermore, the coverage of the surface by boron oxide has to be taken into account. Boron oxide might be a product of the oxidation of the boron organyl part of the precursor molecule. However, the percentage of

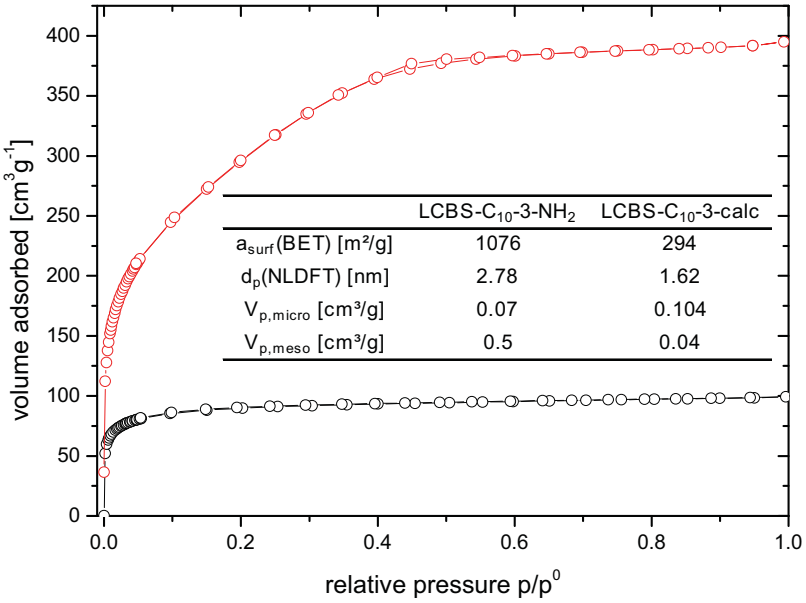

Figure 3.12: Nitrogen adsorption results of aminated (-) and calcined (-) LCBS-C_{10}-3

boron oxide is too small to be exclusively responsible for the lower porosity. It is assumed that the loss in porosity is therefore a combination of shrinkage of the pores and the surface coverage with boron oxide. A boron oxide doping of the silica surface might lead to highly thermal and mechanically stable porous material, as it is known for Duran® glasses,[132] leading perhaps to a high durability of catalyst supports. Additionally, the incorporation of boron oxide has a decisive influence on the surface acidity which was reported by CHISTOVSKAYA to enable good catalytic activity for the reaction of methanol to alkenes.[133]

Throughout the above mentioned experiments, it became obvious that the optimal condition for the condensation of the LCBS-C_{10} precursor is a 20 mol% mixture of the precursor in TEOS under solvent mediation by ethanol. Thus, all further investigations are based on this procedure.

3.4 Variation of alkyl groups in LCBS

The hydroboration reaction offers a unique opportunity to tailor the properties of the precursor (Figure 3.13). All precursors used, exhibit the same structural features except for the length of the alkyl moiety. Here, the influence on the final porosity of these different alkyl chains of the LCBS precursor will be investigated. Considering the results of the previous chapter, the material characteristics after condensation of the precursor show a

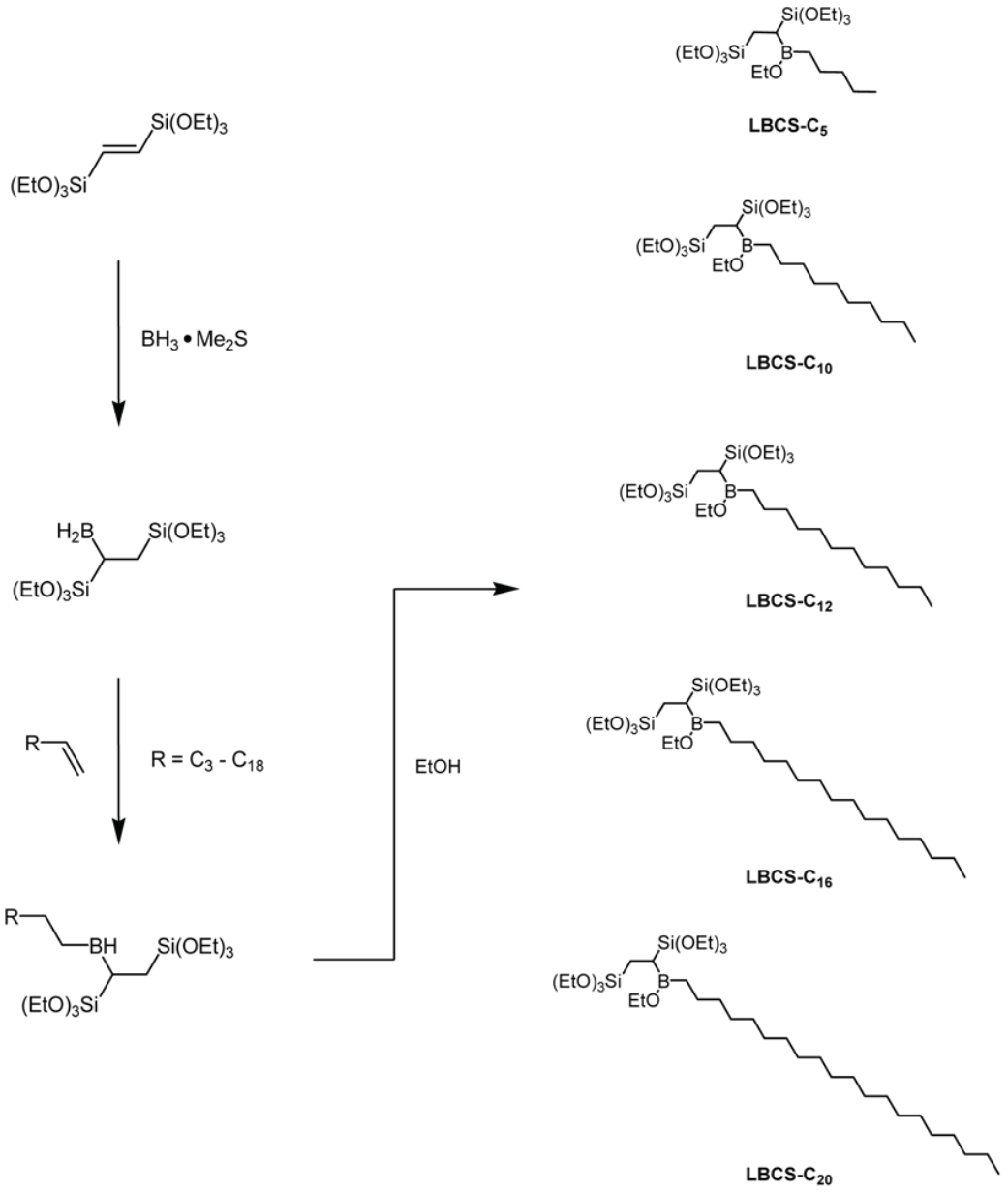

Figure 3.13: Hydroboration for the fine tuning of hydrophobicity in LCBS-C_x precursors

strong dependence on the reaction conditions. Therefore, all LCBS-C_x precursors synthesized here are condensed and functionalized following the procedure given above (mixture of 20 mol% LCBS-C_x-precursor in TEOS and ethanol as solvent) but using 50 °C for stirring the reaction mixture to ensure complete homogenization especially for the very hydrophobic LCBS-C_{20} precursor. All condensed organosilicas were amine-functionalized in order to remove the porogen and generate the porosity.

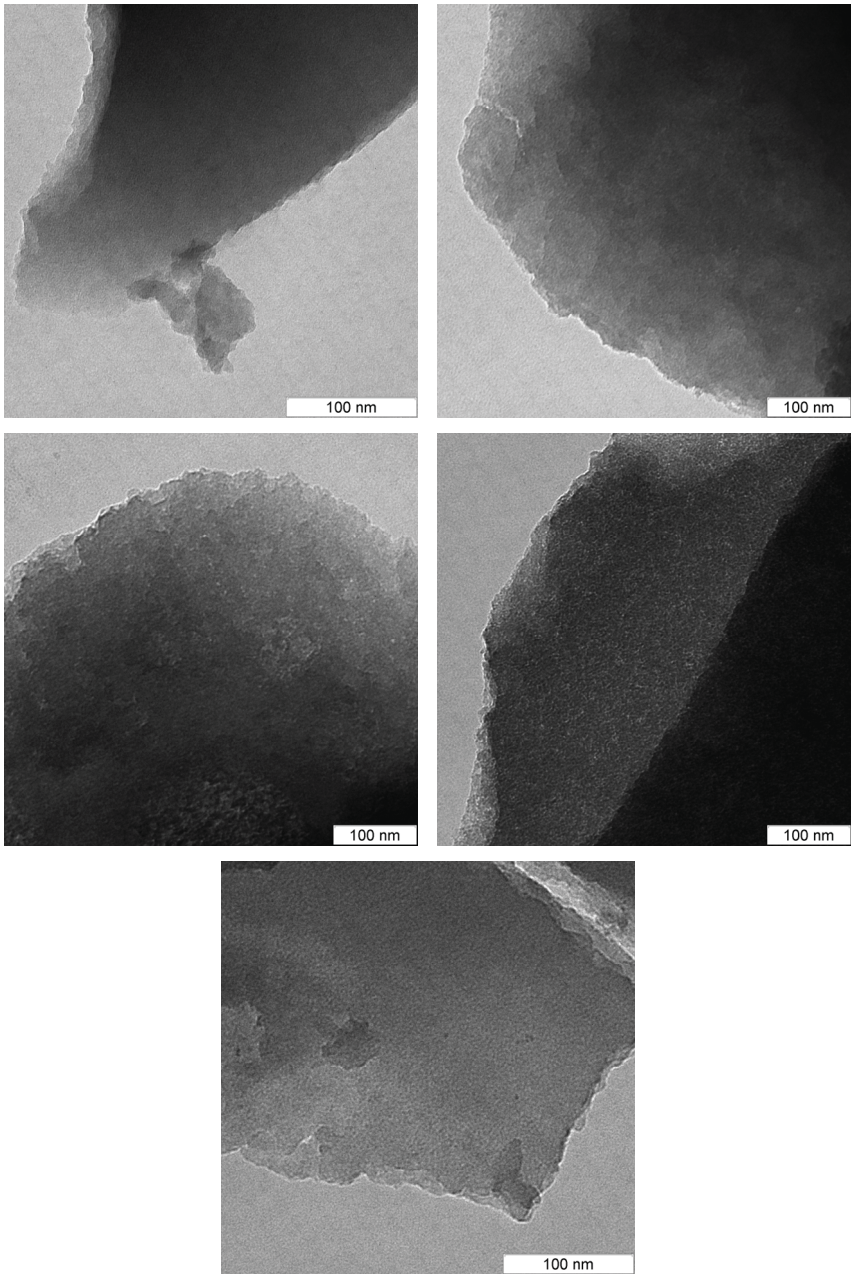

Figure 3.14: TEM micrographs of amine-functionalized LCBS-C_x films: first row: LCBS-C_5-NH_2, LCBS-C_{10}-NH_2, second row: LCBS-C_{12}-NH_2, LCBS-C_{16}-NH_2, third row: LCBS-C_{20}-NH_2

Electron microscopy micrographs of the obtained organosilicas give a hint of their pore structure and the rigidity (Figure 3.14). While for LCBS-C_5-NH_2 the resolution of the TEM is not high enough to make the pores visible, all other samples exhibit disordered wormlike pores. The material density of the sample seems to depend on the alkyl chain length of the involved LCBS-C_x precursor. The longer the chain length the larger and more numerous pores can be observed. Additional XRD measurements were carried out and the absence of Bragg-peaks confirmed non-periodicity of the pores. This shows that even though the alkyl-

attachments are able to form hydrophobic aggregates and subsequently lyotropic phases these phases are not long range ordered. While materials with incorporated pentyl groups show the highest density and apparently, less pronounced porosity, the maximum porosity is obtained for LCBS-C_{16}-NH_2. For LCBS-C_{20}-NH_2, a decrease of the porosity is found. These findings are supported by the nitrogen adsorption (Figure 3.15). All organosilicas (except LCSB-C_5-NH_2) exhibit high surface areas up to 800 m²/g and bear different micropore/mesopore ratios (Table 3.2). It should be noted that the surface area for the aminated LCBS-C_{10} organosilicas in this chapter is lower by 350 m²/g than these obtained from the network stabilization study in the previous Chapter 3.3.1. This is presumably caused by the change of homogenization conditions for the sol which was necessary in order to avoid macrophase separation for the longer precursor homologues. As the LCBS / TEOS molar ratio was held constant throughout experimentation, a higher overall organic loading for organosilicas with increasing alkyl chain length is assumed. This is reflected in the increasing porosity in the series LCBS-C_{10} - C_{16}. On the other side, the surface area stays more or less constant, proving that the bridged silanol groups are indeed forming the major part of the pore walls. For LCSB-C_5 and LCSB-C_{20} a different aggregation behavior of the precursor is observed. Thus, for LCSB-C_5 a very low hydrophilic-hydrophobic contrast of the silanol head groups and the short alkyl chain can be assumed, leading to partial incorporation of pentyl chains into the framework. Thus, these alkyl groups are inaccessible for further functionalization and extraction. In contrast, for

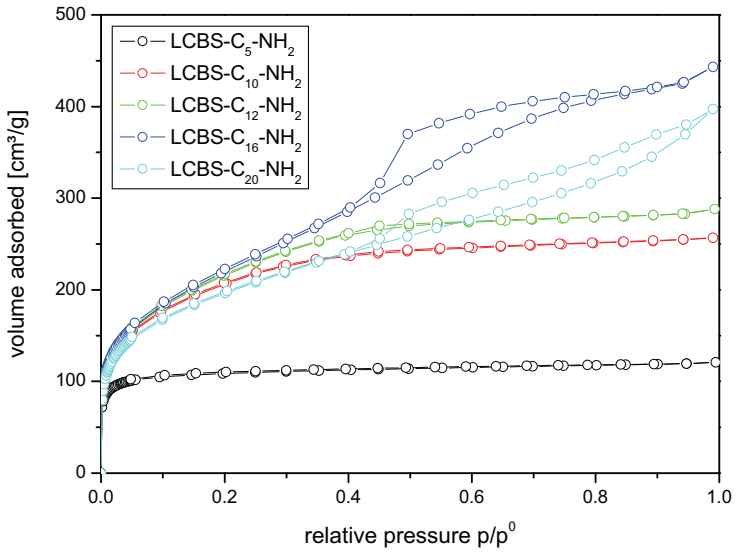

Figure 3.15: Isotherms of functionalized LCBS-C_x-NH_2 silicas

Table 3.2: BET surface area and pore size characterization for organosilica materials: [a] Specific surface area; [b] Average pore diameter ($D = 4V_P/(S_{total}-S_{ext})$); [c] Micropore volume of pores < 2 nm in diameter; [d] Mesopore volume of pores between 2 and 50 nm; [e] Total pore volume (sum of micro- and mesopore volume)

entry	a_{surf} (BET)[a] [m²/g]	d_P (NLDFT)[b] [nm]	$V_{P,micro}$ (NLDFT)[c] [cm³/g]	$V_{P,meso}$ (NLDFT)[d] [cm³/g]	$V_{P,tot}$ (NLDFT)[e] [cm³/g]
LCBS-C_5	372	1.43	0.142	0.033	0.175
LCBS-C_{10}	732	2.49	0.086	0.285	0.371
LCBS-C_{12}	758	2.74	0.066	0.347	0.413
LCBS-C_{16}	799	4.06	0.019	0.611	0.630
LCBS-C_{20}	699	3.87	0.059	0.504	0.563

LCBS-C_{20} the length of the alkyl moiety is to large to support the formation of well-defined hydrophobic domains surrounded by the inorganic network. Thus, a more ill-defined material is observed exhibiting a rather broad pore size distribution. Indeed, the hydrophobicity of this precursor increases to such a degree that solutions in ethanol are already slightly turbid. Pentyl- or eicosyl chains can therefore be seen as the borderline cases for the here shown approach. Nitrogen sorption isotherms revealed the shift of the average pore size with increasing chain length. While LCBS-C_5-NH_2 exhibit a Type I isotherm typical for microporous materials, LCBS-C_{10}-NH_2 and LCBS-C_{12}-NH_2 show isotherms described for so-called "super-microporous" materials[134,135] or materials with small mesopores. The NLDFT pore size distributions of these two organosilicas reveal an average pore size of 2.49 nm and 2.74 nm, respectively. For LCBS-C_{16}-NH_2 and LCBS-C_{20}-NH_2 Type IV isotherms are observed with a well defined hysteresis in the case of C16, showing an average pore size of 4.06 nm with a defined pore size maximum of 5.0 nm (Figure 3.16). Obviously, there is a tendency to form larger pores when LCBS-C_x precursors with increasing alkyl chains are used. Thus, after hydrolysis the precursors behave like surfactants forming micelles in which the diameter of the hydrophobic domain gets larger with increasing chain length of the hydrophobic tail. After ammonolysis the hydrophobic domains give rise to the porosity of the resulting organosilicas.

The pore size distributions determined by NLDFT is based on assumptions for the interactions of the adsorbate (nitrogen) on an adsorbent (silica) with ideal cylindrical pores. Since the aminated organosilica surface of LCBS-C_x-NH_2 materials, obviously, differs in its

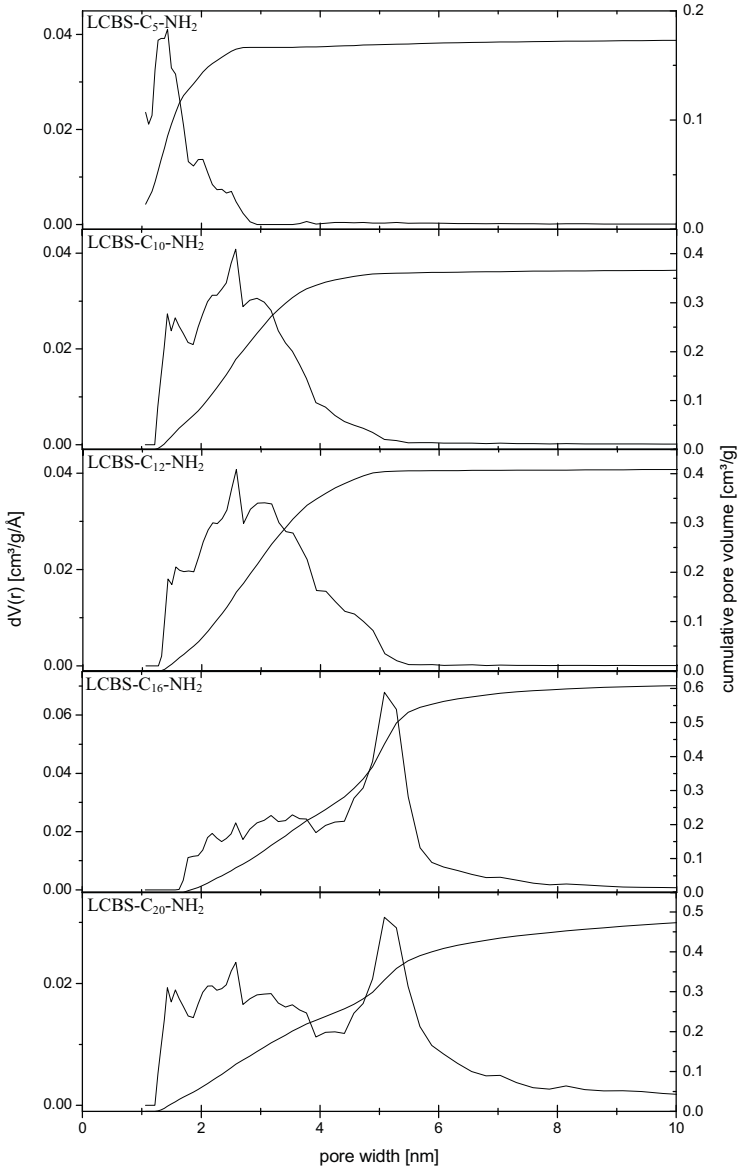

Figure 3.16: NLDFT pore size distributions of LCBS-C_x-NH_2

surface characteristics from pure silica, this somewhat simplistic assumption might lead to deviations of the real pore diameter from the one determined by NLDFT. For that reason, this part of the work is dedicated to additional determinations of the pore size by SAXS measurements. Thus, the determination of the POROD length will be discussed in the following to provide an insight into the pore size. Typical deviations from the s^{-4} descent were observed for all LCBS-C_x-NH_2 organosilicas and were corrected using the appropriate 3D density fluctuation correction (Figure 3.17).[136] All SAXS calculations and results are based on measurements with pin-hole focused beam and the assumption for the bulk density

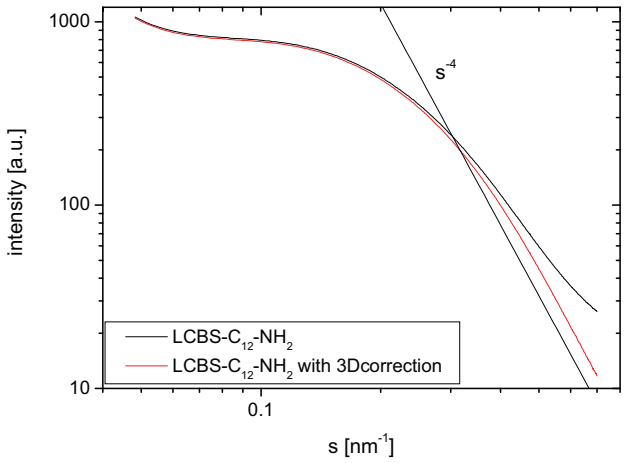

Figure 3.17: SAXS pattern of LCBS-C_{12}-NH_2 with and without 3D density fluctuation correction, exemplary for results of all LCBS-C_x-NH_2

of ρ = 2.0 g/cm³ for the amorphous organosilica. The density is slightly lower than this of pure amorphous silica (ρ = 2.20 g/cm³) because of the incorporation of organic moieties.[137]

From the 3D-density fluctuation corrected SAXS curves, the POROD lengths l_P and subsequently, the average pore diameters were calculated for all LCBS-C_x-NH_2 organosilicas according to Equation 2.7 (Table 3.3). While the nitrogen adsorption experiments show a particular maximum for the pore diameter at 4.06 nm for LCBS-C_{16}-NH_2, SAXS analysis reveals a constantly increasing POROD length and consequently, an increase of the pore diameter with increasing alkyl chain length from 0.75 nm to 2.81 nm. Although SAXS results directly prove the expected influence of alkyl chain length on the pore diameter, the obtained average pore sizes show deviations from the pore diameters obtained by nitrogen adsorption. Furthermore, the TEM micrographs show pronounced mesoporosity for LCBS-C_{12} and -C_{16}

Table 3.3: Pores sizes for LCBS-Cx organosilicas determined with SAXS (POROD length, pore diameter) and nitrogen adsorption (NLDFT): [a] POROD length; [b] average pore diameter, according equation 2.7; [c] average NLDFT pore diameter ($d = 4V_P/(S_{total}-S_{ext})$)

entry	l_P[a] [nm]	d_P(SAXS)[b] [nm]	d_P(NLDFT)[c] [nm]
LCBS-C_5	0.55	0.75	1.43
LCBS-C_{10}	0.85	1.49	2.49
LCBS-C_{12}	0.90	1.63	2.74
LCBS-C_{16}	1.12	2.54	4.06
LCBS-C_{20}	1.32	2.81	3.87

which is not supported mesoporosity for LCBS-C_{12} and -C_{16} which is not supported by SAXS measurements. Thus, it can be concluded that SAXS measurements of the pore size are suited for providing a trend in pore diameters, but the absolute values are probably affected by phase interferences. The major difference between the findings of both methods might be caused by the presence of micropores which are inaccessible for nitrogen adsorption or the incorporation of compact microdomains containing organic groups that are trapped in the pore walls. Both contributions would lead to a smaller average pore diameter determined via the SAXS method.

In general, pore diameters obtained from NLDFT or SAXS calculations are average values, depending on the pore morphology and in the case of SAXS, giving an average value including non-accessible pores. However, the obtained pore diameters directly prove the influence of the alkyl chain length on the porosity. It should be noted that the pore diameters obtained by SAXS are smaller than these obtained from NLDFT for the same reasons as stated above.

3.5 Copper adsorption experiments

A crucial point in the process of tuning surface functionalities is the determination of the accessibility and its quantification. The determination of nitrogen by elemental analysis of the LCBS-C_x-NH_2 gave inconclusive results. Typically, only about one third of the theoretically expected amine functionalities were detected (Table 3.4). This result was, however, reported by several other authors who also found a lack of amine functionalities compared to theoretical calculations. MANN and GABER observed in some cases one third to

Table 3.4: Elemental analysis results of the incorporation of functional groups in organosilicas: [a] values based on elemental analysis for nitrogen

entry	theoretical [mass%][a]	measured [mass%][a]
LCBS-C_5-NH_2	3.62	1.01
LCBS-C_{10}-NH_2	3.62	1.28
LCBS-C_{12}-NH_2	3.62	1.35
LCBS-C_{16}-NH_2	3.61	1.45
LCBS-C_{20}-NH_2	3.62	1.41

one half of the initial functional group content.[138, 139, 140] Their assumption was that different condensation rates lead to an inhomogeneous material by formation of organosilica clusters that can be washed out. However, this cannot be the exclusive reason for this phenomenon. Follow-up experiments on the determination of nitrogen by elemental analysis of pure 3-aminopropylsilica (APTS), also resulted in a lack of amine functionalities. The deviation was 12 % which is somehow smaller than that observed for LCBS-C_x-NH_2, but still proof that elemental analysis is not a sufficient method for the determination of amine functionalities in organosilicas. Furthermore, this finding refutes the theory of MANN and GABER since a leaching in a material composed of one pure silsequioxane cannot result in a deviation of the elemental analysis. For that reason, copper adsorption experiments were carried out to get a better insight in the surface coverage with amines.

The adsorption of copper ions is frequently used in order to verify the surface density of amine groups of the LCBS-C_x-NH_2 materials.[141,142] Copper, an electron deficient metal, possesses a strong complexation affinity towards nitrogen, an electron donor which results in very stable complexes. This affinity of copper is combined with several applications like copper adsorption onto porous materials for water treatment[143,144] and metal-ion affinity chromatography.[145]

The total copper uptake for all synthesized, amine-functionalized organosilicas was carried out by determining the metal capacity. The silicas were loaded with copper(II)-ions by dispersing the silica material in a concentrated solution of copper(II)-chloride. After removal of the excess of non-complexed copper the adsorbed copper was released under acidic conditions and the copper concentration in the resulting solution was analyzed by atomic adsorption spectroscopy (AAS). All copper loaded silica materials have a typical blue color,

Table 3.5: Copper loading of hydroxyl and amine-functionalized LCBS-C_x silicas

entry	BET surface [m²/g]	Cu loading (mmol/g)	Cu loading (mmol/g)	BET surface [m²/g]	entry
LCBS-C_5-NH_2	372	**0.150**	**0.035**	74	LCBS-C_5-OH
LCBS-C_{10}-NH_2	732	**0.311**	**0.038**	427	LCBS-C_{10}-OH
LCBS-C_{12}-NH_2	758	**0.301**	**0.037**	541	LCBS-C_{12}-OH
LCBS-C_{16}-NH_2	799	**0.349**	**0.037**	500	LCBS-C_{16}-OH
LCBS-C_{20}-NH_2	699	**0.341**	**0.035**	562	LCBS-C_{20}-OH

proving the successful formation of copper complexes. LCBS-C_{10-20}-NH_2 silicas exhibits a similar copper uptake of about 0.32 mmol/g, while the uptake for LCBS-C_5-NH_2 is significantly lower (Table 3.5). In order to evaluate the influence of surface functionalization, the copper (II) uptake for all amine-functionalized samples was compared with similar, but hydroxyl-functionalized organosilicas. Obviously hydroxyl functionalization does not yield the same porosity as can be seen in the slightly different surface areas (Table 3.5). This can probably be explained by the diminished reactivity of the hydrophobic organosilanes for removal of the boronorganyl in aqueous media. In contrast, ammonolysis was carried out in an organic solvent that ensures the complete removal of the boron organyl. However, the slight difference in surface area between hydroxyl- and amine-functionalized silicas can be neglected. The determination of the copper uptake on hydroxyl-functionalized organosilicas was carried out exactly like determination on amine-functionalized organosilicas. Indeed, hydroxyl-functionalized samples exhibit about one order of magnitude lower copper uptake than the amine-functionalized organosilicas (Figure 3.18). Thus, pure surface-adsorption effects can be excluded. Even though it should be noted that the overall surface areas of the hydroxyl-functionalized samples are somewhat smaller compared to the amine-functionalized samples. Considering that all organosilicas were prepared using the same molar ratio of LCBS and TEOS, a constant amount of amine groups has to be expected for all materials after ammonolysis. This should principally result in the adsorption of a similar amount of

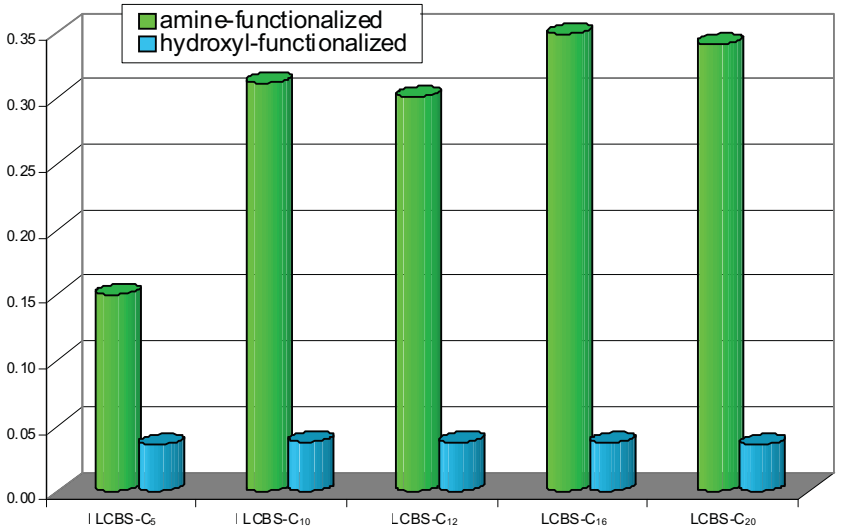

Figure 3.18: Comparison of copper loading of hydroxyl and amine-functionalized LCBS-C_x silicas

copper ions in these samples, provided that all amine groups are accessible for the ions. Indeed, comparable amounts of copper loading are observed for materials prepared from longer chain LCBS, with a slightly higher adsorption in organosilicas with larger pore sizes. In contrast, for LCBS-C_5-NH_2 a much lower adsorption of copper is found which can be explained by the small pores and lowered surface area generated in these samples, thus decreasing the accessibility of the functional groups for the bulky hydrated copper ions.

Multiple complex interactions of copper with the amine-functionalized surface impede calculations on the amine surface density. However, a rough estimation on the surface density of amine functionalities should be given. KLONKOWSKI et al. assumed a coordination form of copper on amine-functionalized silica surfaces involving one amine-group, three silanol moieties, and two water molecules.[146] Considering this assumption, the average copper loading of 0.32 mmol/g for LCBS-C_{10}-C_{20} correlates to a 12 % loading of amine functionalities, with respect to theoretical possible loading. This value is comparable low and most likely a hint that either the assumption on the coordination is inaccurate or the pore accessibility for copper is not fully granted. It should be noted that the diameter of a hydrated copper ion $Cu(H_2O)^{2+}$ is 1.2 nm[147] which already indicates the scope of this method. Thus, amine functionalities in small micropores are not fully accessible for the copper ion, resulting in an underestimation of the amine functionalities in the partial microporous LCBS-C_x-NH_2 materials. For that reason an absolute determination of the amine functionalities in the LCBS-C_x-NH_2 materials via copper adsorption is not feasible. However, a comparison of the copper loading of the obtained materials with similar amine functionalized materials allows drawing a conclusion on the surface amine coverage.

Copper adsorption characteristics of several primary amine-functionalized organosilicas, mainly using 3-aminopropylsilane precursors, can be found in the literature and will be compared to the values for the here presented LCBS-C_x-NH_2 organosilicas. These reported organosilicas differ mainly in their synthetic pathway, either grafting or co-condensation of APTS and TEOS was applied. Generally for cocondensed organosilicas smaller copper adsorption capacities of 0.1 and 0.16 mmol/g were reported.[148,149] DAI et al. applied an approach which is to some extent analogous to the one described here. He also predefined the position of the amine functionalities but using a copper aminopropyl-trimethoxypropyl imprinting complex in contrast to the boron-silane approach.[150] With this, a material which is supposed to have all functionalities exclusively located on the surface is obtained showing a

copper loading of 0.1 mmol/g. However, it should be mentioned that higher copper uptakes were reported for some APTS grafted materials, reaching up to 0.767 mmol/g[151,152]. Considering that the synthetic pathway of the latter examples differ significantly from the one described in this work, one can hardly compare these materials between each other. Nevertheless, comparison of amine functionalized and similar hydroxyl functionalized as well as similar amine functionalized materials reported in literature, proving the good surface accessibility of the functionalities in LCBS-C_x-NH_2 materials.

3.6 Summary

The present study has demonstrated that long-chain-boron-silanes (LCBS) enable a rational access for tuning the porosity of highly functionalized organosilicas. By a double hydroboration firstly at an ethylene bridged silane and secondly at a long-chain alkene a precursor was synthesized combining the function of a network builder and a porogen in one molecule. Upon hydrolysis of the inorganic moieties the pendant alkyl chains self-organize into hydrophobic domains of different sizes. These hydrophobic domains are, after splitting of the carbon-boron bonds via ammonolysis, reflected in the pores with surface amine functionalities in the resulting organosilicas. Exemplary for this precursor system, the decyl substituted precursor (LCBS-C_{10}), was shown to possess an exceptional capability for the formation of highly porous materials even in mixtures with a high amount of network stabilizer (pure SiO_2). Thus, no encapsulation of these precursors in the silica matrix was observed, resulting in accessible pores after ammonolysis. In this way materials with very high surface areas up to 1080 m²/g were synthesized.

The precursor concept enables anchoring of various alkyl chains to the silica source, resulting in a tunability of the porogens which yields functionalized micro- and mesoporous organosilicas after condensation and functionalization. Microporous organosilicas are observed when short chains (pentyl) are attached to the precursors, while decyl- and dodecyl chains yield materials with super-micropores and small mesopores and hexadecyl-chains mesoporous organosilicas. Thus, depending on chain length micro- to mesoporous materials with average pore sizes from 1.5 nm to 4.1 nm for attached pentene to hexadecene chains, respectively, are observed. Furthermore, the reaction pathway via boron groups enables the subsequent introduction of various functional groups into the pore walls of the organosilica networks. Amine or hydroxyl functionalities have been introduced into the organosilica

walls, dependent on the experimental conditions used during the borane cleavage and extraction step.

It turns out that the determination of functional groups in organosilicas by elemental analysis is not a sufficient method, since values are usually about one third of the theoretically calculated. Therefore application of copper adsorption was exploited for the characterization of surface functionalities. The investigations revealed a decisive difference of copper affinity with respect to amine and hydroxyl-functionalized organosilicas, documenting the accessibility and the successful surface modification.

4. Silane functionalized polymers

4.1 Introduction

Homopolymer templates for the synthesis of porous silicas can be divided into two classes. Either compact bulk materials such as styrene beads[153,154] or self-assembled molecular aggregates like poly(L-lysine)[155] or hydroxypropyl cellulose[156] can be employed for the sol-gel-process. However, more often amphiphilic block-copolymers are used as templates because of the ability to influence directly the structure and morphology of the resulting material by tailoring the blocks of the copolymer.[157,158] Commonly poly(ethylene oxide) (PEO) based copolymers, such as poly(ethylene oxide)-poly(propylene oxide)-poly(ethylene oxide) (PEO-PPO-PEO) triblock copolymers denoted as Pluronics®,[159] PB-PEO poly(butadiene-*b*-ethylene oxide) block copolymers,[160,161,162,163] PS-PEO poly(styrene)-poly(ethylene oxide)[164] and poly(ethylene-co-butylene)-block-poly(ethylene oxide) denoted as KLE are used.[165] SBA-15 is probably the most common polymer surfactant mediated porous silica made with Pluronic P123 with two-dimensional (2D) hexagonal (p6mm) mesostructure. Using PB-PEO based surfactants it was shown how the morphologies of the lyotropic phases and consequently the porosity in the resulting silicas can be tailored.[166,167] Changing the temperature, surfactant concentration and block length of the polymeric surfactant, cylindrical, lamellar and vesicular structures were observed. These examples illustrate the interest in the morphological design of silica materials by the use of block-copolymers.

In the following the hydroboration approach will be used to enable a covalent grafting of a bridged silane, namely BTSE onto a homopolymer. Poly-1,2-butadiene (PB) provided a suitable unsaturated polymer, since it was shown in the previous chapter that borane addition on terminal alkenes is easily feasible. Furthermore, PB is an attractive substrate because it is easy to synthesize via anionic polymerization and is also commercially available, both as a homo- or block-copolymer. Block-copolymers with polystyrene have found widespread applications, as it shows mesophase formation in the bulk state (e.g. high tensile strength materials or high impact polystyrene).[168] Therefore, in the second part of this chapter the hydroboration approach involving the homopolymer PB will be extended to grafting of BTSE

onto PS-PB. Since the anchored silanes enable a cross-linking via silanol condensation it was possible to solidify the polymer structure.

4.2 Silane functionalization of 1,2-polybutadiene

The functionalization of the polymer was achieved by hydroboration with borane dimethylsulphide complex on bis(triethoxysilyl)ethylene BTSE followed by the addition on 1,2-polybutadiene (PB) (Figure 4.1). The remaining free reactive BH site was then reacted with ethanol yielding silane functionalized polybutadiene denoted as PB-SIL. The general processing is rather simple since all reagents are well soluble in the reaction solvent THF. However, the high cross-linking tendency of the polymer aggravates the purification and characterization of the resulting PB-SIL. Reprecipitation of the PB-SIL in ethanol or methanol leads to an irreversible cross-linked polymer insoluble in THF, ethanol and ethyl acetate. If the reagents are used in equimolar ratio no formation of side products can be expected, thus a further purification step can be avoided provided that the reaction degree reaches 100 %. Thus, reaction conditions for the hydroboration were chosen according to this consideration.

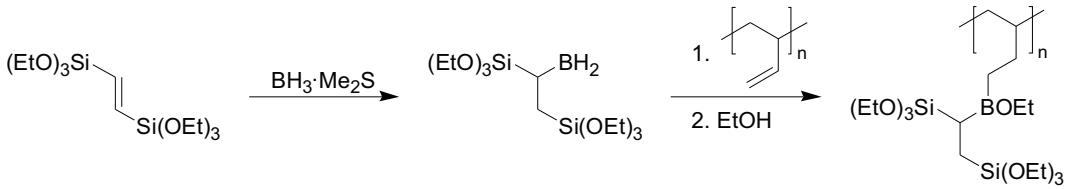

Figure 4.1: Synthetic pathway for hydroboration of polybutadiene

The reaction was monitored by ^{1}H NMR and shows the complete conversion of both unsaturated compounds (Figure 4.2). Peaks shown in the inlay at 4.9 and 5.4 ppm or 6.6 ppm originating from double bonds of PB or BTSE, respectively, were not observed after hydroboration. The spectrum was directly recorded from the reaction mixture since the tendency towards a high degree of cross-linking in the polymer hinders the removal of solvent. Thus, peaks assignable to dimethylsulphide and THF can be found in the ^{1}H NMR spectrum. The recorded spectrum of the reaction mixture prior to the addition of ethanol shows ethoxy peaks which are arising exclusively from the silane functionalized homopolymer PB-SIL. However, as expected proton resonances of the aliphatic polymer backbone are less resolved and very small because of the high order signal splitting due to

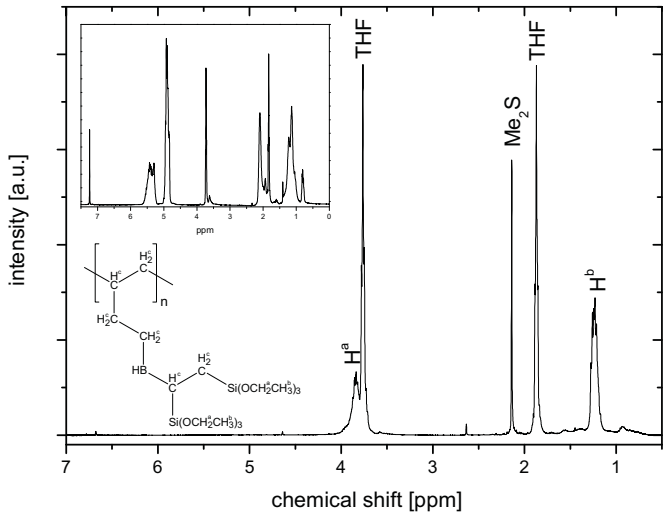

Figure 4.2: NMR of reaction mixture before adding ethanol, inlay: NMR of initial polybutadiene

the vicinal proton coupling. For that reason, the polymer backbone and the ethylene bridge protons H^c appear as low intensity signals between 0.5 and 1.7 ppm but they can hardly be exactly addressed.

Interestingly, condensed PB-SIL already exhibits remarkable morphologies depending on the condensation conditions used, despite the absence of an obvious self organization motive. While condensation in acidic media or condensation in organic solvents (i.e. THF, ethanol and methanol) leads to rather undefined amorphous structures, condensa-tion under similar conditions in aqueous ammonia yields fibrous aggregates (Figure 4.3). The condensation was

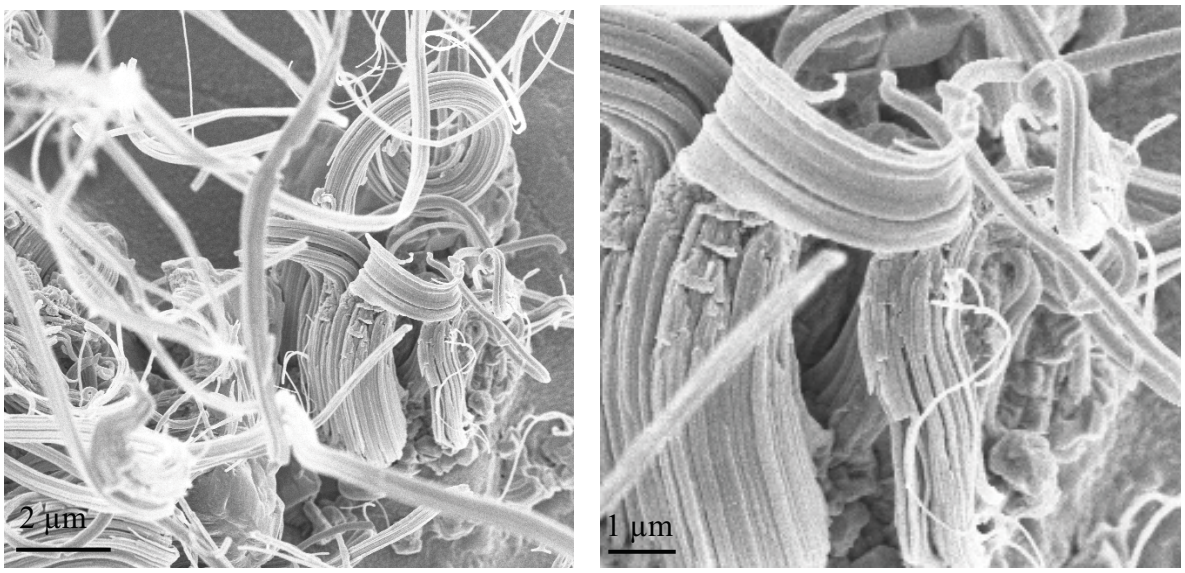

Figure 4.3: Silica fibers made from silane functionalized polybutadiene

carried out by mixing an ethanolic PB-SIL solution with aqueous ammonia followed by aging of the first clear solution for two days. The sol was not stirred and the precipitation occurred slowly indicating a real self-organization process. The formed fibers were used as received for SEM investigations. The larger fibers are 30-100 µm in length and 1-2 µm in width. They appear to be aggregates of coaxial aligned fibrillar structures, each fibril having a diameter of ~ 1 µm. The overall length of a single fibril reaches in some cases up to 60 µm. XRD measurements on the obtained fibers show no peaks, indicating the absence of crystallinity in the samples.

TGA and IR measurements were carried out in order to prove the incorporation of the organic polymer backbone into the silica matrix (Figure 4.4). IR measurements of the condensed materials document the successful formation of an inorganic-organic composite. CH_3, CH_2 and CH stretching vibrations between 2900 and 3000 cm^{-1} can be assigned to the aliphatic PB, the broad peak at 1365 cm^{-1} (deformation vibrations) indicate the successful incorporation of B-C, B-O and the peak at 1035 cm^{-1} can be attributed to Si-OH deformation vibrations.[169] TGA measurements, carried out under an oxygen atmosphere result in the combustion of all organic compounds, yielding a residue that is 64.5 % of the original sample mass. The remaining residue is assumed to consist of SiO_2 and B_2O_3 in a molar ratio similar to the precursor's stochiometry. Based on these assumptions the content of inorganic compounds is only 81 % of the theoretically calculated. This deviation can be explained by either chemisorbed or physisorbed water. The adsorption of 1 mol water per mol of repeating polymer unit resulted in a 100 % agreement with the TGA measurements. Thus, it is assumed

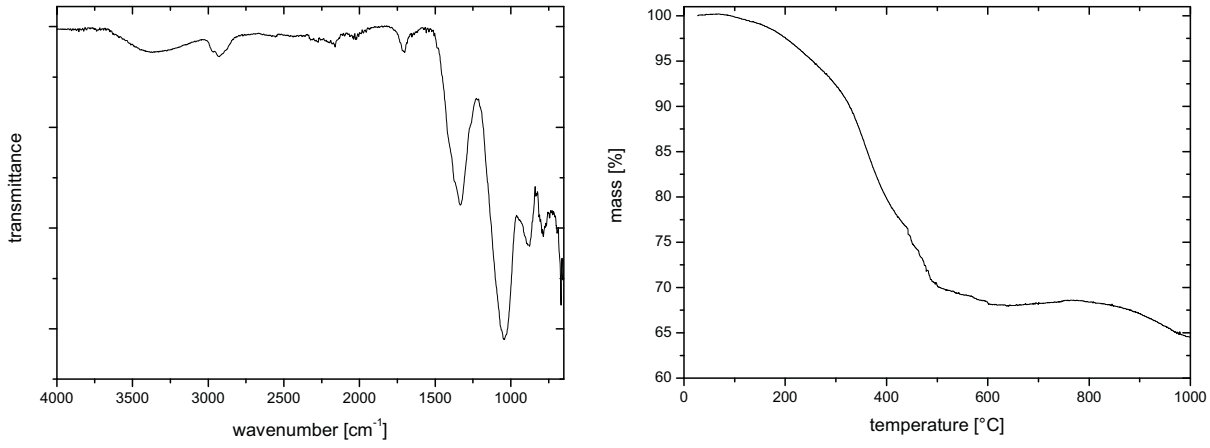

Figure 4.4: Infra red spectra (left); and TGA results (right) of silane functionalized PB

that water is additionally to the organic compounds liberated during thermal treatment in the TGA, originated from incomplete condensed silanol functionalities.

On first glance, it seems like the bulky polymer silane side chains are responsible for the formation of a stiff polymer which can undergo condensation and thus solidify the molecule structure. This could lead to the observed fibrils. However, it should be noted that the close vicinity of the silane functionalities is obligatory for fibril formation. However, in general the steric requirement of the side chains in PB-SIL is not crucial for the formation of a stiff "bottle brush"-like polymer as it was reported by BÖRNER.[170,171] In these polymers, the side chains reaching molecular weights of more than one order of magnitude higher than for PB-SIL. Thus, it is supposed that the formation of these fibers is caused by a sequential, growth-like mechanism. This theory is supported by the observation of the pH-dependence for the formation of fibrils. Since fibrils were obtained only under basic conditions (amorphous structures under acidic conditions) the hydrolysis/condensation rate has a decisive influence. As already mentioned the rate of hydrolysis at pH values higher than 5 is lower than the rate of condensation and vice versa. Thus, in the case of acidic catalysis, the high rate of hydrolysis yields a preformed polymer with many reactive silanol functionalities allowing an undirected inter- and intramolecular cross-linking. This might explain the obtained

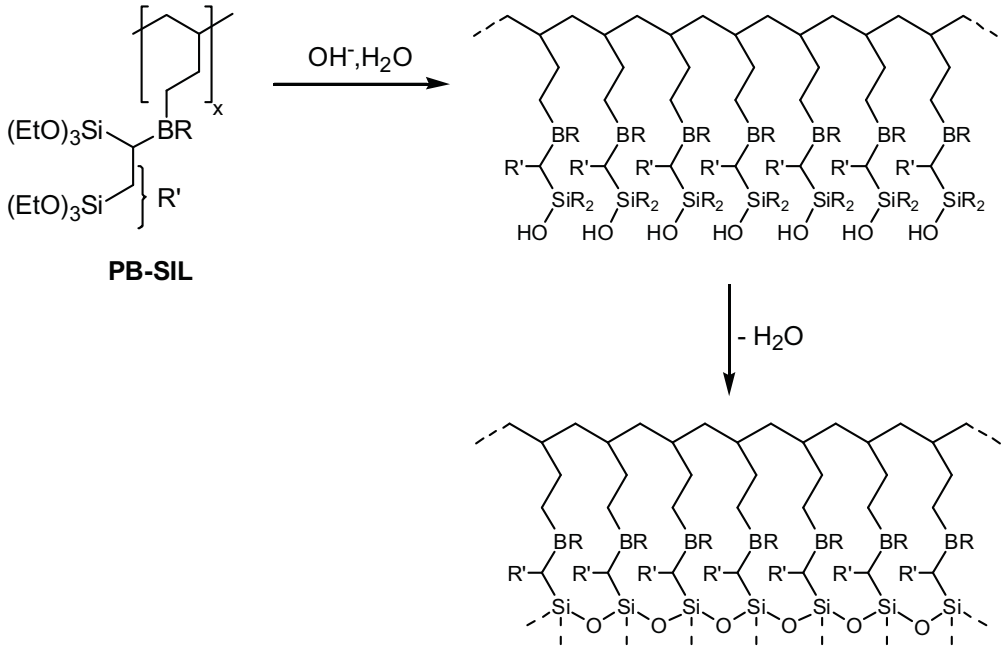

Figure 4.5: Assumed mechanism for the formation of PB-SIL fibres

amorphous structures. In contrast, under basic conditions the hydrolysis rate is low but the condensation rate is high. Thus, it is assumed that the condensation of the few existing silanol functionalities is favored between proximate silanol side chain functionalities. This intramolecular condensation of PB-SIL is supported by the dense distributed silane side chain functionalities yielding a ladder-like polymer. This stiff condensed polymer combines an organic backbone with a newly formed polysiloxane (Figure 4.5). A further accretion, precisely an intermolecular condensation of several polymer strands leads to the formation of fibrils.

In this section, the synthesis of a silane functionalized polybutadiene was realized via the hydroboration approach. The unexpected structure formation via a self organization process in the PB-SIL homopolymer was a stimulus for expanding this concept to block-copolymers which will be discussed in the following.

4.3 Silane functionalization of poly(styrene-*b*-butadiene)

While the formation mechanism in the above described homopolymer PB-SIL can only be assumed, the self assembly of amphiphilic block-copolymers can be easier addressed. The aim of this part of the work is to investigate the self-assembly of a silane functionalized block-copolymer, made according to the boron-silane approach. Silane functionalization of

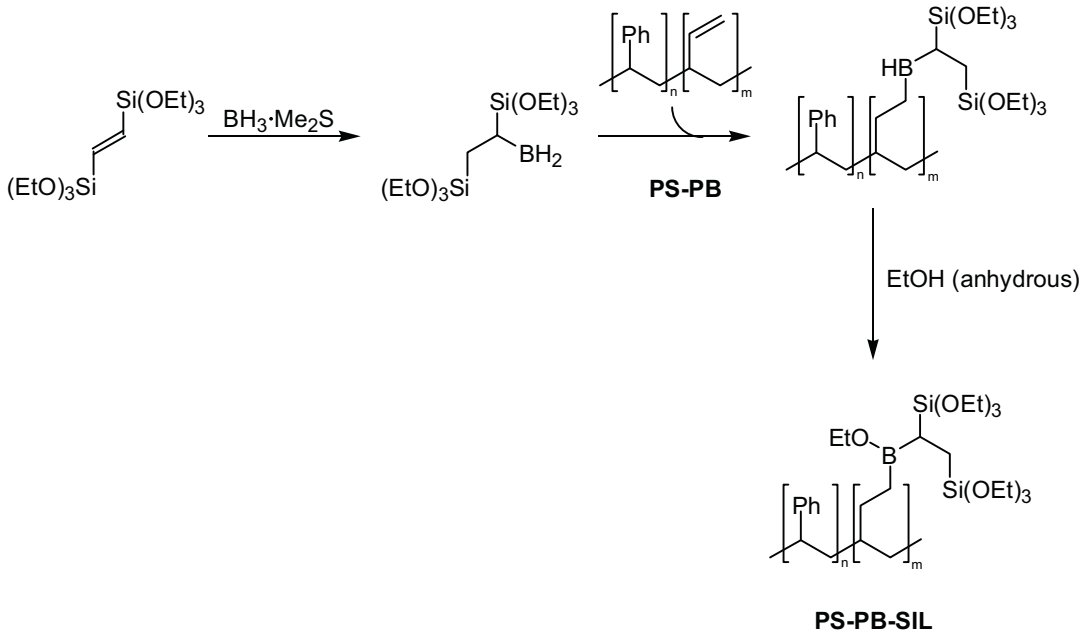

Figure 4.6: Synthetic pathway for the synthesis of PS-PB-SIL block-copolymer

$PS_{122}PB_{161}$ with an apparent number-average molecular weight of 21400 mol/g was carried out using the double hydroboration route yielding PS-PB-SIL (Figure 4.6). The reaction processing is rather simple, all reagents are soluble and the equimolar use of reagents ensures complete conversion.

The reaction was monitored by ^{1}H NMR and shows the successful double hydroboration firstly on BTSE and secondly on PS-PB (Figure 4.7). Since solvents could not be removed due to the disposition to cross-linking of the silane modified polymer the spectrum contains peaks arising from dimethylsulphide and THF. After functionalization, peaks assignable to non-aromatic alkenes as they could arise from BTSE at 6.6 ppm and PS-PB at 4.9 ppm and 5.4 ppm were not observed. However, the broad, flat peaks centred at 6.6 ppm and 7.1 ppm are exclusively arising from aromatic polystyrene protons and proving in combination with the non-observable alkene protons the complete conversion of PS-PB. Peaks at 1.8 ppm and 3.8 ppm can be assigned to the ethoxy groups of the silane. Since this spectrum was recorded before admixing ethanol the integrals of these peaks can be used for quantitative evaluation of the reaction and document 100 % conversion. It should be noted, that low intensity peaks arising between 0.5 and 1.6 ppm can be attributed to the aliphatic polymer backbone but are not exactly assignable due to the high order signal splitting. The high cross-linking tendency

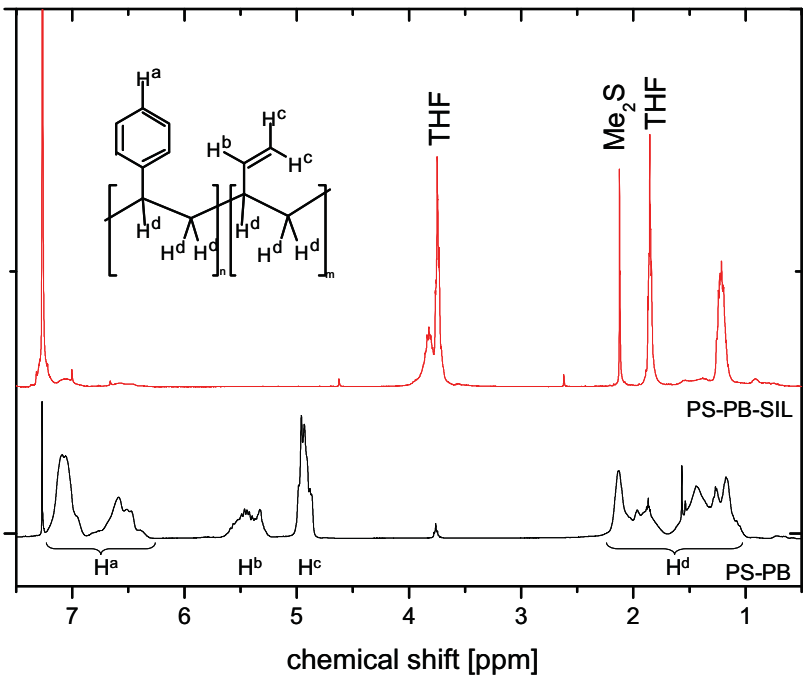

Figure 4.7: ^{1}H NMR of PS-PB (-) and PS-PB-SIL (-) before adding ethanol to oxidize the vacant BH-site

of the polymer hinders the purification of PS-PB-SIL by reprecipitation (e.g. precipitation in ethanol or methanol yields a product insoluble in organic solvents). Thus, purification of the PS-PB-SIL prior to condensation was carried out by dialysis in THF or ethyl acetate.

The dialyzed PS-PB-SIL was characterized by ultra-centrifugation and gel permeation chromatography (Figure 4.8). The sedimentation coefficient of the starting polymer was 0.42 S and increased after functionalization to 2.00 S which proves the increase of the molecular weight and density of the polymer, and thus the successful silane functionalization of PS-PB. This finding is supported by GPC measurements by the obvious change of the elution volume for the PS-PB copolymer to the silane functionalized PS-PB from 17.6 ml to 15.5 ml respectively. However, conclusions based on the polydispersity index (PDI) are vague. While ultra-centrifugation indicates an increase of the PDI after functionalization to PS-PB-SIL the elugram of the GPC analysis shows a similar peak width for the starting polymer PS-PB and the silane functionalized PS-PB-SIL, indicating a similar PDI which is expected for polymer analogous reactions. In general the dialyzed PS-PB-SIL was observed to be stable in solution for several weeks and leads to very low condensation rates, whereas the precipitated polymer undergoes fast cross-linking, forming an insoluble composite. After 2 months the gelation of the diluted polymer was observed.

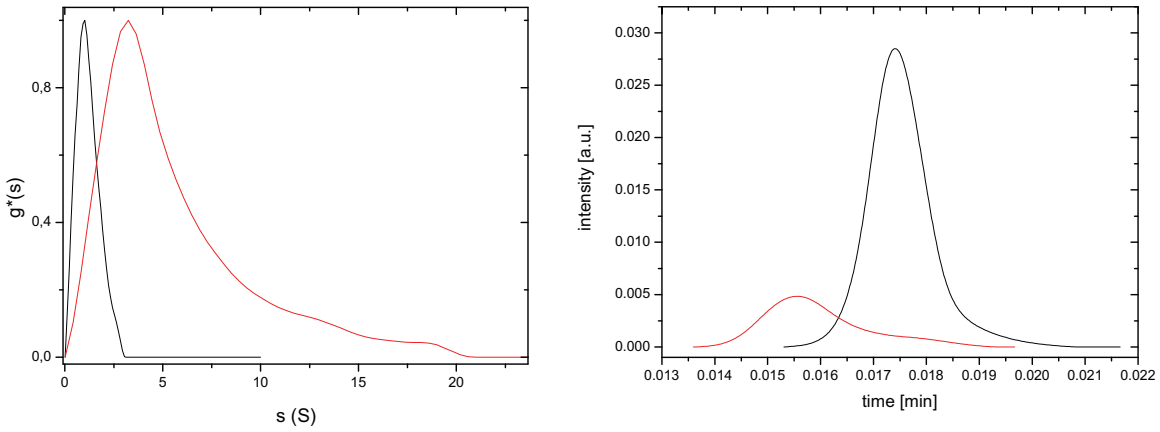

Figure 4.8: left: UC results and right: GPC (eluent: THF, detector RI) results of PS-PB-SIL (-) and PS-PB (-)

Dynamic light scattering of the PS-PB-SIL was used to gain an insight into the average size of the aggregates formed in polar solvents. These investigations were done in an organic solvent and not in aqueous media in order to avoid cross-linking of the polymer caused by

Table 4.1: Result of dynamic light scattering for PS-PB-SIL and literature comparisons: [a] measured in ethyl acetate, [b] literature reference[172], measured in water

entry	M_n PS	M_n block B	R_h [nm]
PS-PB-Sil[a]	12700	8700	19.4
PS-PEO[b]	11200	17500	22.0
PS-PEO[b]	3700	10400	14.0

condensation of the silane functionalities. Furthermore the hydrophobicity of PS-PB-SIL hinders its solubility in water. It was shown by mean of dynamic light scattering that ethyl acetate is a proper solvent to allow the self-assembly of the pure PS-PB-SIL. Measurements of the hydrodynamic radius for PS-PB-SIL polymer in ethyl acetate gave $R_h = 19.4$ nm ($R_G = 13.1$ nm). The ratio of R_G/R_H equals 0.67 which points towards homogenous spheres namely PS-PB-SIL micelles. Furthermore, the hydrodynamic radius of PS-PB-SIL is in the same range as the radius of similar polystyrene block-copolymers (Table 4.1). Although PS-PB-SIL differs chemically from PS-PEO and the used solvents for the dynamic light scattering experiment are not identically, the similarity of the hydrodynamic radii proves that it is possible to compare both block copolymers.

Condensation, carried out by mixing the THF dialyzed PS-PB-SIL and hydrochloric acid (pH = 2) results in a cross-linked, solid organosilica. Both, IR and TGA analysis of this material prove the incorporation of organic moieties and silica into the composite (Figure 4.9). C-H stretching modes at 2858, 2920, 2972 cm^{-1} arising due to the various aliphatic

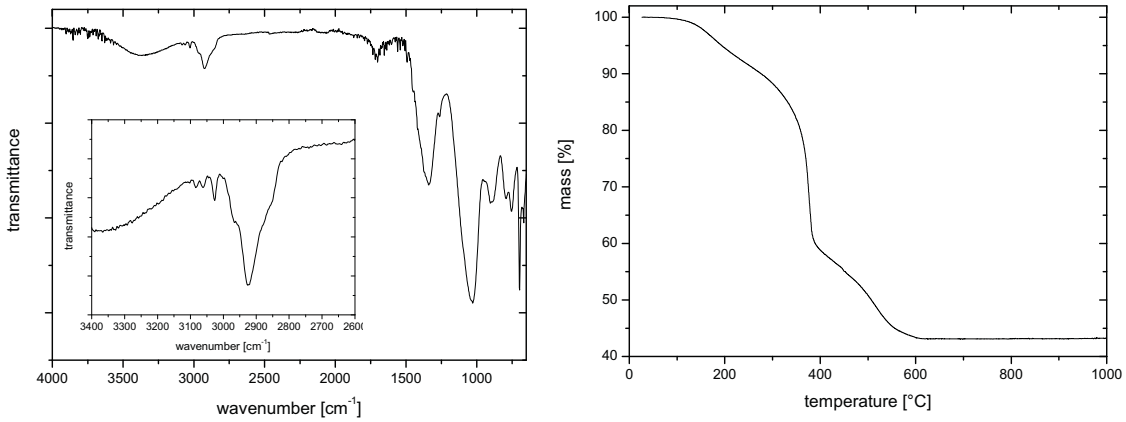

Figure 4.9: Infrared spectra (left) and TGA (right) analysis of the as condensed PS-PB-SIL; inlay: enlargement of the spectrum at 3000 cm^{-1}

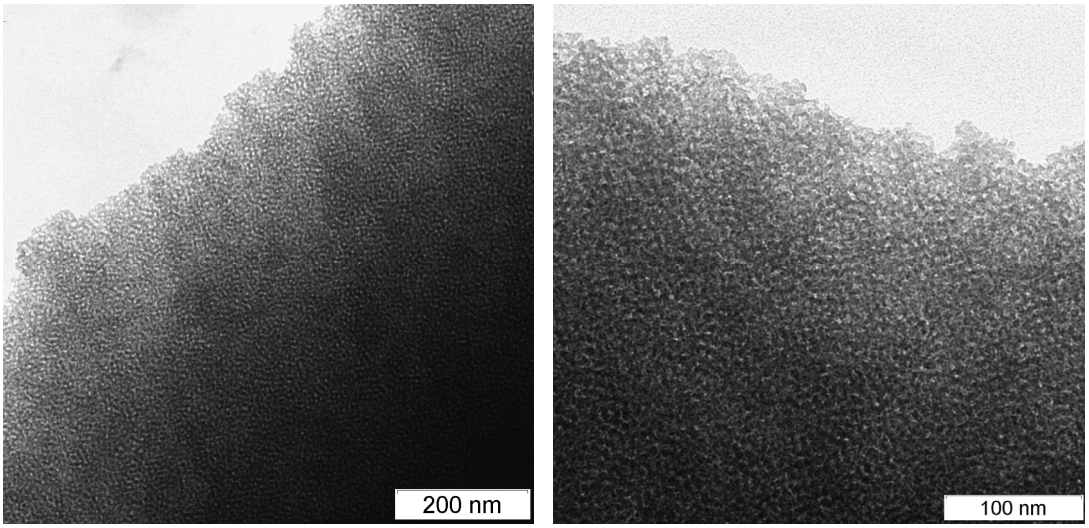

Figure 4.10: TEM micrographs of condensed and calcined PS-PB-SIL following bulk condensation approach

hydrogen nuclei accompanied by aromatic CH stretching modes at 3019 and 3061 cm^{-1} attributable to the PS-block. The strong absorptions at 1340 and 1027 cm^{-1} can be assigned to B-O, B-C and Si-O-Si, Si-O-C vibrational modes, respectively. Based on TGA measurements and the assumption that the remaining residue at 1000 °C consists of SiO_2 and B_2O_3, equal to the precursor stoichiometry, the inorganic amount of the composite is 89 % of the theoretically calculated. This deviation can be explained by either chemically or physically adsorbed water as in the PB-SIL material. The adsorption of 1 mol water per mol repeating unit polymer resulted in a 100 % agreement with the TGA measurements. Thus, it is assumed that chemisorbed or physisorbed water is liberated in addition to the organic compounds during thermal decomposition, originating from incomplete condensed silanol functionalities.

The attempt to remove the polymer moiety by chemical cleavage via ammonolysis followed by solvent extraction as described in Chapter 3 failed in the condensed PS-PB-SIL. It is obvious that a polymer can hardly be removed by extraction when trapped in a close-fitting silica matrix, especially when spherical aggregates are observed. Thus, removal of the organic moiety was realized by calcination, yielding porous silica (Figure 4.10). It should be noted that the removal of the template by calcination can cause changes in the materials density, as it was shown in Chapter 3.3.3.

The generation of porosity in condensed and calcined PS-PB-SIL can be explained by a self-organisation of the amphiphilic PS-PB-SIL polymer (Figure 4.11). This hydrophilic/ hydrophobic contrast is supposed to be a result of the hydrolysis of the silane functionalities.

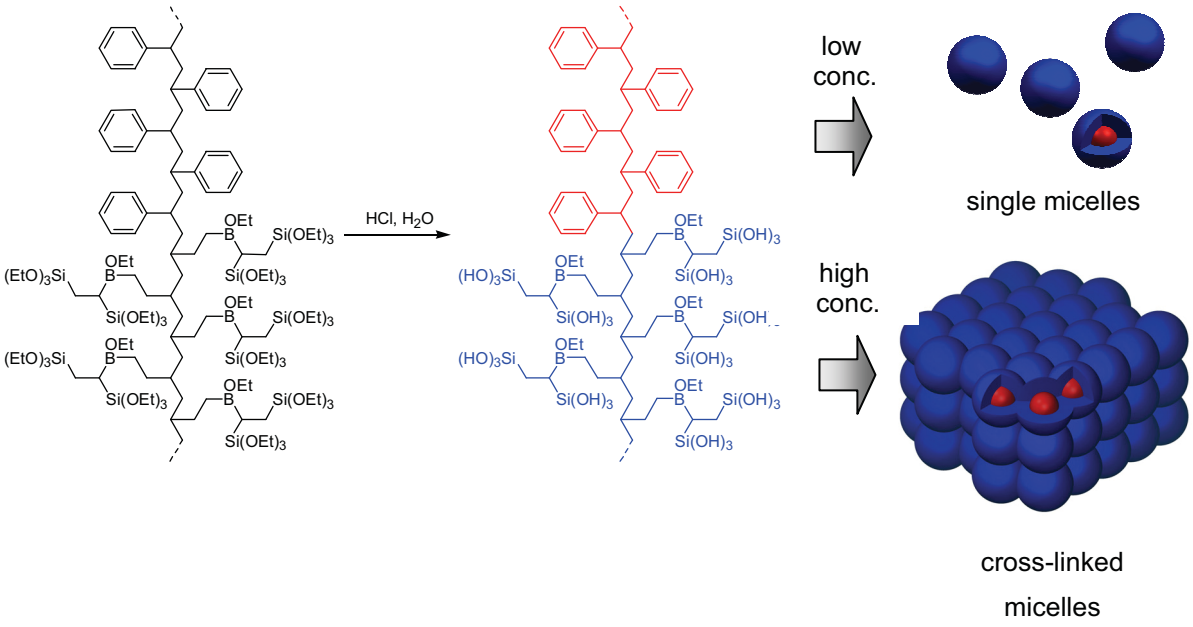

Figure 4.11: Formation of amphiphilic block-copolymer of PS-PB-SIL: change from hydrophobic PS-PB-SIL to amphiphile with hydrophilic block (blue marked species) and hydrophobic block (red marked species)

While the silane functionalized PB-block is rather hydrophobic the substitution to silanol functionalities causes the change to a hydrophilic block. Solidification of the resulting micelles takes than place by the condensation of the silanol functionalities. The morphology of the micellar aggregates should then be possible to be tailored by the choice of reaction conditions. While high PS-PB-SIL concentrations will yield a porous bulk material (Figure 4.10) the use of diluted polymer solutions might yield single micelles. The latter was investigated by the condensation of PS-PB-SIL as film on a gold TEM grid followed by calcination.

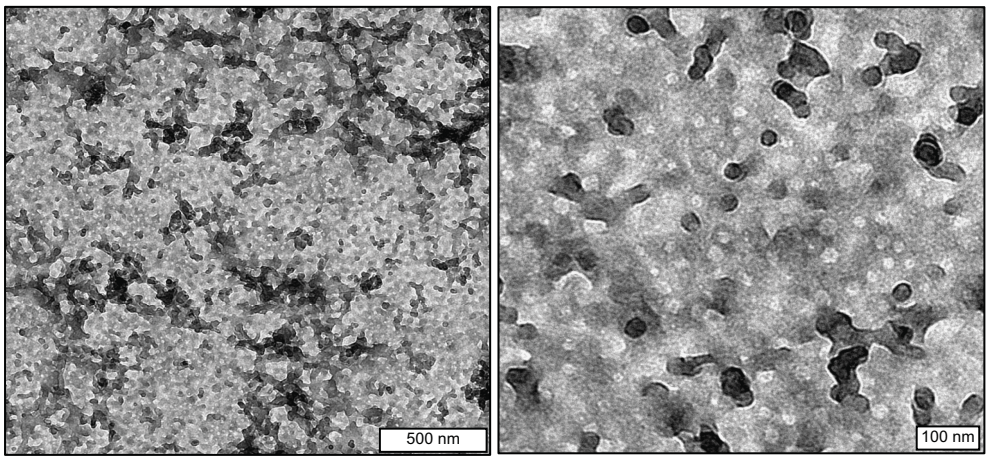

Figure 4.12: TEM micrographs of calcined PS-PB-SIL (dilution 1/50 of dialysed polymer solution)

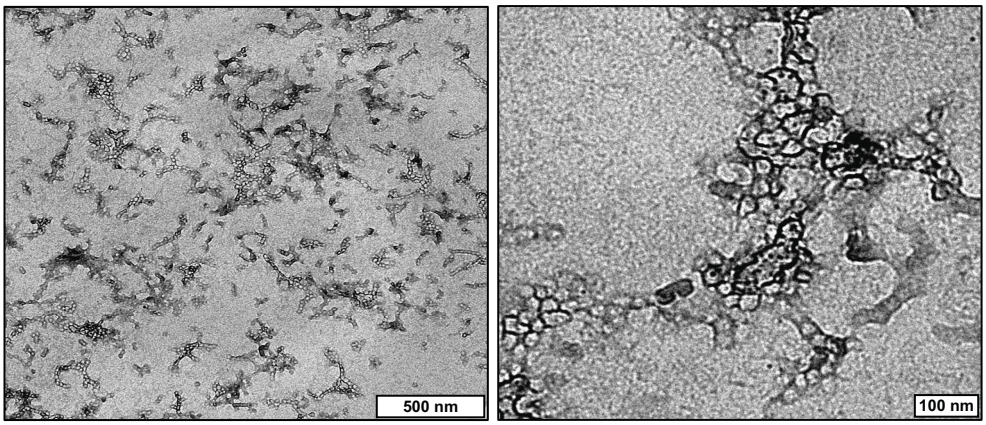

Figure 4.13: TEM micrographs of the calcined PS-PB-SIL micelles (dilution 1/2500 of dialysed polymer solution)

Condensation of PS-PB-SIL was carried out in ethanol by admixing hydrochloric acid (pH = 2). The reaction pathway followed a film condensation approach (for exact detail see experimental section). The freshly prepared sol was applied on a gold grid and left at RT to dry. After calcination, the polymeric template structure is mirrored in the pores of the porous silica, as can be seen in the TEM micrographs (Figure 4.12). A closer look at the thin sections furthermore reveals monodisperse pores of 14 nm in size which is in good agreement with aggregate size obtained from dynamic light scattering. Additionally, it seems that the porous silica material consists of cross-linked micelles rather than the bulk structure observed at high concentrations (Figure 4.10). Further dilution of the initial PS-PB-SIL solution yield separated or loosely aggregated silica hollow particles after the condensation-calcination sequence (Figure 4.13). The similar average pore diameter in the materials obtained from a concentrated and the 100 fold diluted PS-PB-SIL solution proves that the self assembly behaviour was not affected over the used concentration range. Thus, using this approach it seems possible to petrify micelles by subsequent condensation of the covalent anchored silanes into a solid shell.

4.4 Summary

In this chapter it was shown that the double hydroboration concept can be expanded from alkyl porogens (chapter 3) to polymeric silane functionalized precursors. Polybutadiene and poly(styrene-*b*-butadiene) was covalently linked with a sol gel precursor, yielding PB-SIL and PS-PB-SIL with condensable silane functionalities respectively. Although PB-SIL does not show an obvious amphiphilic character or obvious affinity to form molecular aggregates

(e.g. charge transfer), the condensed precursor yields a structured, fibrous material. It is assumed that the formation is a controlled intramolecular condensation process supported by the stiffness of the polybutadiene equipped with very bulky side chain functionalities. In contrast, the silane functionalized poly(styrene-*b*-butadiene) (PS-PB-SIL) possess an obvious amphiphilic character. Hydrolysis of the silane functionalities results in a transformation of the substituted PB into a hydrophilic block while PS remains hydrophobic. Consequently, condensation of the silanol functionalities results in the solidification of the microphase-separated structure. After removal of the organic porogen by calcination a porous silica is obtained. The high affinity for phase separation even in diluted solution was proven. Single solidified silica hollow shells with diameters of 14 nm were obtained.

These findings illustrate the versatility of the double hydroboration approach for the design of silica precursors which after condensation yield various predefined morphologies. Hence, it is an incentive for anchoring further structure directing agents such as e.g. mesogens to silica precursors.

5. Organosilica with chiral bridges

5.1 Introduction

Organosilicas provide an enormous variety of modifications. According to the 13 million known organic compounds, it is theoretically possible to combine all of them with the inorganic silica matrix to design new materials with extraordinary properties. Beside the possibility of changing functionalities, one can additionally generate chiral surfaces. These materials are promising candidates in applications such as chromatography for optical isomers or enantioselective catalysis. For surface functionalization with chiral compounds, mainly two methods are distinguished, namely immobilization of a chiral compound on the surface (grafting) or the direct condensation of a chiral silane in the presence or absence of a network stabilizer, such as TEOS. The grafting approach is often reported for the functionalization of stationary phases.[173,174] In contrast, direct condensation of chiral bridged silanes commonly applied for the synthesis of heterogeneous catalysts and the formation chiral imprinted structures.[175,176,177,178,179,180] It was shown that these chiral mesoporous organosilicas (ChiMOs) display optical activity and even exhibit enantioselective discrimination. However, in most approaches the chiral organic groups were attached to the silane groups via long and flexible linkers. Even though bridge bonded, these organic groups can hardly be regarded as a supporting component of the pore walls and consequently the addition of high amounts of pure inorganic precursors was necessary to stabilize the porous framework. Recently, POLARZ et al. synthesized a chiral PMO precursor related to the here described boron silane precursors.[181] An ethylene-bridged precursor was converted into a chiral alcohol using a metal-catalyzed, enantioselective hydroboration with subsequent oxidative alcoholysis. Hydrolysis and condensation of this precursor in presence of surfactants yielded in chiral PMOs, while the preservation and accessibility of the chiral functions in the resulting silica was not further proven. It is obvious that the here presented approach involving a structure directing moiety (see Chapter 1.6) that ensures the surface positioning, shows significant advantages.

Herein, the rational design of a new chiral organosilica-precursor based on boron silanes will be discussed. This precursor is convertible into an amine-functionalized, chiral mesoporous organosilicas via a condensation-ammonolysis sequence. The so prepared organosilicas

exhibit a tunable functionality, porosity and a very high and accessible surface area. Furthermore, the as-made monomers do self-organize when hydrolysis of their inorganic part takes place, resulting in an aggregation of the organic parts into hydrophobic domains and subsequently, after their removal, in porous materials with the activated amine-sites accessible at the pore interface. The size of the hydrophobic domains can be tailored by attaching sterically demanding alkenes or alcohols to the monomers, resulting in different pore sizes. Stereoselective splitting of the carbon-boron bonds after condensation of the organosilica network yield a chiral functional group localized at the pore wall by the template moiety.

5.2 Synthesis and characterization of chiral organosilicas

Porous chiral amine-functionalized organosilicas were synthesized *via* enantioselective hydroboration of an ethylene-bridged organosilica precursor, condensation of this precursor and finally ammonolysis of the boron moieties (Figure 5.1). The chirality in this case is

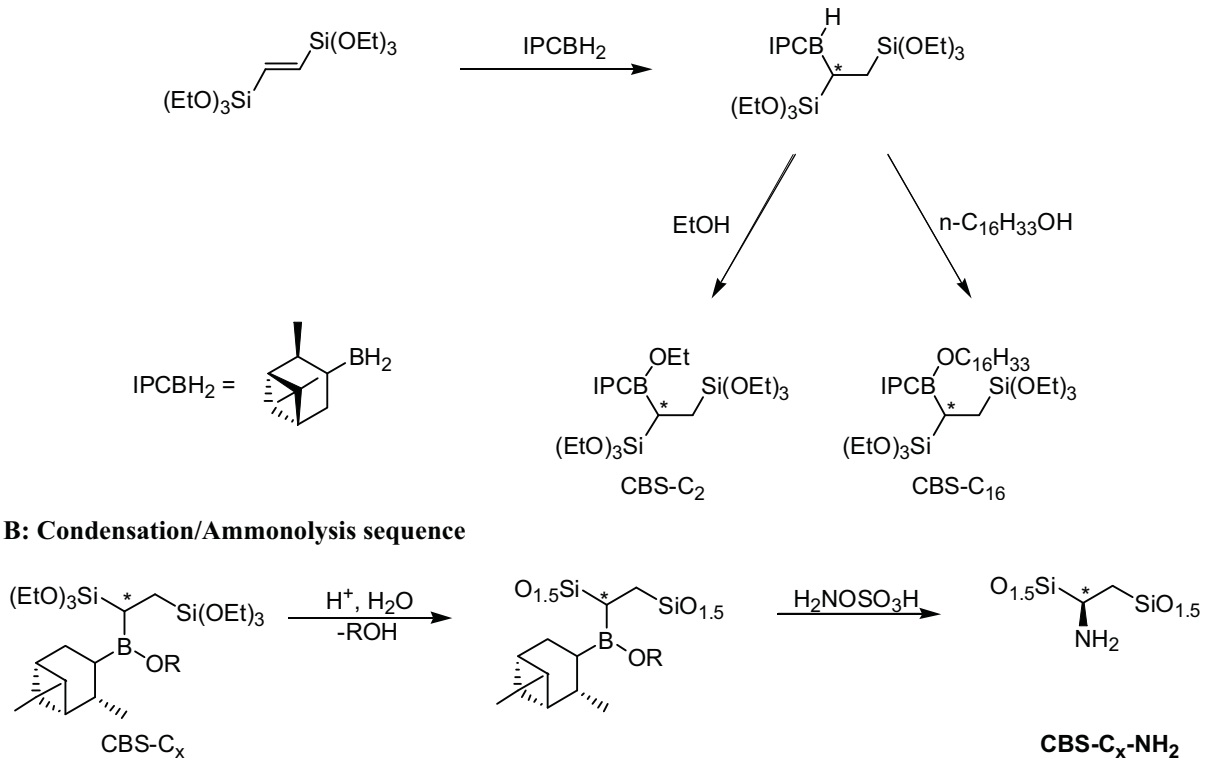

Figure 5.1: Synthesis of chiral MO precursors via hydroboration with *S*-monoisopinocampheylborane and hydrolysis, condensation and ammonolysis of the precursor.

obtained by an enantioselective hydroboration using *S*-monoisopinocampheylborane. This approach has several advantages: Compared to metal catalyzed reactions, higher enantioselectivities were reported (*E*-alkenes are converted with up to 95% ee).[182]

As enantioselective hydroboration reagent, commercially available *S*-monoisopino-campheylborane was used. The reaction was either quenched with ethanol yielding CBS-C_2 or the intermediate was further reacted with hexadecanol (yielding CBS-C_{16}). The incorporation of different alkyl groups cause an increase of the hydrophobic domain and is supposed to promote the self-organization of the precursor. In general, the reactivity of the remaining BH- bond, enable the incorporation various alcohols and also terminal alkenes. Precursors synthesized using 1-hexadecene however yield comparable results as for those reacted with hexadecanol, thus just data of the alcohol-quenched precursors are described in the following section.

The reaction can be monitored using 1H-NMR measurements (Figure 5.2). It is seen that the ethylene protons of the starting material have vanished completely in the spectra of the products, proving the full conversion by addition of the borane. Additional signals corresponding to alkane protons can be attributed to the campheyl, hexadecyl and bridging ethane group, respectively. The hydroboration reaction was further verified by FT-IR measurements (Figure 5.2). The appearance of C-H, C-B, O-B deformation modes between 1250-1460 cm^{-1} support the successful hydroboration. Additional peaks arising at 858 and 888 cm^{-1} can be assigned to CH vibration of branched alkenes. Furthermore, an increased

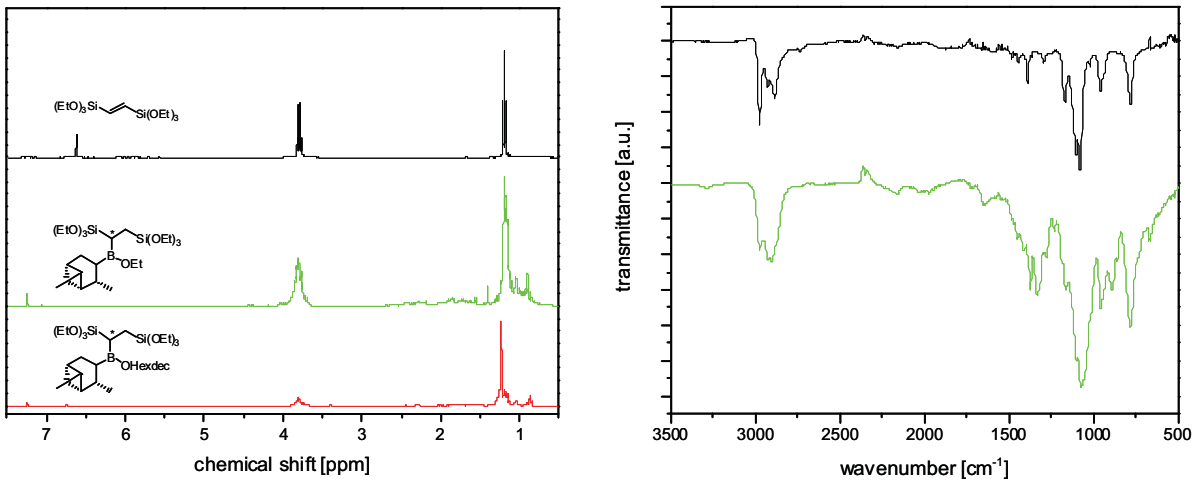

Figure 5.2: ^{1}H-NMR and IR spectra of the bis(triethoxysilyl)ethene (-) and the products CBS-C_2 (-) and CBS-C_{16} (-)

intensity of the CH stretching modes between 2880 cm^{-1} and 2980 cm^{-1} is observed due to the incorporation of the campheyl moiety. As expected, no signals above 3000 cm^{-1} are observed for CBS precursors which would be indicative for C=C-H vibrational modes. A comparative IR-measurement of bis(triethoxysilyl)ethane and bis(triethoxysilyl)ethene, however, revealed that CH-double bond vibrational modes are unobservable weak for this precursors. Therefore, they are not suitable for monitoring the here described hydroboration.

Different organosilicas were synthesized by the condensation of the CBS-C_x precursor in hydrochloric acid. The synthetic details are given in Table 5.1.

Table 5.1: Chiral organosilicas prepared from CBS-C_x precursors

entry	Si_{CBS}/Si_{TEOS} ratio	Precursor [mmol]	TEOS [mmol]	HCl [ml]	EtOH [ml]
CBS-C_2-NH_2-1	1/0	CBS-C_2 / 2.50	-	0.6	3.0
CBS-C_2-NH_2-2	1/2	CBS-C_2 / 1.25	2.50	0.6	3.0
CBS-C_2-NH_2-3	1/4	CBS-C_2 / 0.83	3.33	0.6	3.0
CBS-C_2-NH_2-4	1/8	CBS-C_2 / 0.50	4.00	0.6	3.0
CBS-C_{16}-NH_2-1	1/0	CBS-C_{16} / 2.50	-	0.6	3.0
CBS-C_{16}-NH_2-2	1/2	CBS-C_{16} / 1.25	2.50	0.6	3.0
CBS-C_{16}-NH_2-3	1/4	CBS-C_{16} / 0.83	3.33	0.6	3.0

In the first series, a set of silicas were produced from the CBS precursor and different amounts of TEOS and HCl (pH = 2). Stereoselective splitting of the carbon-boron-bonds after condensation of the organosilica network was carried out by stirring the materials in hydroxylamine-*O*-sulfonic acid/diglyme solutions. This procedure leads to functionalization on the organic bridges to give the chiral silicas (denoted as CBS-C_x-NH_2). Extraction of the cleaved organic attachments is mainly accomplished during this functionalization step, while the complete removal of the organic moieties can be obtained after an additional extraction with ethanol and THF. It should be noted that this approach can also naturally lead to other functional groups attached to the bridges, as the various transformations towards versatile functionalities are known from chiral organoboranes.[95]

The condensation and functionalization step was analyzed using ^{29}Si, ^{11}B and ^{13}C NMR measurements (Figure 5.3). For the condensed, but not functionalized material ^{29}Si NMR resonances appear between -60 and -85 ppm representative for T-Type organosilica species, while the weak signal for Q-units at -110 ppm confirms the Si-C bond cleavage is only

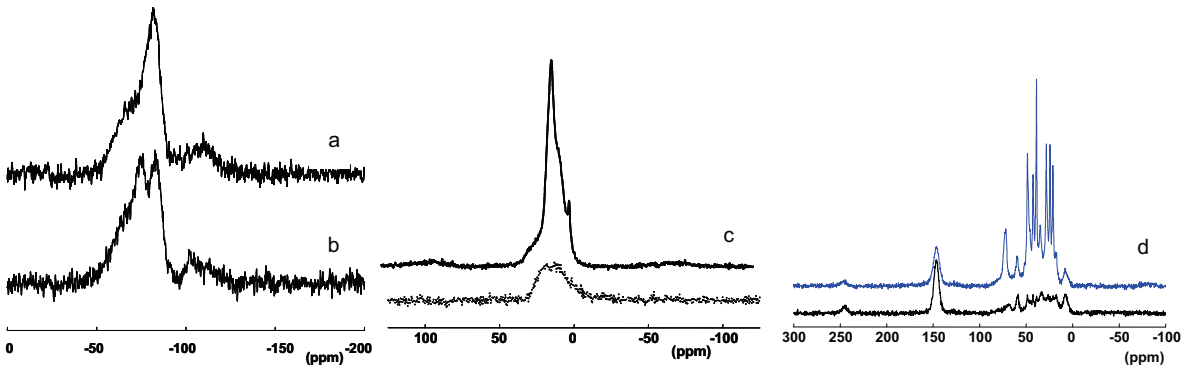

Figure 5.3: ^{29}Si and ^{11}B MAS NMR spectra before and after ammonolysis of organosilica CBS-C_2-NH_2-1:a) ^{29}Si, before ammonolysis, b) ^{29}Si after ammonolysis; c) ^{11}B, before and after (dotted line) ammonolysis; d) ^{13}C, before(blue) and after (black) ammonolysis**;**

minor. Deconvolution of the spectra resulted in an integral proportion of about 10 % for the Q-sites. The same is true for materials after ammonolysis, proving that the bridge-bonded organic group is maintained throughout the reaction. Changes in the coordination of the bridge bonded organic group after ammonolysis have a distinct influence on the ^{29}Si signals. The spectrum in Figure 5.3b can be simulated with at least three different T species at -83 ppm, -75 ppm and -65 ppm, respectively. These signals can be attributed to T^1, T^2 and T^3 species, however a reliable assignment is difficult because these T-sites are also likely to be observed due to the (rarely described) asymmetric composition of the organosilica, where the silica atoms are bound to two different carbon species of the bridging group. This asymmetric bridging group should therefore result in the emergence of e.g. two T_3-species. The strong signal at -75 ppm after ammonolysis, exhibiting a one-to-one ratio to the strong signal at -83 ppm therefore can be attributed to the formation of a new T_3 species as expected for this reaction.

A comparison of the ^{11}B-NMR spectra for both materials shows a strong signal for the as-made organosilica which is significantly weakened after ammonolysis. However, the appearance of this, even though weak, signal indicates that a few boron moieties are trapped in the silica framework and thus, not accessible for further functionalization. A comparison of the spectra in Figure 1c indicates the existence of at least two boron species before functionalization, and only one, the accessible one, disappears after ammonolysis. Comparable results are observed from the ^{13}C-NMR spectra where the signals attributable to the boron attached campheyl and ethanol group have weakened significantly, showing the almost complete cleavage of the boron moieties.

Additional IR measurements on the condensed materials before and after functionalization support these results (Figure 5.4). The CH_3, CH_2 and CH stretching vibrations at 2900 cm^{-1} nearly disappear in the amine-functionalized samples, proving the successful cleavage and removal of the campheyl and hexadecyl moieties. The same is true for the CH_3, CH_2, CH and B-C, B-O, C-H deformations vibrations which can be attributed to the broad band at 1365 cm^{-1}. As functionalization yields almost complete removal of the hydrocarbons, the remaining CH groups causing only very weak signals. Due to the high amine loading, especially for sample CBS-C_2-NH_2-1, a new peak at 1632 cm^{-1} can be identified after functionalization which can be assigned to NH_2 deformation modes. The typically existing NH stretching modes at 3100 cm^{-1} are presumably buried under the broad vibration band of adsorbed water and therefore not suitable for characterization.

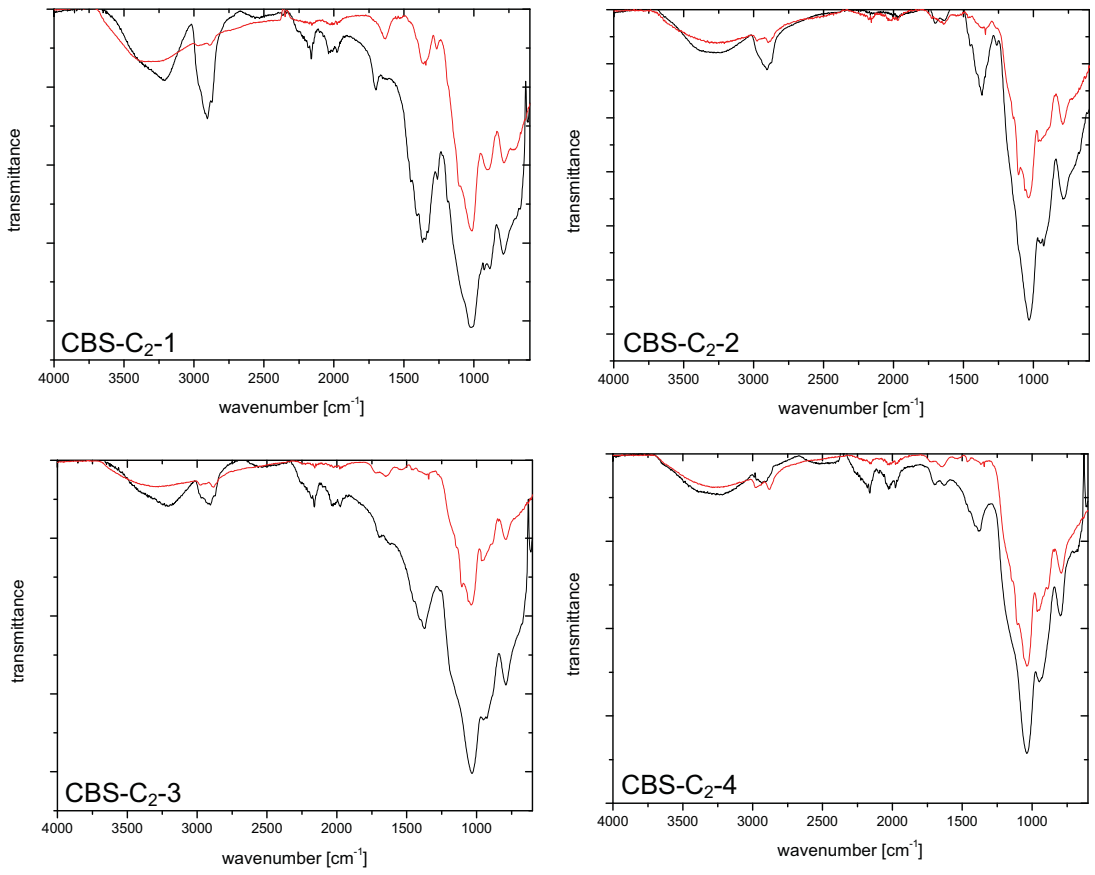

Figure 5.4: Infrared spectra of condensed CBS-C_2-1 to 4 (-) and amine functionalized CBS-C_2-NH_2-1 to 4 (-)

It is important to note that the removal of the organic moiety is not accompanied by a significant bridge cleavage. This shows that the ethylene bridge of the organosilica, responsible for the network formation is preserved during the functionalization by

ammonolysis and the extraction step. Therefore, it can be assumed that the resulting organosilica framework is also stable enough to maintain porosity after removal of the organic moieties.

The resulting materials where analyzed using nitrogen sorption, TEM and XRD measurements. All organosilicas showed no detectable porosity and surface area prior to ammonolysis. However, after this functionalization, defined porosities and high surface areas are observed. Nitrogen isotherms of the materials CBS 1-4 after ammonolysis are shown in Figure 5.5.

The nitrogen isotherm for organosilicas made from the pure precursor (CBS-C_2-NH_2-1) exhibit a high nitrogen uptake at low relative pressures and a less pronounced hysteresis, indicating the existence of mainly micropores (< 2.0 nm) and some additional mesopores (> 2.0 nm) in this sample (Figure 5.5a). Furthermore, the surface area is considerable lowered compared to the materials with admixed TEOS. It is also observed that the adsorption and desorption branch do not close at low relative pressure, indicating a soft, polymer-like material. This probably yields a partial collapse of the porous system for the pure organosilica (CBS-C_2-NH_2-1) after functionalization and extraction of the organic moiety.

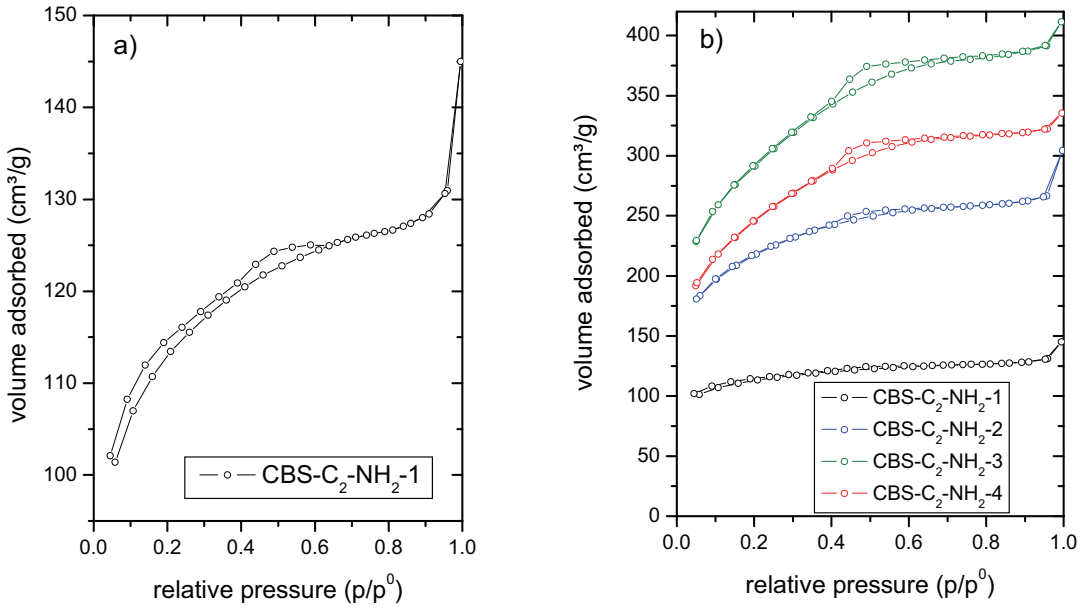

Figure 5.5: a) N_2-sorption isotherms of sample CBS-C_2-NH_2-1 and b) comparison of samples CBS-C_2-NH_2-1-4 showing the influence of different CBS /TEOS ratios on the observed porosity and surface area.

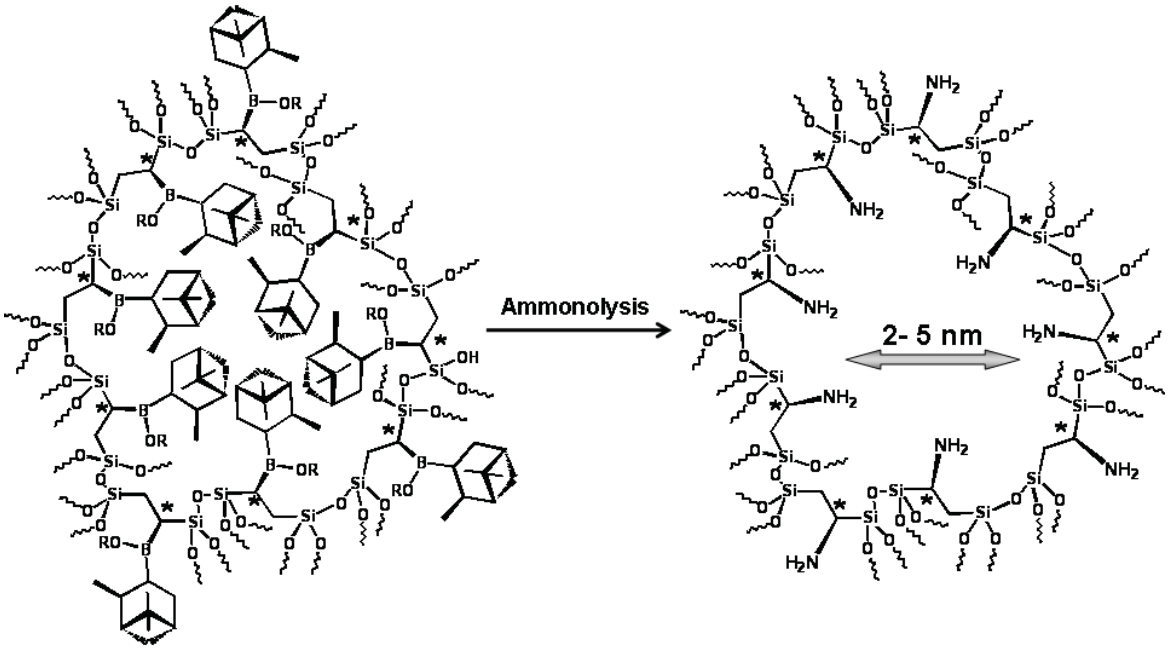

Figure 5.6: Self-assembly of CBS-precursors and the porosity generate dafter ammonolysis

All other organosilicas exhibit high surface areas of up to 1000 m^2/g for CBS-C_2-NH_2-3 and average pore sizes in the range of 2.2 - 2.6 nm which is significantly higher than found for molecular imprinting of related organic molecules (0.8 nm).[183] Regarding the results shown in the previous chapter on boron-functionalized organosilicas, an aggregation of the hydrophobic moieties of the monomer can be assumed, yielding an increased pore size compared to silicas generated by single-molecule templating (Figure 5.6).

Table 5.2 compares the BET surface areas, the average pore diameter from DFT evaluation as well as the micro- and mesopore volume of samples CBS-C_2-NH_2-1-4. Distinctly higher

Table 5.2: BET-surface area and pore size characterization for organosilicas CBS-C_2-NH_2-1-4 after ammonolysis [a] Specific BET surface area. [b] Average pore diameter. [c] Micropore volume of pores < 2 nm diameter. [d] Mesopore volume of pores between 2 to 50 nm diameter. [e] Total pore volume (sum of micro- and mesopore volume)

Sample	a_{surf}(BET)[a] [m^2/g]	d_P(NLDFT)[b] [nm]	$V_{p,micro}$(NLDFT)[c] [cm^3/g]	$V_{p,meso}$(NLDFT)[d] [cm^3/g]
CBS-C_2-NH_2-1	367	2.0	0.143	0.041
CBS-C_2-NH_2-2	731	2.2	0.186	0.166
CBS-C_2-NH_2-3	1010	2.6	0.165	0.379
CBS-C_2-NH_2-4	853	2.5	0.141	0.316

surface areas and increasing average pore diameters are observed for materials prepared with addition of pure silica precursor, more precisely for intermediate TEOS/CBS ratios. This can be attributed to a stabilization of the organosilica framework with increasing amount of the stiff inorganic parts. To avoid pore collapse, reinforcement of organosilica frameworks by addition of pure silica precursors is frequently used throughout the literature, especially for chiral mesoporous organosilicas (however, with much higher TEOS/ChiMO-precursor ratios).[176,177] Note that for long and flexible bridging groups, a significant amount of TEOS has to be added e.g. for the generation of mesoporous organosilicas, yielding an overall decrease of the organic groups in the framework.

Therefore it is interesting to note that also for the pure organosilica (CBS-C_2-NH_2-1 made without addition of the purely inorganic co-monomer) a significant surface area is still observed. This proves that the chiral-bridged organosilica is mechanically strong enough to at least partially support the pore wall, allowing an organic monomer content of 100 %.

The comparison of micro-/mesopore volumes for CBS-C_2-NH_2-1-4 further indicate that, beside the stabilization of the pore walls, the addition of pure silica precursor enhance the aggregation of the organic moieties, as a higher fraction of mesopores is observed in the samples with higher pure inorganic precursor content.

Thus, from the BET measurements, it can be seen that for a TEOS/CBS-C_2 molar ratio of 4:1 the maximal porosity is observed. This is in good agreement with the results of the nitrogen adsorption for the LCBS-C_{10} materials (see Chapter 3.3.1). Further addition of TEOS leads again to a decrease of the surface area which is to be expected due to the increasing silica content and does not contribute to the overall porosity. The ratio of the micro- and mesopore volumes (Table 5.2) of samples CBS-3 and 4 are comparable to other mesoporous silicas exhibiting smaller mesopores, e.g. derived from Brij-surfactants.[184] However, due to the less defined aggregation of the hydrophobic moieties, the CBS-materials possess a less defined pore size distribution.

The pore architectures and specifically the pore size of the resulting mesoporous organosilica can be further modified when long chain alkyl tails are additionally attached to the precursor (CBS-C_{16}). In Figure 5.7 the BET isotherms of pure and TEOS-admixed organosilicas prepared from CBS-C_{16} are shown. The pure precursor (CBS-C_{16}) exhibit already consider-

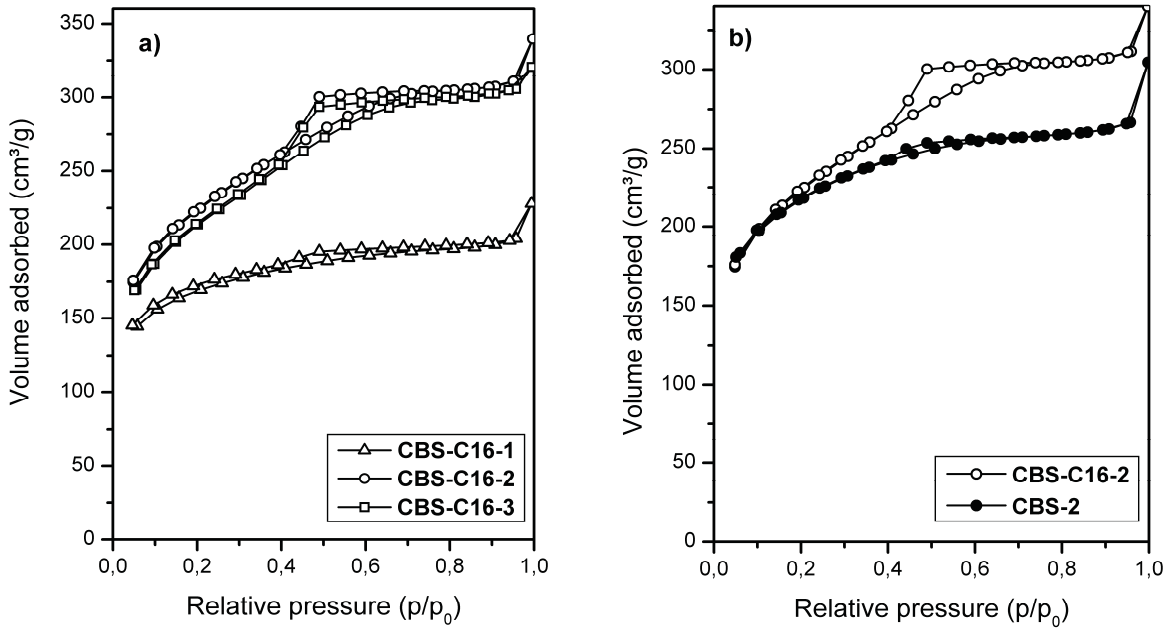

Figure 5.7: a) N2-sorption isotherms of samples CBS-C16-1 - 3 and b) comparison of N_2-sorption isotherms for organosilicas CBS-C_2-NH_2-2 and CBS-C_{16}-NH_2-2

able surface area. However, an average pore size not higher than for the CBS precursors is observed. Comparable to the organosilica CBS-C_2-NH_2-1, this is due to a partial collapse of the porosity, as a result of the high organic fraction in this sample. This is supported by the finding that the highest surface area as well as a more defined mesoporosity is observed for the organosilicas prepared by admixing TEOS. As summarized in Table 5.3, the pore sizes for these organosilicas have increased up to 5 nm, showing the influence of the attached hexadecyl-chains by increasing the hydrophobic domains and the related pore size. The comparison of organosilicas made from CBS-C_2 and CBS-C_{16} under similar conditions nicely illustrates this finding (Figure 5.7 b), as a more pronounced hysteresis, is indicative of larger fractions of mesopores and is observed for the CBS-C_{16}-NH_2.

Table 5.3: BET-surface area and pore size characterization for organosilicas CBS-C_{16}-NH_2-1-3 after ammonolysis: [a] Specific BET surface area. [b] Average pore diameter. [c] Micropore volume of pores < 2 nm diameter. [d] Mesopore volume of pores between 2 to 50 nm diameter. [e] Total pore volume (sum of micro- and mesopore volume)

entry	a_{surf}(BET)[a] [m²/g]	d_P(NLDFT)[b] [nm]	$V_{p,micro}$(NLDFT)[c] [cm³/g]	$V_{p,meso}$(NLDFT)[d] [cm³/g]	$V_{p,tot}$(NLDFT)[e] [cm³/g]
CBS-C_{16}-1	559	2.0	0.167	0.117	0.284
CBS-C_{16}-2	771	5.1	0.129	0.288	0.417
CBS-C_{16}-3	739	4.6	0.116	0.296	0.412

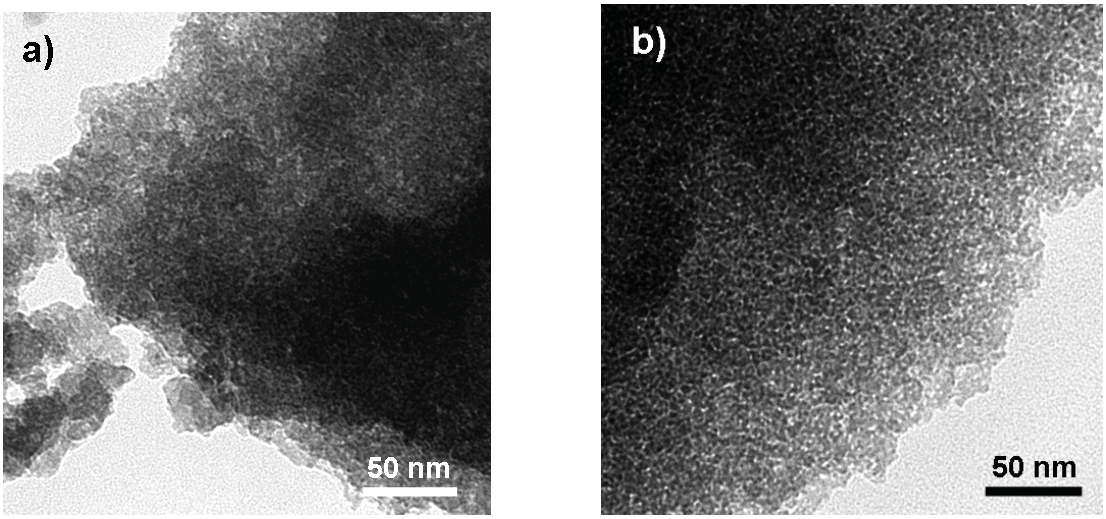

Figure 5.8: TEM measurements on the silicas a) CBS-C_2-NH_2-2 and b) CBS-C_{16}-NH_2-2

TEM measurements (Figure 5.8) on the materials indicate the presence of a disordered, worm-like pore structure. Even though the campheyl-attachments are able to form hydrophobic aggregates and subsequently lyotropic phases these phases are not long range ordered.

For evaluating the chiral properties of the organosilicas, circular dichroism measurements were carried out on the pure precursor and on the condensed organosilica. Circular dichroism spectroscopy is commonly used for determination of the optical activity in the liquid state. However, solid state CD spectroscopy can provide valuable information on chiral interactions or reactions which occur specifically in the solid state.[185] Solid-state CD measurements have been reported on chiral organosilicas using potassium bromide pellets.[186] Here, measurements were carried out on the organosilicas dispersed in trichlormethane which is an approximately isorefractive solvent to avoid scattering contributions and depolarization effects at grain boundaries. However, evaluation of the data from solid-state CD measurements is still difficult, so that the measurements should be considered as qualitative results.

Although CD measurements on the liquid precursor can not methodically confirm the incorporation of a new asymmetric carbon in the ethylene bridge, due to of the synchronous existence of the chiral terpene derivative, it can be exploited to verify that no racemisation of the precursor takes place (Figure 5.9). Hence, in order to verify the chirality of the amine-functionalized organosilica a second experiment was carried out on the pure organosilica

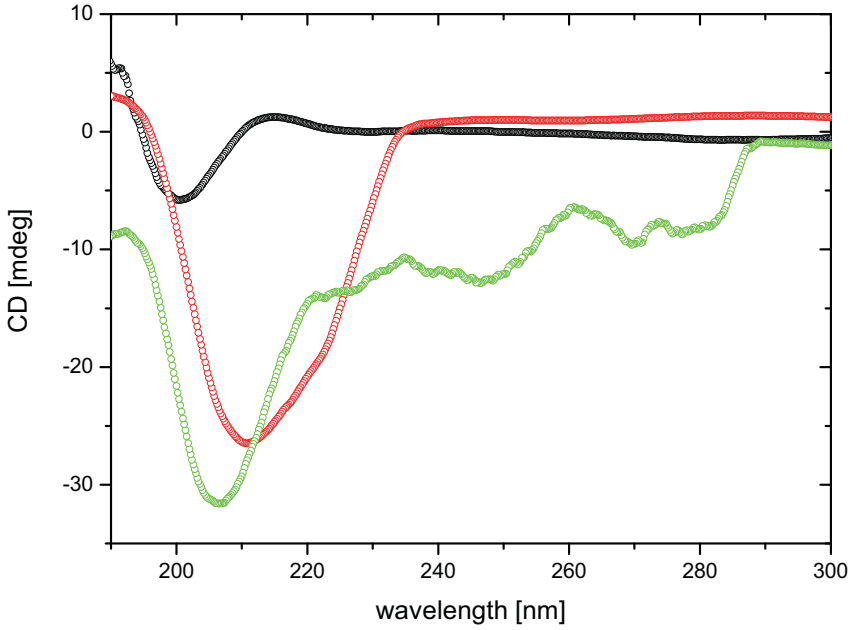

Figure 5.9: Circular dichroism measurements of the precursor CBS-C_2 (-), the corresponding organosilica CBS-C_2-NH_2-1 (-) and its benzoic acid adduct (-)

CBS-C_2-NH_2-1 dispersed in trichlormethane, and then in combination with adsorbed benzoic acid. Assuming that the chiral amine-groups on the organosilica are accessible, interactions with the acidic chromophore should induce a significant optical activity of the otherwise achiral benzoic acid. Such induced circular dichroism is for example observed in solid-state inclusion compounds of achiral chromophores in chiral molecules.[187] For the described experiments, organosilica CBS-C_2-NH_2-1 was used which, although having the smallest surface area, displays the highest organic fraction of the described materials. The signal centered at ~ 210 nm for the pure organosilica (CBS-C_2-NH_2-1) can be attributed to the amine groups attached to the chiral center. After addition of benzoic acid, two additional bands are observed in the CD-spectrum due to the induced optical activity via adsorption on the chiral amines. The peaks centered at 247 nm and 274 nm can be attributed to carbonyl and aromatic adsorption peaks of benzoic acid of the respective UV-spectrum.

Even though a quantitative evaluation of the chirality is difficult due to the fact that the sample is a solid, this measurement clearly proves that the prepared organosilicas are indeed chiral. In addition, this chirality is accessible from the outside and influences molecules entering the pore system.

5.3 Influence of cosurfactants

As described above, the condensation of CBS-C_x precursors lead usually to disordered organosilicas with high surface areas and mesoporosity, but without regularity of pores. This finding, is certainly no disadvantage for most applications, because disordered systems suffice for needs of membrane technology or catalysis which do not directly benefit from mesoscopic order.[188] Nevertheless, to prove the versatility of this precursor, it was also tried to use it in a conventional PMO synthesis, using a common triblock copolymer (Pluronic F127) as an additional template. Pluronic-Type triblock copolymers have been frequently used for the preparation of PMOs.[189,190,191]

As shown in Figure 5.10 organosilicas with an ordered pore structure are formed proving that the present concept and monomer system can also be expanded to periodic mesoporous silicas. Nitrogen sorption measurements reveal a specific BET surface area of 591 m^2/g for this CBS-C_2- NH_2-F127 PMO (Figure 5.11). NLDFT evaluation of the pore diameter using the adsorption branch and SAXS measurements (Figure 5.11) further indicate a narrow pore size distribution with a maximum at 3.8 nm for the amine-functionalized material.

Beside the use of Pluronics for the synthesis of materials with a sharp pore size distribution the use of common ionic surfactants like CTAB was investigated. The aim of this study is to ascertain the possibility of further tailoring of the pore size in CBS materials by admixing

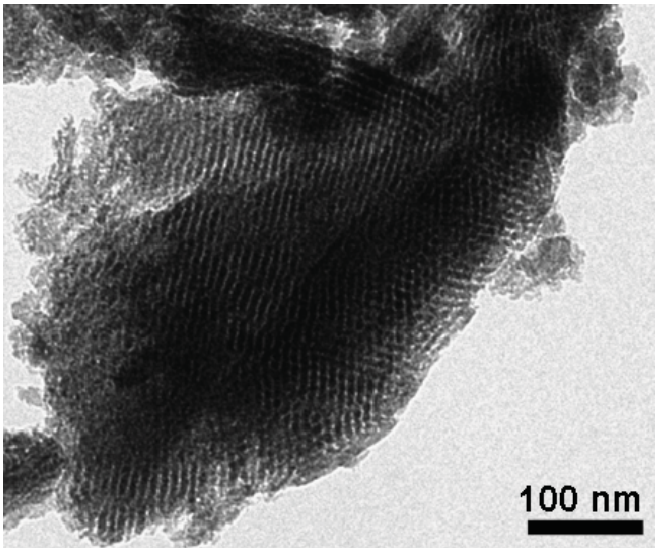

Figure 5.10: TEM-Micrograph of CBS-F127 after extraction of the surfactant and ammonolysis

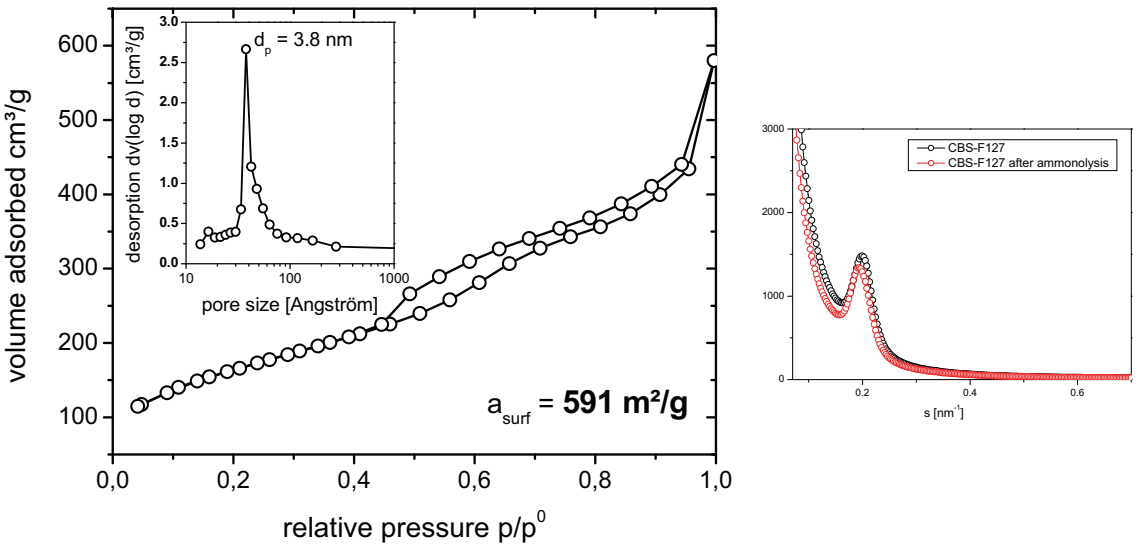

Figure 5.11: Nitrogen adsorption of CBS-C_2-NH_2-F127 and pore size distribution (left), SAXS pattern (right)

CTAB while maintaining the advantages of this approach, such as predefinition of the location of the functionalities and the possibility to vary the functionalities by the choose of the chemical cleavage step. Thus, it would be possible to fine tune the accessibility of the pores, but only if the admixing of CTAB result in mixed micelles. A bimodal pore size distribution caused by separated micelles made of the CBS precursor and CTAB micelles can of course not influence the accessibility of the chiral functionalities. Another question that arises is "does the addition of CTAB to the CBS-C_2 precursor result in the same effect like using the pure CBS-C_{16} precursor?" For this purpose a set of CTAB containing and CTAB free mixtures of CBS-C_2 and CBS-C_{16} organosilicas were investigated (Table 5.4). For all materials, a 20 mol% mixture of precursor in TEOS was used and the condensation was carried out in hydrochloric acid (pH=2) following a bulk condensation pathway. The

Table 5.4: Influence of CTAB on the porosity of CBS-C_2-NH_2 and CBS-C_{16}-NH_2 organosilicas; [a]0.5 equivalents (eq) regarding to the CBS-C_x precursor

entry	CTAB	a_{surf}(BET) m^2g^{-1}	V_p,(NLDFT) cm^3g^{-1}
CBS-C_2-NH_2	-	911	0.63
CBS-$C_{2,CTAB}$-NH_2	0.5 eq[a]	1159	1.04
CBS-C_{16}-NH_2	-	925	0.85
CBS-$C_{16,CTAB}$-NH_2	0.5 eq[a]	1183	1.36
$TEOS_{CTAB}$-NH_2	0.5 eq[a]	1161	0.62

condensed materials were aminated and extracted by ethanol in order to remove the porogens. TEM measurements showing disordered wormlike pores for all organosilicas obtained by CTAB admixing, as described for CBS-C_x-NH_2 (not shown).

Nitrogen adsorption shows a decisive change of the porosity in the resulting material (Figure 5.12, Table 5.4). Note the slight difference of the surface areas of CBS-C_2-NH_2 and CBS-C_{16}-NH_2 compared to the values obtained in the previous section can be caused by the higher amount of ethanol used here in order to support the solubility of CTAB. However, all obtained organosilicas in this studied were synthesized under similar conditions and therefore comparable. The surface area in all CBS materials is comparable high (≈ 1000 m^2/g) but the porosity changes due to the incorporation of long alkyl chains originating from either the CBS-C_x precursor or CTAB. While pores in the CBS-C_2-NH_2 silica are exclusively generated by the hydrophobic moieties of the precursor CBS-C_2 precursor, the addition of CTAB leads to an increase of porosity and an increase of the pore diameter. The same is true for CBS-C_{16}. Thus, the highest porosity is obtained when the effect of the hexadecyl chain origin from the precursor and CTAB sum up. In this case (CBS-$C_{16,CTAB}$), the porosity reaches up to 1.36 cm^3/g. The observation that the surface area remains unaffected in all organosilicas while the porosity undergoes extreme changes can only be caused by a cosurfactant-like character of

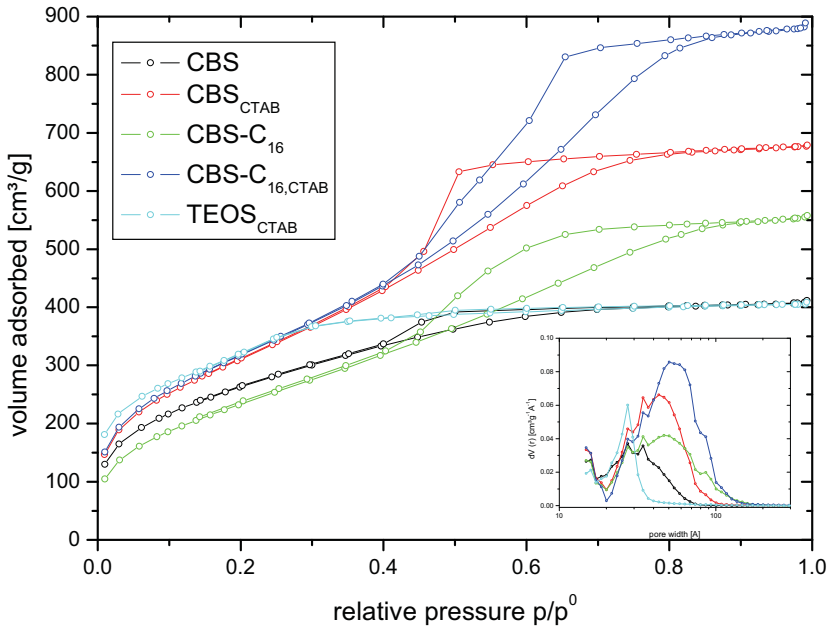

Figure 5.12: Nitrogen adsorption and pore size distribution of CTAB containing CBS and CBS-C_{16} organosilicas

CTAB. This precisely means that the CBS-C_x precursor and CTAB form mixed micelles. This explanation is supported by the pore size distribution. A widening of the average pore size is observed when admixing CTAB to the CBS-C_x precursor (Figure 5.12). Furthermore, the comparative pure silica sample ($TEOS_{CTAB}$) shows a prominent peak at 2.8 nm which is not pronounced in all obtained organosilicas. This is indicative for a non-bimodal pore size distribution. Hence, both findings confirm the existence of mixed micelles and not the existence of additional porosity caused by CTAB.

5.4 HPLC application of chiral organosilicas

Chromatographic separation, especially chiral resolution on chiral stationary phases is of special interest for pharmaceuticals since the early 1970s.[192,193] An unfortunately famous example for the importance of the separation and detection of racemic mixtures is the pharmaceutical Thalidomid, also known as Contergan®. After rollout in 1956 it was sold in more than 50 countries and only 5 years later removed from the market because of its side effects. Thalidomide is a sedative, hypnotic and multiple myeloma medication which was chiefly sold and prescribed to pregnant women as an antiemetic to combat morning sickness and as an aid to help them sleep. While the D-enantiomer produces the intended effect, the L-enantiomer is a teratogene (Figure 5.13). Unfortunately it was not known that the activation of stereogenic α-carbonyl carbon by the carbonyl group is strong enough to allow racemisation even under aqueous conditions at room temperature. This example proves in a very tragic way, the importance of a powerful method for recognition and separation of racemic mixtures. Nevertheless, even in the early 1990s, about 90% of synthetic chiral drugs were still racemic, that is, equimolar mixtures of both enantiomers which reflects the difficulty in the practical synthesis of single-enantiomeric compounds.[194] Today's expenses for both sales and analysis of chiral drugs are more than a 300 billion dollar market.

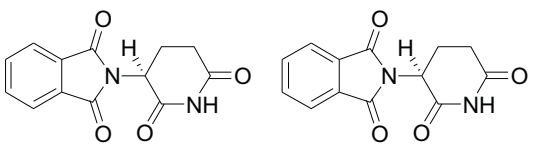

D-enatiomer teratogene L-enatiomer soporifics

Figure 5.13: Enantiomers of Contergan®

In order to categorize here the presented chiral stationary phase and comparing the performance with respect to commercial columns, a brief summary on existing materials will be done in the following paragraphs. In general chiral stationary phases can be classified according to their interactions mechanism with an analyte. A subdivision into five Types was first proposed by WAINER.[195]

Type I chiral stationary phases possessing chiral resolution only by forming temporary complexes. The formation is supported by attractive interactions, such as hydrogen bonds, π-π interactions and dipole stacking. Important representatives of this class are the brush Type phases of PIRKLE.[196] Most common is N-(3,5-dinitrobenzoyl) –phenylglycine bonded to aminopropylsilica. These columns are capable of separating a large number of analytes which have to be aromatic or otherwise a pre-derivatization step to introduce an aromatic moiety into the analyte is necessary. Advantages are very simple accessibility by cheap synthesis and provide high selectivity factors. However, the mobile phases are commonly restricted to relative non-polar organic solvents.

Type II chiral stationary phases showing additionally to the attractive interaction of Type I phases, inclusion complexes which lead to a higher chiral resolution with respect to Type I. These phases are commonly based on cellulose derivatives. For tailoring the stationary phase, with respect to the analyte properties, the hydroxyl groups are substituted mainly by ether esters, and amides.

Type III chiral stationary phases rely exclusively on the formation of inclusion complexes. Most common are cyclodextrines[197], crown ethers and helical polymers (e.g. poly(triphenylmethylmethacrylate)).

Type IV chiral stationary phases separate by means of diasteriomeric metal complexes, also denoted as ***C**hiral **L**igand **E**xchange **C**hromatography* CLEC[198].

Type V chiral stationary phase are based on proteins where the separation rely on co-action of hydrophobic and polar interactions.

Presented here are chiral stationary phases that can be assigned to Type I chiral stationary phases and should therefore possess good separation capability for a vide variety of analytes, especially aromatic compounds. The chiral selector is in all cases an amine derivative. Thus,

amplification of the separation by the formation of inclusion complexes (Type II and III) as it is commonly applied for many commercial columns cannot be expected.

The new stationary phase material for the chiral resolution via HPLC is based on the CBS-C_2 precursor described in the previous chapter. By use of this precursor, access to multiple chiral functionalities is enabled and thus it is a very promising system for the application in a chiral HPLC. It is expected that the presented stationary phases will possess a very high performance because of the close proximity of the asymmetric carbon of the chiral functionality to the silica surface. This effect, most commonly denoted as the "confinement effect" is reported to be responsible for increased interactions.[199] In that point, the presented stationary phase differs from ordinary commercial column materials were the stereogenic centre is anchored via a side chain functionality far away from the silica surface.

First of all, the synthetic pathway towards different kinds of stationary phases will be discussed, namely monolithic and packed particle phases. Both differ in their physical properties, and therefore their chiral resolution.[200] All phases are unified by the material they are made from. In general, silica is used because of its extraordinary properties, such as mechanical/thermal resistance, lack of shrinking or swelling and high compatibility with a broad range of solvents. To further improve the chemical dependability of these stationary phases, especially to pH-values larger than 7, interest is gathering into recent developments on alumina, zirconia and polymer based materials.[201] Most common for the synthesis of highly functionalized materials for the use as stationary phase is the grafting process on pre-prepared pure silica particles or monolith. This is a very reliable method for the formation of surface functionalities and from the point of economy of chemicals. Furthermore, a possible but rather rare approach is the direct condensation of an appropriate silica precursor according to STÖBER.[202] This pathway is limited to particles with a maximum diameter of 1 µm. However, by controlled growth the particle size can be significantly increased until a diameter of 10 µm for the condensation of TEOS, under preservation of a narrow size distribution.[203,204] This method was adapted in order to obtain 5 µm spheres which are supposed to show optimal behavior as stationary phases. Since the CBS-C_2 precursor itself enables the formation of highly amine-functionalized porous organosilica, this material was perfectly suitable for the synthesis of a stationary phase according to the STÖBER process. Condensation of the pure CBS-C_2 precursor was carried out under various conditions, either

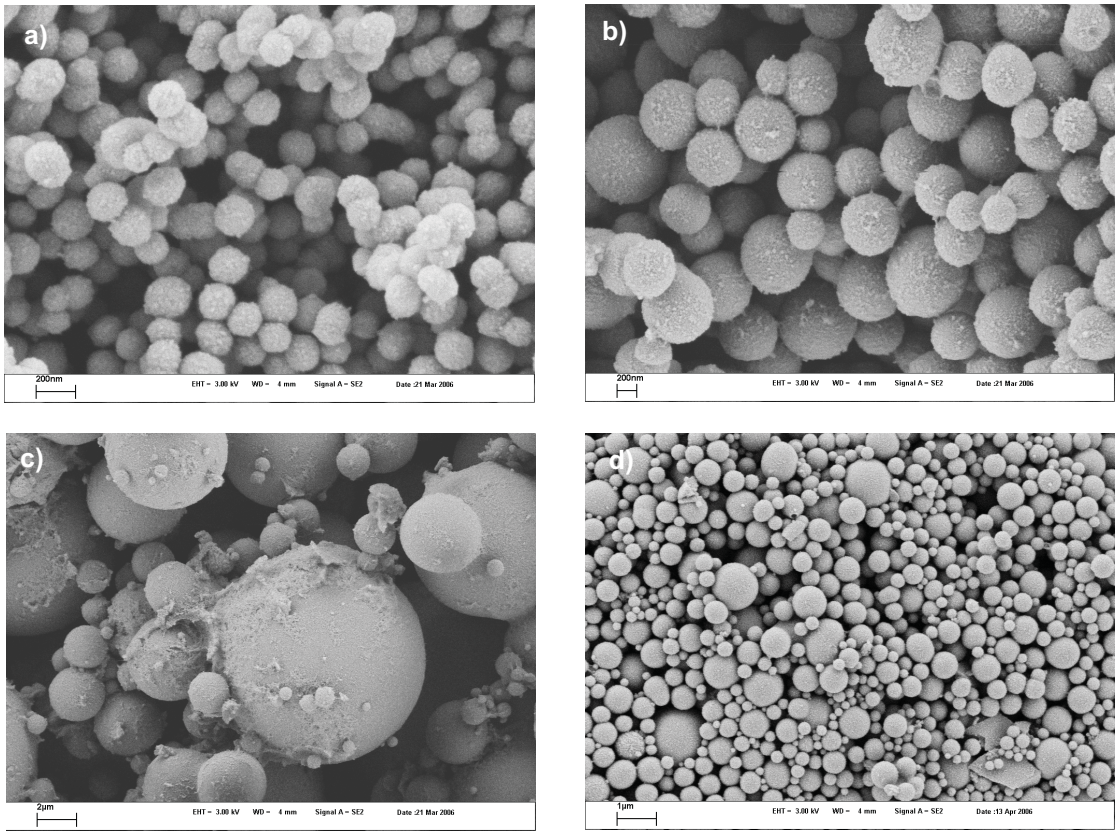

Figure 5.14: SEM micrographs of silica spheres synthesized according STÖBER process; particles were collected after over night aging of the mixed reagents, a) mixture of 60 mg CBS-C_2 in 2.0 ml absolute ethanol and 2.1 ml HCl (7.0 M); b) mixture of 53 mg CBS-C_2 in 3.0 ml absolute ethanol and 2.1 ml HCl (9.0 M); c) mixture of 51 mg CBS-C_2 in 2.5 ml absolute ethanol and 2.1 ml HCl (9.0 M) ; d) a solution of 100 mg CBS-C_2 in 1.0 ml absolute ethanol was slowly added (0.1 ml/h) to 3.0 ml HCl (9.0 M) and 3.0 ml ethanol

slow condensation of a diluted precursor solution or the controlled condensation by slow addition using an automatic injection system. An excerpt of the obtained particles is summarized in Figure 5.14. The range of obtained particles reaches from monodisperse 200 nm particles (Figure 5.14a) via mono-disperse 700 nm particles (Figure 5.14b) to broad size distributions from about 1 µm up to 10 µm (Figure 5.14c) This finding proves that despite of the unusual hydrophobic structural composition of the precursor, CBS-C_2 is very simple to handle and can be used for common methods like the STÖBER process. However, the obtained monodisperse particles were usually less than 1 µm in diameter. Although application of smaller particles leads to a higher chromatographic resolution and the Van-Deemter-Equation is almost linear which leads to a flow independent resolution (for particles <3 µm), the counter pressure raises dramatically evoking the need for a high pressure stable system.

Beside the synthesis of CBS particles for the application as stationary phase, synthesis of monolithic materials with a hierarchically pore structure was also attempted. In general, the development of monolithic silica columns of practical utility is thought to be of much interest, because they show much higher separation efficiency and permeability. Since the chiral amine functionalized organosilicas possess mesoporosity, these CBS materials fulfilling the first criteria (high surface area and accessible pores) for a monolithic stationary phase. Additionally, the appropriate mass transport must be realized via macro pores which are usually obtained by the use of polymeric structure directing agents. This approach was reported by NAKANISHI who exploited the macrophase separation of poly(acrylic acid) and poly(ethylene oxide) during the condensation of TMOS for the generation of macroporosity.[205] Therefore, the condensation process towards monolithic chiral organosilicas was carried out under various conditions using the CBS-C_2 precursor, polyethyleneoxide and different amounts of TEOS as network stabilizer. It was shown that the CBS-C_2 precursor can be used for the synthesis of a hierarchically structured organosilica (Figure 5.15), proving a similar easy usability of the precursors like the commonly used TMOS. However, all obtained monoliths were usually very soft and fragile even when adding 20 fold excess of network stabilizer TEOS. Slight mechanical stress or the solvent extraction results in the destruction of the material. One alternative to use this material might be the “in situ” synthsis of these monoliths directly into HPLC columns, similar to polymeric monolithic stationary phases.[206]

Both the monodisperse particles synthesized according to the STÖBER process, and the synthesis of monolithic materials showed the manageability of the precursor but did not result in the suitable stationary phase for the HPLC. Therefore, for the synthesis of all stationary phases used for the chiral separation in the present work the grafting approach was

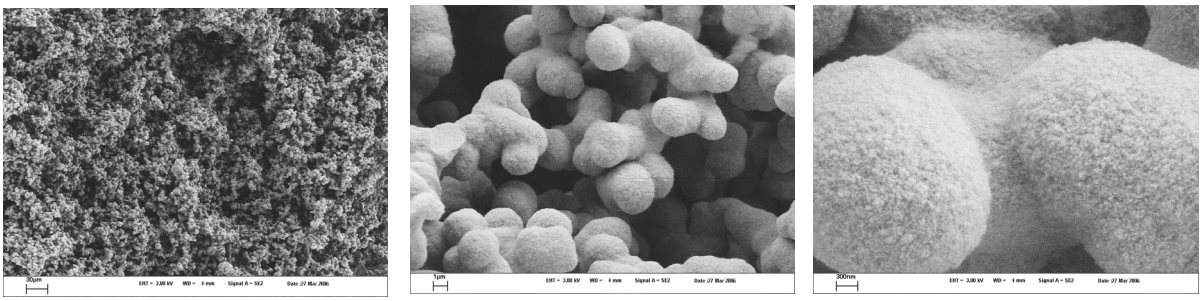

Figure 5.15: SEM micrographs of monolithic column materials made by cocondensation of 60 mg CBS-C_2 and 440 mg TEOS in a solution of 100 mg $PEO_{10'000}$ in 1.0 ml ethanol and 0.25 ml hydrochloric acid (pH=2)

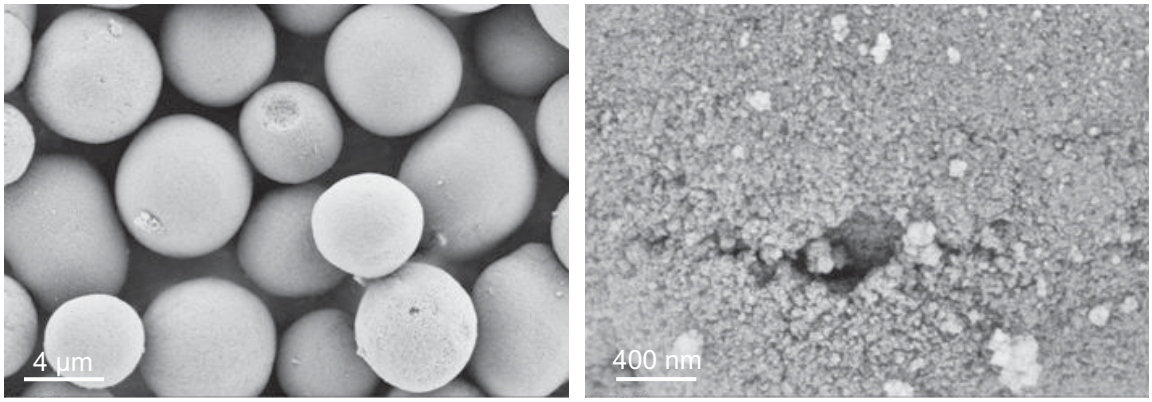

Figure 5.16: SEM micrographs of silica spheres for stationary phases used for the grafting process

chosen. Beside the economical use of the precursor this approach also guarantees that the functional group is located on the particle surface. For the grafting process, 5 µm mesoporous silica spheres from Merck were chosen as the starting material (Figure 5.16). The preparation pathway is simple, involving the synthesis of the chiral precursor CBS-C_2 (see chapter 5.2), followed by covalent attachment of this chiral molecule to the silica surface (Figure 5.17). The grafting of bridged silanes in general is a technique which yields more stable covalent linkage because of two involved bonds. Thus, the organic functionalities can be regarded as part of the wall. Further functionalization of the grafted particles towards amides or carbamates can than be carried out in order to tailor the column material.

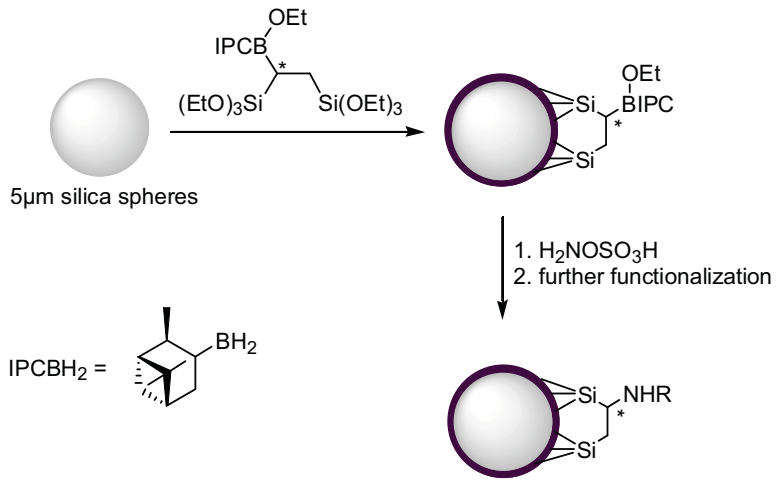

Figure 5.17: Synthetic pathway for surface functionalization of 5 µm silica spheres with CBS precursor

The following stationary phases where prepared and their performance for the chiral resolution of various enantiomers were studied. Furthermore the separation of racemic mixtures was intended to prove the accessibility of amine functionalities of CBS materials. In

order to obtain a maximum of possible interactions, different synthetic procedures were investigated regarding the maximum loading of organic functionalities onto silica spheres.

Two general procedures were used:

(i) grafting under aqueous conditions

(ii) grafting under non-aqueous conditions

For detailed synthetic procedure see the experimental section. In brief summary, aqueous conditions means that silica spheres were dispersed in a mixture of the appropriate solvent and hydrochloric acid followed by admixing of CBS-C_2. Grafting under non-aqueous conditions was carried out by refluxing the dispersed silica spheres and CBS-C_2 in anhydrous toluene. The different grade of functionalization with CBS-C_2, i.e. the campheyl borane derivative, was shown by means of TGA (Figure 5.18). All stationary phases were washed with ethanol and dried under the same conditions prior to the TGA analysis. The result of the analysis reveals a significant influence on the surface density of organic functionalities evoked by the choice of solvent for the synthesis under aqueous conditions. The mass loss is defined by the combustion of the organic moieties of the pure condensed CBS-C_2 precursor, i.e. no amine functionalization was carried out prior to TGA measurements.

While condensation in THF results in the lowest organic loadings, toluene enables an organic loading of 6.4 %. A relation of the reaction temperature and the loading can only be seen in the case of ethanol. The use of non-aqueous conditions yields a 5.5 % loading and gives a

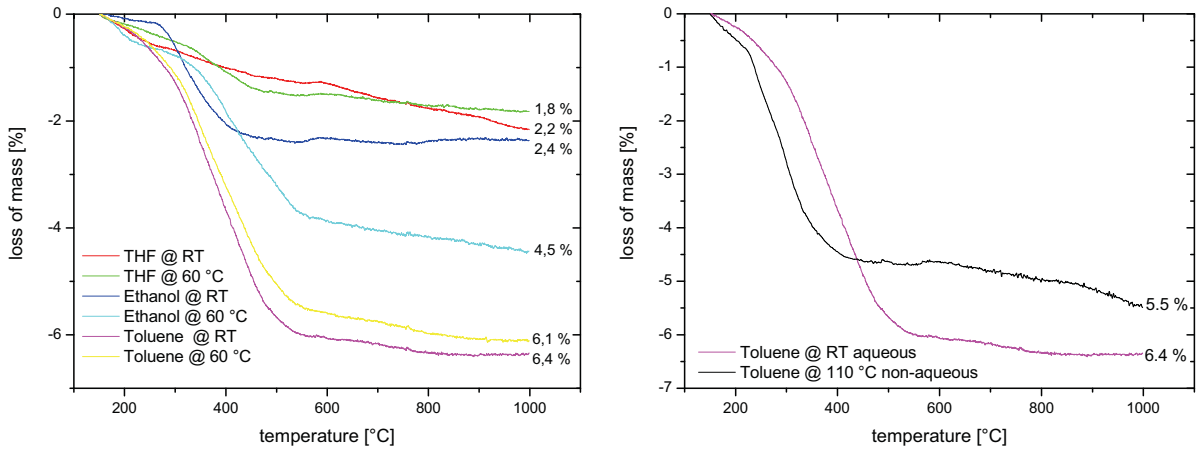

Figure 5.18: TGA results of CBS-C_2 grafted silica beads under various conditions: left → aqueous procedure; right → comparison of aqueous and non-aqueous procedure); all graphs are corrected by subtraction of a blank silica and normalized to 0 % at 150 °C in order to minimize the influence of adsorbed water or solvents

Table 5.5: Summary of stationary phases and their functionalization synthesized in this study: [a] dNPh = 3,5-dinitrophenyl; [b] anhydrous/aqueous refers to grafting conditions of precursor onto silica beads (for details see experimental section)

entry	R[a]	conditions[b]
chi StaPh 1	H	anhydrous
chi StaPh 2	CO-Ph	aqueos
chi StaPh 3	CO-dNPh	anhydrous
chi StaPh 4	CO-dNPh	aqueous

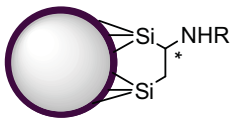

somewhat lower loading than the analogue functionalization done under aqueous conditions.Consequently, both procedures were used to obtain the basic CBS-C_2 functionalized silica spheres for the use as stationary phases.

On the basis of the results for the grafting conditions different chiral stationary phases were prepared under either aqueous conditions or in non-aqueous media. The employed phases are summarized in Table 5.5. While chi StaPh 1 possess only the chiral amine functionalities on the surface, the possibility for stationary phases analyte interactions was further improved by the functionalization to benzamide (chi StaPh 2) and dinitro-benzamide (chi StaPh 3, 4). The latter functionalization is closely related to PIRKLE stationary phases (Type I) and was already shown to provide good separation in a wide variety of aromatic analytes (see HPLC introduction). All stationary phases possess good accessibility of the pores and subsequently

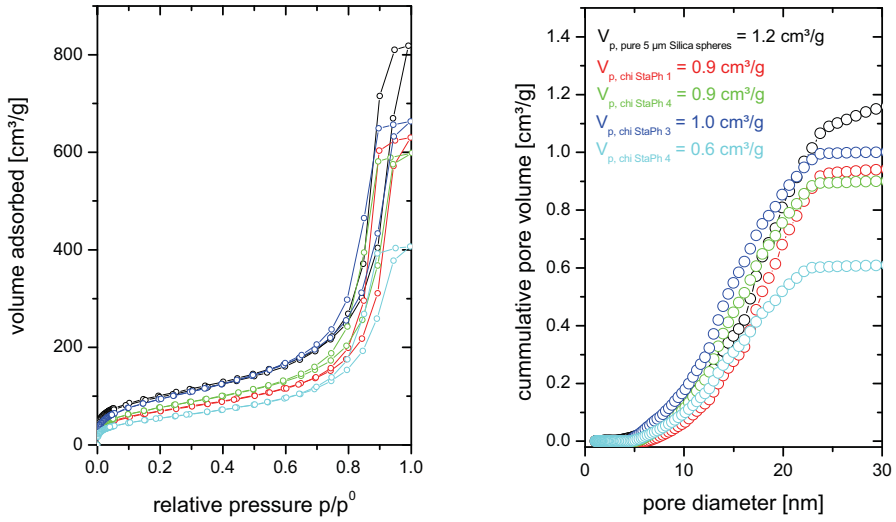

Figure 5.19: Nitrogen adsorption isotherms and NLDFT cumulative pore volume for unfunctionalized pure 5 µm porous silica spheres (-) and stationary phases chi StaPh 1 (-), 2 (-), 3 (-), and 4 (-)

of the selectors after complete functionalization, as indicated by nitrogen adsorption (Figure 5.19). The different nitrogen uptakes and the cumulative pore volume for the chi StaPh 1 to 4 provide a clear conclusion on the surface coverage of functional groups after functionalization (for TGA measurements and elemental analysis see experimental section). Thus, the highest amount of coverage is obtained in the case of chi StaPh 4, followed by the other chi StaPh with a somehow similar organic loading. These findings are important in order to justify the later chiral resolution and give an insight on a possible lack of performance.

The capability for chiral resolution of the pure enantiomers on these 4 stationary phases was studied under isocratic conditions with different mobile phases and analytes (Table 5.6). Even chi StaPhs with simple selectors, such as a chiral primary amine show promising chiral resolution for mandelate esters and indanol with typical separation factors of about 1.05. Further aliphatic and aromatic, polar and unpolar analytes like ethyl lactate, 1-phenyl-1-

Table 5.6: Chiral resolution of mandelate esters and indanol on stationary phase; [a]isocratic mobile phase composition given (hexane:ethyl acetate)

analyte	condition[a]	k	α	N
	chiStaPh 1			
R-methyl mandelate	90:10	3.93	1.04	96
S-methyl mandelate	90:10	4.08		66
	chiStaPh 2			
R-methyl mandelate	90:10	9.44	1.08	56
S-methyl mandelate	90:10	8.74		39
	chiStaPh 3			
R-methyl mandelate	90:10	7.47	1.06	34
S-methyl mandelate	90:10	7.91		36
R-methyl mandelate	85:15	3.77	1.05	34
S-methyl mandelate	85:15	3.95		26
R-indanol	85:15	5.11	1.01	20
S-indanol	85:15	5.14		18
	chiStaPh 4			
R-methyl mandelate	90:10	7.58	1.09	35
S-methyl mandelate	90:10	8.29		32
R-methyl mandelate	85:15	5.06	1.07	34
S-methyl mandelate	85:15	5.42		29
R-indanol	85:15	5.86	1.00	46
S-indanol	85:15	5.85		43

ethylamine, mandelic acid and 1,1-bi-2-naphthol dibenzoate were used but no chiral resolution was observed. Additionally change of the mobile phase to reverse phase conditions like water : alcohol (ethanol, methanol) gave no improve of the performance (not shown). These preliminary results are a good hint for the successful modification of the silica spheres and proving the accessibility of the chiral functionalities. However, an impact of the different surface functionalities (from primary amines via benzamides to nitro benzamides) on the resolution cannot be observed. This is probably caused by the poor resolution of single peaks from the pure enantiomers, expressed by the low number of theoretical plates. This might be the result of either non-specific binding of the analyte with surface silanol groups or the very high loading with the CBS-C_2 precursor. The latter reason might cause the generation of additional microporosity due to the porogenic properties of the precursor. This would lead to a diminished mass transport within the stationary phase. Although the separation factor when the pure enantiomers are injected separately is promising, a separation of a racemic mixture was not observed which can be traced back to the low number of theoretical plates, too. Even though chiral resolution of methyl mandelate was not feasible when changing the substitution of the chiral ester from methyl to butyl an enantio-separation was observed (Figure 5.20). Higher homologues of mandelic acid ester derivatives consequently possess increased hydrophobic interactions with the phenyl functionality of the stationary phase, leading to a higher separation factor (α = 1.26).

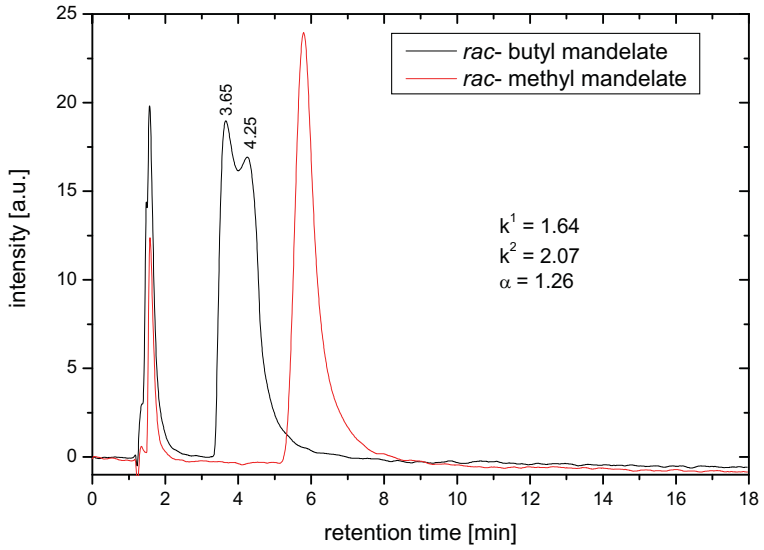

Figure 5.20: Chromatogram of separation of *rac*-butyl mandelate (isocratic mobile phase hexane : chloroform = 70 : 30, UV-detector @ 250 nm, chi StaPh 2)

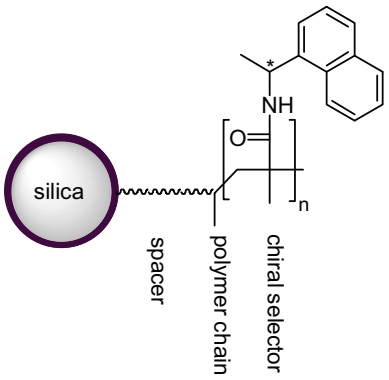

Figure 5.21: Functionalization of commercial YMC chiral NEA® stationary phase (methacrylate-(-α-naphthyl) amine copolymer bonded)

Interestingly, the separation factor obtained for chiral resolutions of methyl mandelate on all presented chiral stationary phases is similar to those of a comparable functionalized commercial column (YMC chiral NEA®) (Figure 5.21). Unfortunately, this does not lead to the same separation since the resolution of single peaks, expressed by the number of theoretical plates, is significant lower for the here synthesized stationary phases compared to the YMC column (Table 5.7). While the commercial column exhibit about 1600 theoretical plates, the chi Staph 4 exhibit less than 100 theoretical plates resulting in broad peaks and an overlay of the peaks for racemic mixture. This can be explained by the use of the Van Deemter Equation and its different contributions (Equation 5.1). H describes the height

$$H = \frac{l}{N} \qquad H = A + B \cdot u + \frac{C}{u} \qquad \textbf{5.1}$$

equivalent to a theoretical plate, N is the number of theoretical plates, l is the length of the column, u is the mobile phase velocity, A is Eddy diffusion, B is longitudinal diffusion and C

Table 5.7: Chiral resolution of methyl mandelate on commercial and here described chi Staph 4 column; [a]isocratic mobile phase composition given (hexane:ethyl acetate)

analyte	conditions[a]	k	α	N
	YMC chiral NEA®			
R-methyl mandelate	90:10	4.46	1.05	1557
S-methyl mandelate	90:10	4.70		1612
	chiStaPh 4			
R-methyl mandelate	90:10	7.58	1.09	35
S-methyl mandelate	90:10	8.29		32

describes the mass transfer between stationary and mobile phase. As observed from this equation, the mobile phase velocity has a strong influence on the final separation. Thus, a variation of this parameter from the standard velocity of 1.0 ml/min which was used for all separations, to 0.5 and 2.0 ml/min was carried out, but results in no significant improvement of the resolution. Since the influence of parameter A and B can be neglected because of the use of a standardized packing material and anyhow shorter columns for the chi StaPh, the C parameter must have a strong influence on the final separation. This mass transfer dependent parameter is defined by the characteristics of the stationary phase, like transport in pores or the interaction of the analyte with the surface. Thus, it can be recommended for further investigations to use first, lower loaded stationary phases, because a high CBS loading on the stationary phase might lead to the formation of additional micropores that will hinder the mass transport. Furthermore the analyte-stationary phase interactions need to be tailored to avoid non-specific analyte stationary phase interactions (e.g. modifying the chiral selector or the use of end capping).

However, these considerations adress the challenge of how to control the surface interactions and can explain the broadening of peaks by strong adsorption of the analyte on the surface. Since the stationary phases described in this work can hardly be compared with macromolecular commercial phases the rather low resolution can be explained. Chiral resolutions obtained with the here presented chi StaPh is a proof of the accessibility of the functionalities and more important a proves the chirality of the amine functionalities.

5.5 Catalytic activity of chiral amine functionalized silicas

Amine-functionalized chiral organosilicas with very high surface area and accessible functionalities were presented in Chapter 5.2. The amine functionalities in the CBS-C_2-NH_2 materials combine chirality with BRÖNSTED and LEWIS basicity (Figure 5.22). Hence, it was obvious to investigate the catalytic activity of these organosilicas for chiral discrimination. A set of typical base catalyzed reactions were chosen for investigation such as the catalytic activity for either chiral resolution or asymmetric synthesis. The difference in both principles for the synthesis of chiral substances lies in the reaction course. While chiral resolution starts from a racemic mixture, and the enrichment of one enantiomer is achieved by its higher reaction rate, asymmetric synthesis allows a stereo-specific reaction from

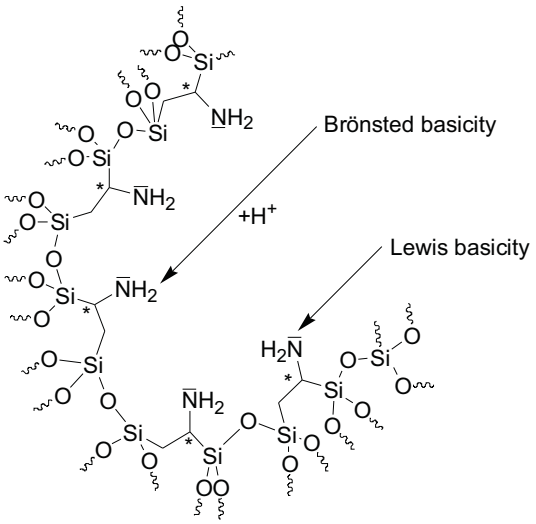

Figure 5.22: Basic functionalities in CBS-C_2-NH_2 materials

prochiral substrates to a chiral product. Comparing both methods, asymmetric synthesis offers a theoretical maximum yield of 100 % whereas chiral resolution provides a maximum yield of 50 % due to the employment of a racemic substrate. Thus, chiral resolution can be considered as a purification method leading to a pure enantiomer and is consequently a widely applied tool for purification of pharmaceuticals. Furthermore, by choosing both chiral resolution and asymmetric synthesis a distinctive difference in the chiral discrimination is expected. A general guideline is that reactions which take place in the presence of two chiral reagents are elevated in terms of stereoselectivity compared to reactions where only one chiral centre is involved.[207] Thus, the usage of a chiral resolution like transesterification is supposed to result in a higher enantiomeric excess (ee) compared to an asymmetric synthesis. Therefore, chiral discrimination by the use of the CBS-C_2-NH_2 catalysts was investigated for chiral resolution, namely esterification, transesterification, and KNOEVENAGEL reaction and for asymmetric synthesis, namely aldol reaction (Figure 5.23). In general, the catalytic activity for the transesterification of β-ketoesters by aminopropyl functionalized silica[208] and the primary amine catalyzed KNOEVENAGEL condensation of ethyl cyanoacetate with various aldehydes and ketons is described.[209,210,211] The aforementioned reactions were carried out by use of the CBS-C_2-NH_2-1 organosilica (see Chapter 5.2) as catalyst. The reaction conditions are summarized in the following. The heterogeneous catalyst was prior to use treated with ammonia followed by removal of the excess ammonia by washing with ethanol and evaporation of the solvents. This step ensures the deprotonation of the ammonium functionalities of the catalyst to the needed basic amines. For the reaction, the

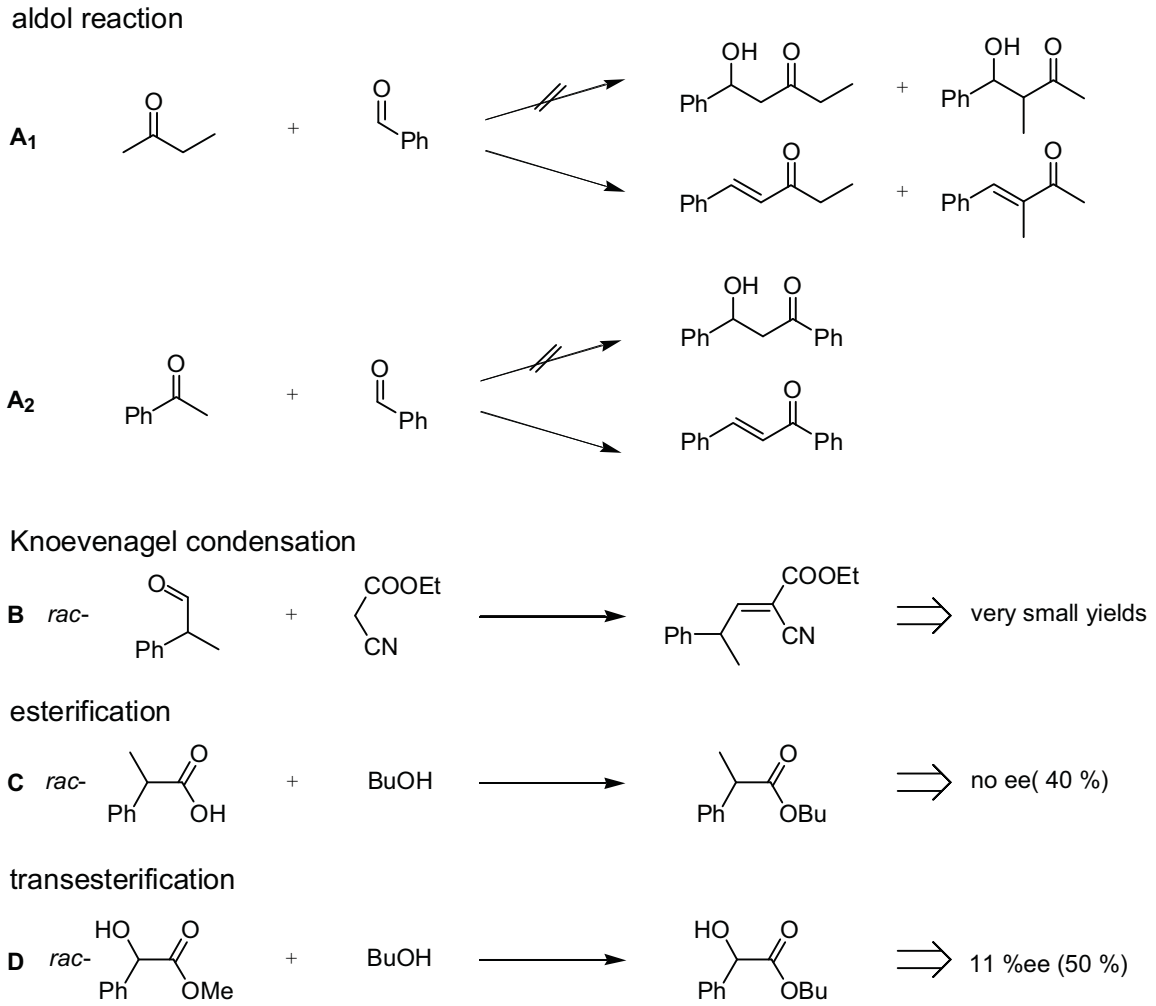

Figure 5.23: Catalytic activity of CBS-materials

catalyst was dispersed in either the reagents or in an appropriate solvent. The exact reaction conditions are described in the experimental section. The reaction courses were first monitored with GC-MS and ^{1}H NMR to verify the products and in a second step the obtained products analyzed with HPLC equipped with chiral-NEA(R)-NP column.

Under the applied conditions the aldol reaction of benzaldehyde with either 2-butanone (A_1) or benzophenone (A_2) do not yield the addition products but went one step further with very high conversion towards the condensation products (Figure 5.23). As a result of the formation of the double bonds, no stereogenic centre is generated and thus, no enatiomeric excess is observed. The KNOEVENAGEL condensation (B) led to only very small yields. This was probably caused by chemical adsorption of 2-phenyl-1-propanal on the catalyst, as indicated by GC measurements. The substrate can not be detected after adding the catalyst. The esterification (C) of 2-phenylpropionic acid was observed but the reaction was proved to

be non-stereoselective. In contrast, transesterification of methyl mandelate (D) shows a clear enatiomeric excess of 11 %, proving the asymmetric induction caused by the catalyst. This validates the accessibility of the chiral functionalities and is another proof for the chirality of the amine functionalities in CBS materials. The finding of 11 %ee of course do not convince compared to other asymmetric catalysts but considering that the catalytic active species is a chiral amine only, and not a difficile constructed catalyst which has to be synthesized by tedious efforts, this result is promising. Catalysts described in literature are usually based on the kinetic resolution induced by enzymes[212] (e.g. the kinetic resolution of *rac*-1-phenylethanol to the corresponding acylester was catalyzed by P. aeruginosa lipase)[213]. These macromolecules possess a very high catalytic activity and can for that reason hardly be compared with the CBS materials. In addition, hydrolysis in aqueous media is often preferred instead of transesterification because of the position of the equilibrium state and need of water for the kinetic resolution by lipases[214]. Therefore the kinetic resolution obtained here shows an interesting venture towards the kinetic resolution in non-aqueous media with a simple catalyst.

5.6 Summary

A new organosilica precursor for the synthesis of chiral, amine-functionalized micro- and mesoporous organosilicas is presented. The final material is obtained after a condensation-ammonolysis sequence. This precursor combines three roles of a network builder, a chiral and latent functional group and a porogen. It was shown that these precursors do self-organize after hydrolysis of their inorganic part via an aggregation of their organic moieties into hydrophobic domains. Furthermore, the size of these hydrophobic domains can be tailored depending on the boron substituents. The tri-valent boron centre enables not only the linkage of the silica source and the porogens but furthermore the covalent linkage with an alcohol. Thus reaction with ethanol yields a smaller template and correspondingly small pores with average diameters of 2.0-2.6 nm while the observed pore sizes are much larger (up to 5 nm) when hexadecanol is added as a pendant side chain. All materials possess very high surface areas but the highest surface areas were observed for organosilicas prepared with admixed pure inorganic precursors in a TEOS/CBS molar ratio of 4:1 yielding an organosilica with a surface area of 1010 m^2/g.

All synthesized organosilicas displayed disordered, worm-like pore systems but it was shown that the precursors can be also used in a similar fashion as conventional PMO precursors. Common surfactants, such as the block-copolymer F127, can be admixed to further control and tailor the resulting mesoporous system and finally create chiral *periodic* mesoporous organosilicas.

The chirality of the material which is a vital point for applications was proven using circular dichroism measurements. Furthermore the accessibility of the chiral functional groups was successfully validated via enatiomeric discrimination by chiral HPLC and asymmetric catalysis.

6. Conclusion

The aim of this work was to open new pathways in structuring and functionalizing organosilica materials. This was successfully achieved through the presented developments on boron-silane precursor concept. The approach resulted in micro- and mesoporous organosilicas with all necessary properties already embedded in the molecular architecture of the precursor. These precursors combine the properties of a network builder, a latent functional group and a porogen. The precursors are prepared by the convenient hydroboration which enables by sequential reaction management the linkage of a silica source and a structure directing moiety. In this work bis(triethoxysilyl)ethene was exclusively used as inorganic substrate for the hydroboration but the concept can be expanded to a variety of unsaturated silanes as well. More important is the possibility to tailor the structure directing moiety (porogen) and therefore directly influence the morphology of the resulting organosilica. Here, the investigated range of porogens reached from *n*-alkenes with different alkyl chains length to polymeric porogens. Another benefit that arised from borane chemistry is the potential of generating chiral organosilicas by exploiting asymmetric hydroboration.

In general, it could be shown that these boron-silane precursors do self-organize after hydrolysis of their inorganic part *via* an aggregation of their organic parts into hydrophobic domains. Thus, after chemical cleavage of the boron linkers and extraction, a porous, functionalized organosilica is obtained. The former pendant porogenes determine the resulting pore size and are decisive for formed functionalities to be exclusively located on the pore walls. Utilizing this procedure, materials with different pore sizes ranging from micropores to mesoporous were obtained. Additionally, it was shown that various functional groups can be addressed by the appropriate chemical cleavage reaction of the boron linker. This is one of the major advantages of the hydroboration approach since substitution of organoboranes provide a multitude of functional groups that can be incorporated into the silica network.

Here, the results in each chapter referring to the boron-silane precursor concept will be summarized. Starting with the possibility to tailor the pore size using different alkyl group porogens which include a full characterization of these organosilicas and the validation of the accessibility of amine functionalities. Then continuing with the expansion of this concept to

polymeric porogens and finally leading to chiral organosilicas and their application in chromatography and catalysis:

LCBS

Long chain boron silane precursors (LCBS) were synthesized by the covalent linkage of a bridged sol-gel-precursor (BTSE) and a porogen (long chain alkene) using hydroboration. This facile, one-pot synthesis enables the grafting of alkyl chains with different chain length (pentyl, decyl, dodecyl, hexadecyl, eicosyl) onto the precursors. Upon hydrolysis of the inorganic moieties these pendant alkyl chains self-organize into hydrophobic domains of different sizes. These hydrophobic domains are, after splitting of the carbon-boron bonds via ammonolysis, reflected in the pores of the resulting amine-functionalized organosilicas. Microporous organosilicas are observed when short chains (pentyl) are attached to the precursors, while decyl- and dodecyl chains yield materials with super-micropores and small mesopores and hexadecyl-chains mesoporous organosilicas. Thus, depending on chain length micro- to mesoporous materials with average pore sizes from 1.5 nm to 4.1 nm for attached pentene to hexadecene chains, respectively, were obtained. All synthesized organosilicas show wormlike pore structure with high surface areas (beside LCBS-C_5) between 700 and 800 m^2/g. Furthermore, the reaction pathway *via* boron groups enables the subsequent introduction of various functional groups into the pore walls of the organosilica networks. Amine or hydroxyl functionalities have been introduced into the organosilica walls, dependent on the experimental conditions used during the borane cleavage and extraction step. Copper adsorption experiments proved the accessibility of these functionalities by a significant metal adsorption onto the amine-functionalized organosilica walls.

Stabilization of the somehow flexible ethylene bridged silica network can be achieved by admixing TEOS to the LCBS-C_{10} precursor yielding organosilicas with very high surface areas of up to 1080 m^2/g. It should be noted that the stiffness of the pure precursor itself is sufficient to generate a highly porous material and as opposed to mixtures containing 90 % TEOS, yielding materials that still has accessible and interconnected pores. Thus, by the use of the pure precursor without admixing a network stabilizer like TEOS, high loadings of functionalities can be realized. In contrast, the possibility to synthesize organosilicas with a high concentration of TEOS under preservation of the porosity and accessibility of the functionalities makes the LCBS approach very efficient and therefore affordable.

Furthermore, it was exemplary shown for LCBS-C_{10} that the use of ethanol to mediate the solubility of the hydrophobic precursor is not necessary. Although the condensation of the precursor shows macrophase separation, indicated by strong turbidity, the final porosity was not significantly affected. In contrast, under the aid of ethanol to support the precursor solubility, a transparent gel is obtained proving the homogeneity of the material. Chemical removal of the boron organyl versus thermal removal was investigated, showing that calcination yields denser material with a lower porosity. This can be explained firstly by the removal of the organic bridges, resulting in a partial structural collapse, and secondly the coverage of the surface with boron oxide.

It can be assumed that a continuous tailoring of the pore size is further possible by mixing precursors with different chain lengths, as it is observed for alkyl surfactants.[49] Furthermore, the self-organization hydrophobic motif can be possibly varied from alkyl chains to other structure directing motifs. Precursors of this Type might yield organosilicas with predefined and adjustable pore sizes, functionalities and morphologies.

Polymeric Porogenes

This chapter of the work proves the applicability of the double hydroboration for the formation of boron silane precursors with anchored polymeric porogenes. This is therefore an expansion of the presented LCBS concept to homopolymers with grafted silane groups (PB-SIL) or block-copolymers with silane groups grafted on one block exclusively (PS-PB-SIL). Although PB-SIL does not show an obvious amphiphilic character or obvious affinity to form molecular aggregates (e.g. charge transfer), the condensed precursor yields a structured, fibrous material. It is assumed that the formation is induced by a controlled intramolecular condensation of the silane functionalities of PB-SIL. In contrast, the silane functionalized poly(styrene-*b*-butadiene) (PS-PB-SIL) shows an obvious amphiphilic character. Dynamic light scattering experiments on PS-PB-SIL revealed structures with a hydrodynamic radius of 19.4 nm in ethyl acetate. It is assumed that hydrolysis of the silane functionalities results in a transformation to a hydrophilic block while PS remains hydrophobic. Condensation of the silanol functionalities then results in a solidification of the microphase separated structure. After removal of the organic porogen by calcination a porous silica is obtained which reflects the structure of the polymeric porogen. The microphase separation takes place even in highly

diluted state. Thus, the cast of single monodispersed micelles with a diameter of about 14 nm is possible.

These findings are an incentive for anchoring further porogens to the precursor to generate predefined material morphologies.

Chiral Organosilicas

A new organosilica precursor for the generation of chiral and amine-functionalized organosilicas was presented. The synthetic pathway is simple involving enantioselective hydroboration using *S*-monoisopino-campheylboran on an ethylene bridged silica precursor. It can be shown that the size of the hydrophobic domains and therefore the resulting pore sizes can be tailored, depending on the boron substitution. Thus, the termination-reaction of the silane functionalized monoisopino-campheylboran with ethanol leads to a smaller template and corresponding small pores with average diameters of 2.0-2.6 nm, while the observed pore sizes are much larger (up to 5 nm) when hexadecanol is added as a pendant side chain. After a condensation-ammonolysis sequence, amine-functionalized, chiral mesoporous organosilicas are obtained. The highest surface areas were observed for organosilicas prepared with admixed pure inorganic precursors in a TEOS/CBS molar ratio of 4:1 yielding an organosilica with a surface area of 1010 m^2/g. However, it was also shown that the pure organosilica precursor is stable enough to at least partially maintain porosity, so that porous organosilicas with an organic monomer content of 100% can be prepared. All these direct organosilicas displayed disordered, worm-like pore systems.

It was shown that the presented monomers can also be used in a similar fashion as conventional PMO precursors: common surfactants, such as the block-copolymer F127, can be admixed to further control and tailor the resulting mesoporous system and finally create chiral *periodic* mesoporous organosilicas.

The chirality of the resulting organosilicas was proven using circular dichroism measurements. A strong optical activity was observed for the pure organosilica, attributable to the chiral amines in the framework. Addition of the achiral chromophore benzoic acid leads to an additional signal in the CD-spectrum indicative for the interaction of the benzoic acid with the chiral amines, proving that the chiral functional groups are indeed accessible for molecules entering the pores.

The described properties of the presented organosilicas make them interesting for a variety of applications which was verified by asymmetric catalysis and chromatographic separation of optically active compounds. For the latter case a new stationary phase modified with the here presented chiral precursor was prepared. Both, the chiral resolution by HPLC and the kinetic resolution by catalysis show a remarkable enantiomeric discrimination, proving the accessibility of the amine functionalities and more important the chirality of the surface.

The insights gained based on the boron-silane precursor approach open a multitude of prospects for the targeted structuring and functionalization of mesoporous organosilicas. This work can therefore contribute to the enormous developments of the past decade and further demonstrates the potential of siliceous sol-gel chemistry.

7. Appendix

7.1 Characterization

Transmission Electron Microscopy (TEM) images were taken using a Zeiss EM 912Ω operated at an acceleration voltage of 120 kV. Samples were ground in a ball mill and dispersed in ethanol. One droplet of the suspension was applied to a 400 mesh carbon-coated cooper grid and left to dry in air. For imaging micelles of the condensed PS-PB-SIL, one droplet of the acidified ethanolic solution was applied to a 400 mesh carbon-coated aurum grid and left to dry in air for 20 min and then heated up to 350 °C within a half hour.

Scanning Electron Microscopy (SEM) was performed on a LEO 1550- Gemini instrument. The samples were loaded on carbon coated stubs and coated by sputtering with a Au/Pd alloy prior to imaging.

Nitrogen adsorption data were obtained with a Quantachrome Autosorb-1 or Qudrasorb at liquid nitrogen temperature (77 K). Before measurement all samples were degassed at 80 °C for 20 hours. Evaluation of the obtained data was done by using the instrument software provided by Quantachrome. Therefore classical BET and NLDFT models were used. Micropore analysis was done by the use of the equilibrium model for the adsorption of nitrogen on silica under assumption of cylindrical pores.

Elemantal Analysis (EA) was done using a Vario EL Elementar. The samples were analyzed for Carbon, Hydrogen and Nitrogen content.

Ultra Centrifugation (UC) Analytical ultracentrifugation was performed with a Beckman Optima XL-I centrifuge (Beckman/Coulter, Palo Alto, CA) with a scanning absorption optics and on-line Rayleigh interferometer.

Thermogravimetric Analysis (TGA) measurements were carried out on a Netzsch thermoanalyzer TG 209 F1, measuring under oxygen form room temperature to 1000°C.

Gel Permeation Chromatography (GPC) Thermo Separation Products GPC setups were used equipped with UV (TSP UV1000) and refractive index (Shodex RI-71) detectors. The column set employed was 30 x 0.8 cm, 5 µm MZ-SD*plus*: 10^3, 10^5, and 10^6 Å. Analyses were performed at 30 °C with THF as the eluent at a flow rate of 1.0 ml/min.

Dynamic light scattering DLS measurements were carried out at 20 °C with a spectrometer consisting of an argon laser (λ= 488 nm, 500 mW; Coherent Innova 300), a self-constructed goniometer, a single-photon detector (ALV SO-SIPD), and a multiple-τ digital correlator (ALV 5000/FAST).

Small Angle X-ray Scattering (SAXS) measurements were performed using a rotating anode x-ray source with pin-hole geometry for the generation of Cu-K_α radiation. Detection of the scattered beam was realized with a two-dimensional marccd camera. The sample to detector distance was 740 mm.

Fourier-Transform Infrared Spectroscopy (FTIR)-spectra were collected using a BIORAD FTS 6000 spectrometer equipped with an attenuated total reflexion (ATR) setup.

^{1}H, ^{13}C NMR spectra were recorded on a Bruker DPX 400 spectrometer in $CDCl_3$ solution. For the calibration $CDCl_3$–signals for ^{1}H (δ = 7.24 ppm) and ^{13}C (δ = 77.0 ppm) were used

^{29}Si, **^{11}B** and **^{1}H→^{13}C CP MAS NMR** spectra were recorded on a Bruker AVANCE 400 spectrometer (Larmor frequencies: ν_{29Si} = 79.5 MHz; ν_{11B} = 128.4 MHz, ν_{1H} = 400.1 MHz, ν_{13C} =100.6 MHz) using a 4mm MAS probe (Bruker Biospin) and applying a spinning speed of 10kHz.

^{29}Si MAS NMR (I=1/2) spectra with 2750 accumulations were recorded with a π/2 pulse duration of p1=4.25 μs, a spectrum width of 20 kHz and a recycle delay of 120 s. ^{11}B MAS NMR (I=3/2) spectra were recorded with an excitation pulse duration of 1μs and referenced with respect to the chemical shift of ^{11}B in $BF_3{\cdot}OEt_2$. The recycle delay was chosen as 1s, the accumulation number was 1800.

The contact times of the ^{1}H→^{13}C CP MAS NMR experiments were optimized as 1ms for the boron containing precursor and 0.25ms after ammonolysis. Values of the isotropic chemical shifts of ^{1}H, ^{13}C and ^{29}Si are given with respect to TMS.

Circular Dichroism (CD) A J-715 spectrometer from Jasco was used. All samples were dispersed in $CHCl_3$ and measured in a 1 mm quartz cuvettes (data pitch: 0.2 nm; band width: 2.0 nm; response: 2 sec). For each spectrum 5 single measurements were accumulated and corrected by subtraction of the baseline.

Atomic Adsorption Spectroscopy (AAS) of copper was done using a Perkin Elmer AAS at 324.8 nm. For the calibration a standardized $Cu(NO_3)_2$ (c= 1,000+/-0,002 g/L) solution purchased from Merck was used and further diluted with bidistilled water to final concentration.

High Performance Liquid Chromatography (HPLC) was done with an Agilent 1200 series instrument equipped with a diode array detector. The detection wavelength was set at 254 nm, the cartridge cooling system was thermostated to 25 °C. The stationary phase material was approved in self-packed VERTEX columns (dimensions 120 x 4 mm). If not mentioned else, the flow was set to 1.0 ml/min and 5 µl of the sample was injected.

7.2 Experimental Section

Chemicals:

Bis(triethoxysilyl)ethene was synthesized by alkene metathesis of triethoxysilylethene.[215] Triethoxysilylethene was purchased from Gelest. Hydroxylamine-o-sulfonic acid, borontrifluoride diethyletherate, tetraethoxysilane (TEOS), borane-dimethylsulphide complex (2M in THF), all 1-alkenes and (*S*)-Alpine-Boramine™ were obtained from Aldrich. Copper standard solution was obtained from Merck as $Cu(NO_3)_2$ (c_{Cu} = 1,000 +/- 0.002 g/L and further diluted with 0.5 M nitric acid to obtain the desired concentration. Solvents for reactions under moisture exclusion were prepared according standard procedures. All further commercial chemicals were used without additional purification.

7.2.1 Synthesis of long-chain-boron-silanes (LCBS)

Synthesis of the LCBS-C_x precursors:

The reaction was carried out under N_2-atmosphere. In a typical synthesis 2.13 g (6.04 mmol) of bis(triethoxysilyl)ethene was dissolved in 25 ml dry THF at 0°C and then 3.02 ml (6.04 mmol) borane-dimethylsulphide complex was added. The mixture was stirred for 19 hours and allowed to warm up until RT. According to the desired product the appropriate 1-alken (6.04 mmol) was added at RT and the solution was stirred for another 3½ hours, followed by the addition of 0.53 ml (9.06 mmol) dry ethanol. The solvent was removed under vacuum to give the corresponding LCBS-C_x precursor.

^{1}H-NMR:

LCBS-C_5: colorless liquid
3.82 (m, 2 H, BOCH), 3.80 (t, J= 7.0 Hz, 6 H, SiOCH), 3.79 (t, J= 6.3 Hz, 6 H, SiOCH), 1.53 (m, 2 H, $CH_{alliphat}$), 1.24 (m, 6 H, $CH_{alliphat}$) 1.18 (m, 21 H, $CH_{alliphat}$) 0.87 (m, 6 H, $CH_{alliphat}$).

LCBS-C_{10}: colorless liquid
3.81 (m, 2 H, BOCH), 3.80 (t, J= 7.1 Hz, 6 H, SiOCH), 3.79 (t, J= 6.3 Hz, 6 H, SiOCH), 1.54 (m, 2 H, $CH_{alliphat}$), 1.18 (m, 37 H, $CH_{alliphat}$), 0.86 (m, 6 H, $CH_{alliphat}$).

LCBS-C_{12}: colorless liquid
3.82 (m, 2 H, BOCH), 3.80 (t, J= 7.1 Hz, 6 H, SiOCH), 3.79 (t, J= 8.6 Hz, 6 H, SiOCH)), 1.54 (m, 2 H, $CH_{alliphat}$), 1.23 (m, 41 H, $CH_{alliphat}$), 0.86 (m, 6 H, $CH_{alliphat}$).

LCBS-C_{16}: colorless viscous liquid
3.82 (m, 2 H, BOCH), 3.80 (t, J= 7.1 Hz, 6 H, SiOCH), 3.79 (t, J= 6.7 Hz, 6 H, SiOCH)), 1.55 (m, 2 H, $CH_{alliphat}$), 1.23 (m, 49 H, $CH_{alliphat}$), 0.86 (m, 6 H, $CH_{alliphat}$).

LCBS-C_{20}: white solid

3.82 (m, 2 H, BOCH), 3.80 (t, J= 7.0 Hz, 6 H, SiOCH), 3.79 (t, J= 6.8 Hz, 6 H, SiOCH)), 1.55 (m, 1 H, $CH_{alliphat}$), 1.23 (m, 58 H, $CH_{alliphat}$), 0.86 (m, 6 H, $CH_{alliphat}$).

Condensation of LCBS-C_x:

Differnent silicas were synthesized by the use of appropriate LCBS-C_x precursor. All silicas were synthesized according to the following molar ratio, LCBS:TEOS:EtOH:HCl:H_2O=1:4:9.5:2.77:15.4. In a typical synthesis 0,54 mmol of the LCBS precursor and 450 mg (2,16 mmol) TEOS were dissolved in 300 µl (5,14 mmol) ethanol and then 150µl hydrochloric acid (pH = 2.0) added. The solution was stirred in a closed vial for 10 minutes accompanied with slight heating to approximately 50 °C to ensure complete homogenization. The silica solution was then aged for 2 days at 60 °C to give the monolithic solids.

Amine functionalization yielding LCBS-C_x-NH_2:

The crude silica condensate was mechanically crushed, and then the proper quantity of silica powder consisting of 0.42 mmol of boron dispersed in 5.0 ml diglyme. To this mixture 0.21 g (1.86 mmol) hydroxylamine-*O*-sulfonic acid were added and stirred at 60°C for 4 hours. After the suspension was cooled down to RT the solvent was removed by centrifugation. The obtained solid was stirred in a mixture of 20 ml HCl (pH = 2) and 20 ml ethanol over night and then extracted with EtOH and THF. Additional purification of the organosilica was realized by washing with ammonia 1N and then repeated centrifugation and washing with THF. All solvents were removed under vacuum at 60°C to give a white solid.

Hydroxyl functionalization yielding LCBS-C_x-OH:

0.25 g of the mechanically crushed organosilica was dispersed in a solution of 1.0 ml hydrogen peroxide (30 %) and 30 µl sodium hydroxide (0.1 M) and stirred at RT for 5 hours. The reaction mixture was neutralized with 0.5 ml hydrochloric acid (pH=2) and 5 ml EtOH was additionally added. The liquid phase was centrifuged of and the solid was repeatedly washed with water (twice), ethanol (twice) and THF (twice). All solvents were removed under vacuum at 60°C to give a white solid.

Cu-adsorption experiments

50mg of the appropriate mechanical crushed silica were dispersed in a 0.1 M $CuCl_2$ in 0.1 M sodium acetate solution and shaken for 1 hour. The resulting mixtures were centrifuged and then 4 times washed with in total 4 ml of bidest water. The Cu loaded samples were dried at 60°C for 16h and then 40 mg these silica extracted with 3.0 ml hydrochloric acid. After 1.5 hour of shaking the solid material was centrifuged off and 4 times washed with bidest water. The combined aqueous phases were diluted to a total volume of 25 ml and then directly measured with AAS.

7.2.2 Synthesis of silane functionalized polymers (PB-SIL, PS-PB-SIL)

1,2- polybutadiene (PB)

Monomers and solvents were purified using conventional methods reported elsewhere in literature[216,217]. 1,2-PB(OH) was synthesized by anionic polymerization of 1,3-butadiene under dry argon atmosphere in THF solution at -78 °C using sec-butyl lithium as initiator. After 1 day, ethyleneoxide was added, and the solution was stirred for 3 days at RT. The polymer was precipitated into methanol and dried under vacuum.

$M_n^{(app)}$ 991 g/mol, PDI (polydispersity index) = $M_w^{(GPC)}/M_n^{(GPC)}$ = 1.5

Poly-(ethoxy(but-3-en)(1,2-bis(triethoxysilyl)ethylene)-borane (PB-SIL)

The reaction was carried out under nitrogen atmosphere. In a typical synthesis 1.40 g (4.00 mmol) bis(triethoxysilyl)ethene and 2.0 ml (4.00 mmol) borane dimethylsulphide complex (2M in THF) were dissolved in 20 ml anhydrous THF at 0 °C and stirred for 15 hours whereas the mixture was allowed to warm up to RT. Then 0.11 g 1,2-polybutadiene were added, followed by another 4 hours of stirring. Slow addition of 0.5 ml anhydrous ethanol gave the resulting polymer solution which was used as synthesized for the condensation.

Condensation of the silane functionalized polybutadiene

An ethanolic solution of the polymer (50 µl) was slowly added to 4.0 ml aqueous ammonia (0.25 %) and the resulting clear solution was aged in a sealed vial under static conditions for two days. SEM of the as synthesized material was carried out of the solid directly collected from the solution.

1,2-Poly(butadiene-*b*-polystyrene) (PB-PS)

Monomers and solvents were purified using conventional methods reported elsewhere in literature[216,217]. 1,2-PS-*b*-PB was prepared by sequential anionic polymerization of 1,3-butadiene and styrene under dry argon atmosphere in THF at -78 °C using sec-butyl lithium as initiator. 1,3-butadiene was condensed into a reactor containing a mixture of dry THF and sec-butyl lithium, and the solution was stirred over night at -78 °C. After withdrawal of an aliquot from the reactor, styrene was condensed into the reactor and polymerized for 1 h at -78 °C. The reaction was quenched with degassed methanol, and the polymer was precipitated in methanol and dried under vacuum at 40 °C.

$M_n^{(app)}$ 21390 g/mol, PDI (polydispersity index) = $M_w^{(GPC)}/M_n^{(GPC)}$ = 1.2 (polystyrene calibration)

Poly(styrene-*b*-(ethoxy)(but-3-en)(1,2-bis(triethoxysilyl)ethylene)-borane) (PS-PB-SIL)

The reaction was carried out under nitrogen atmosphere. At 0 °C 0.715 g (2.03 mmol) bis(triethoxysilyl)ethene was dissolved in 10 ml anhydrous THF and 1.01 ml borane dimethylsulphide complex (2M in THF) were admixed. The mixture was stirred for 18 h and allowed to warm up to RT. Then 0.359 g PS-PB dissolved in 2.0 ml anhydrous THF were added and the mixture was stirred at RT for another 3 h. Finally 0.14 ml anhydrous

ethanol were slowly added and the reaction mixture dialyzed in either EE or THF followed by ethanol, if needed.

Condensation of PS-PB-SIL

Condensation on Au-grid (imprinting of single micelles or cross-linked micelles)

Depending on the targeted micelle covering on the gold grid the initial PS-PB-SIL solution was obtained by diluting the dialysis solution with the appropriate amount absolute of ethanol. This mixture was than acidified with hydrochloric acid (pH=2) and applied to the gold grid. Drying of the gold grid at ambient temperature followed by rapid heating to 350 °C (1/2 hour) leads to the stabilization of the condensed PS-PB-SIL. The so prepared grids were directly used for TEM investigations.

7.2.3 Synthesis of silanes with chiral bridges (CBS)

Preparation of chiral boron silane precursor CBS-C_2 and CBS-C_{16}

The reaction was carried out under N_2-atmosphere. In a typical synthesis 4.80 g (11.7 mmol) of the (*S*)-Alpine-Boramine™ was dissolved in 40 ml dry THF at 0°C and then 2.90 ml (23.3 mmol) borontrifluoride diethyletherate was added. After 20 minutes the reaction mixture was warmed to RT and stirred for another 4 hours. The precipitate was filtered of and washed with dry THF. The clear solution was cooled to -20°C and 8.06 g (22.9 mmol) bis(triethoxysilyl)ethene was slowly added. While stirring for 18 hours the mixture was allowed to warm up to RT. According to the desired product the appropriate alcohol (22.9 mmol) was added at 0°C and the solution was stirred for another 2 hours. The solvent was removed under vacuum. Addition of heptane leads to precipitation of a white solid which was centrifuged off. The solid was washed with heptane and the solvent was removed to give the corresponding chiral precursor.

^{1}H NMR(CBS, 400 MHz): δ 0.95 (m br, 18 H, aliphatic H), 1.17 (t, *J* = 6.8 Hz, 9 H, $SiOCH_2C\underline{H}_3$), 1.18 (t, *J* = 6.8 Hz, 9 H, $SiOCH_2C\underline{H}_3$), 1.41 (m br, 5 H, aliphatic H), 3.79 (q, *J* = 6.8 Hz, 6 H, $SiOC\underline{H}_2$), 3.80 (q, *J* = 6.9 Hz, 6 H, $SiOC\underline{H}_2$), 3.84 (q, *J* = 6.8 Hz, 2 H, $BOC\underline{H}_2$).

^{1}H NMR(CBS-C16, 400 MHz): δ 0.87 (m, 7 H, aliphatic H), 1.06 (m, 4 H, aliphatic H), 1.18 (m, 16 H, aliphatic H), 1.23 (m, 39 H, aliphatic H), 1.51 (m, 3 H, aliphatic H), 3.80 (m, 14 H, $BOC\underline{H}_2$, $SiOC\underline{H}_2$).

Condensation of CBS-C_x

Various silicas were synthesized by modifying the precursor/TEOS ratios (see table 1). Regardless of the ratio Precursor/TEOS, all reactions mixtures contained a total amount of 5.00 mmol of silicon. These mixtures were dissolved in 3.0 ml ethanol and then 0.6 ml hydrochloric acid (pH = 2.0) added. The solution was homogenized in a closed vial for 5 minutes at RT. The silica solution was then aged for 2 days at 60 °C to give the monolithic solids.

Amine functionalization of CBS-C_x to CBS-C_x-NH_2

The crude silica condensate was mechanically crushed, and 0.35 g of the crude powder was dispersed in 5.0 ml diglyme. For every 1 mmol of boron containing in the silica, 2 mmol of hydroxylamine-*O*-sulfonic acid were added. The mixture was stirred at 60°C for 3 hours. After the suspension was cooled down to RT the solvent was removed by centrifugation. To completely remove the excess hydroxylamine-*O*-sulfonic acid and the cleaved organic residue the resulting material was stirred in 20 ml HCl (pH = 2) for 4 hours and then repeatedly washed with water, ethanol and THF. All solvents were removed under vacuum at 60°C to give a white solid.

CBS-C_2 PMO-Synthesis (CBS-F127)

For the synthesis of a chiral periodic mesoporous organosilica 0.5 g Pluronic® F-127 was dissolved in 10.0 ml absolute ethanol and then 0.10 g (0.19 mmol) chiral precursor, 0.16 g (0.76 mmol) TEOS and 50 µl HCl (pH = 2) were added. The mixture was stirred for 20 minutes at RT. The clear solution was filled into a petri dish and aged at RT for 5 hours and then additionally at 80 °C for 23 hours. The pale solid was mechanically crushed and dispersed in 20 ml ethanol and stirred over night at 60 °C to extract the surfactant. Functionalization by ammonolysis was carried out analogous to the CBS samples prepared without surfactants. Further purification was carried out by repeated washing/centrifugation with 20 ml ethanol and 20 ml acetone. After drying under vacuum for 2h at 60 °C a white solid was obtained.

Experimental section HPLC:

The 5µm silica beads (Si 100) spheres were obtained from Merck, the CBS-C_2 precursor for the functionalization was synthesized according to the procedure given above. Anhydrous toluene was dried under standard conditions. Benzoylchloride, anhydrous pyridine, and 3,5-dinitrobenzoylchloride were obtained from Merck.

Packing of the stationary phases was realized by a packing station from Knauer equipped with a P 1900 pneumatic pump. The methanolic slurry of the beads was pumped into the column and the pressure was kept static for another three minutes to ensure a tight packing.

General procedure for the activation of the silica beads:

5.0 g of the 5 µm silica beads were dispersed in a mixture of 100ml water and 100 ml concentrated hydrochloric acid and refluxed for 1 day. The beads were washed with deionized water and THF and then dried under argon stream at 100°C for 3 hours.

chi StaPh 1

1.07 g of the activated silica beads and 1.1 g CBS-C_2 precursor was dispersed in 100 ml dry toluene and then 0.3 ml hydrochloric acid (pH = 2)added. The mixture was shacked for 18 hours at 50 °C and then washed three times with ethanol, 50 ml each. After removal of all solvents under vacuum at 60°C the CBS-loaded silica beads were obtained. This material was then further amine-functionalized.

For the amine functionalization 2.05 g of the before synthesized CBS-loaded silica beads was dispersed in 10 ml anhydrous diglyme and 0.8 g hydroxylamine-*O*-sulfonic acid was admixed. This mixture was shaken at 70 °C for 3 hours. After cooling down to RT the beads were washed with water and ethanol, and then dried at 60 °C under vacuum to give amine-functionalized silica beads.

TGA: mass loss correlates to organic loading with C_2H_5N: 4.9 %

Elemental Analysis: N 0.96 %, C 2.41 %, H 0.963 % , Sum C,H,N = 4.3 %

chi StaPh 2

2.40 g of the activated silica beads and 1.55 g CBS-C_2 precursor was dispersed in 120 ml dry toluene and then 0.5 ml hydrochloric acid (pH = 2) added. The mixture was shacked for 18 hours at 50 °C and then washed three times with ethanol, 50 ml each. After removal of all solvents under vacuum at 60 °C the CBS-loaded silica beads were obtained. This material was then further amine-functionalized.

Therefore 2.05 g of the before synthesized CBS-loaded silica beads was dispersed in 10 ml anhydrous diglyme and 0.8 g hydroxylamine-*O*-sulfonic acid was admixed. This mixture was shaken at 70 °C for 3 hours. After cooling down to RT the beads were washed with water and ethanol, and then dried at 60 °C under vacuum to give amine-functionalized silica beads.

Further functionalization of the aminated silica was carried out under nitrogen atmosphere. Therefore 1.7 g of the aminated silica spheres were dispersed in a solution of 0.17 ml benzoylchloride, 0.5 ml dry pyridine in 5.0 ml dry methylenechloride at stirred for 2 hours at RT. The resulting material was washed three times with ethanol, 50 ml each and then dried under vacuum at 60 °C to give the benzoylamide functionalized silica spheres.

TGA: mass loss correlates to organic loading with C_9H_9NO: 5.2 %

Elemental Analysis: N 0.99 %, C 2.92 %, H 0.98 % , Sum C,H,N = 4.9 %

chi StaPh 3

Under argon atmosphere 3.06 g of the activated silica beads were dispersed in 60 ml dry toluene and then 2.00 g CBS-C_2 precursor added. The reaction mixture was refluxed for 13h and then the solvent completely removed at 60°C under vacuum. After washing three times with ethanol and drying under vacuum at 60°C the CBS-loaded silica beads were obtained which were then further functionalized to 3,5-dinitrobenzoyl amides.

Therefore 2.34 g of the before synthesized CBS-loaded silica beads were dispersed in 10 ml anhydrous diglyme and 0.8 g hydroxylamine-*O*-sulfonic acid were added. This mixture was shaken at 70 °C for 3 hours. After cooling down to RT the beads were washed with water and ethanol, and then dried at 60 °C under vacuum to give amine-functionalized silica beads.

2.0 g of these aminated beads, 3.13 g 3,5-dinitrobenzoylchlorid and 1.0 ml anhydrous pyridine were dispersed in 40 ml anhydrous methylenchloride and the mixture shaken for 10 hours at RT. The resulting material was

washed with methylenchloride, water and ethanol. After drying at 60 °C under vacuum the chi StaPh 3 was obtained.

TGA: mass loss correlates to organic loading with $C_9H_7N_3O_5$: 6.7 %

Elemental Analysis: N 1.14 %, C 3.47 %, H 0.992 %, Sum C,H,N = 5.6 %

chi StaPh 4

4.16 g of the activated silica beads and 2.77 g CBS-C_2 precursor were dispersed in 100 ml dry toluene and then 0.5 ml hydrochloric acid (pH = 2)added. The reaction mixture was refluxed for 13h and then the solvent completely removed at 60°C under vacuum. After washing three times with ethanol and drying under vacuum at 60°C the CBS-loaded silica beads were obtained. This material was then further functionalized to 3,5-dinitrobenzoyl amides.

Therefore 3.71 g of the before synthesized CBS-loaded silica beads were dispersed in 15 ml anhydrous diglyme and 1.2 hydroxylamine-*O*-sulfonic acid were added. This mixture was shaken at 70 °C for 3 hours. After cooling down to RT the beads were washed with water and ethanol, and then dried at 60 °C under vacuum to give amine-functionalized silica beads.

3.0 g of these aminated beads, 3.13 g 4,5-dinitrobenzoylchlorid and 1.6 ml anhydrous pyridine were dispersed in 60 ml anhydrous methylenchloride and the mixture shaken for 10 hours at RT. The resulting material was washed with methylenchloride, water and ethanol. After drying at 60 °C under vacuum the chi StaPh 4 was obtained.

TGA: mass loss correlates to organic loading with $C_9H_7N_3O_5$: 9.8 %

Elemental Analysis: N 1.76 %, C 6.35 %, H 1.184 % , Sum C,H,N = 9.3 %

7.3 Symbols and Abbreviations

AAS	atom adsorption spectroscopy
APTS	3-aminopropylsilane
BET	Brunauer-Emmet-Teller (Surface area chracterizeation)
BTSE	bis(triethoxysilyl)ethene
CBS	Chiral Boron Silane
Cp	cross polarization
CTAB	Cetyltrimethylammonium bromide
FTIR	Fuorir Transform infrared
LCBS	Long Chain Boron Silane
MTMS	Methyltrimethoxysilane
NLDFT	non linesr density function theory
NMR	nuclear magnetic resonance
PB	polybutadiene
PS	polystyrene
PSD	pores size distribution
SAXS	Small angle X-Ray scattering
TEM	transmission electron microscopy
TEOS	tetra ethoxysilane
THF	tetrahadrofurane
TGA	Thermo gravimetric analysis
TMOS	tera methoxysilane
XRD	X-ray difractometry

α	separation factor
a_0	cross section area
a_{surf}	surface area
b	broad
γ	surface tension
δ	chemical shift
d	dublett
d_P	pore diameter
F	packing factor
G	free energy
k	capacity factor
l	length
J	coupling constant
λ	wave length
L	Avogadro constant
m	mass / multiplett
$M_n^{(app)}$	apparent number-average molecular weight
ξ_{Prec}	relative precursor concentration
υ	electron velocity
p	pressure
p^0	saturation pressure
PDI	polydispersity index
σ	cross sectional area
R	ideal gas constant

s	scattering vector / sedimentation coefficient / singulett
T	temperature
t_R	retention time
U	voltage
V	volume
$V_{p,micro}$	micro pore volume
$V_{p,meso}$	meso pore volume
$V_{p,tot}$	total pore volume
W	peak width

7.4 Bibliography

[1] Prato, M. *J. Mater. Chem:* **1997**, *7*(7), 1097-1109.

[2] Ebbesen, T.W.; Ajayan, P.M. *Nature* **1992**, *358*(6383), 220-222.

[3] Baughman, R.H.; Zakhidov, A.A.; Heer W.A. *Science* **2002**, *297* (2), 787.

[4] Lee, N.S. *Diamond Relat. Mater.* **2001**, *10*, 265. Baughman, R.H.; Zakhidov, A.A.; Heer W.A. *Science* **2002**, *297* (2), 787.

[5] Vrieling, E.G.; Beelen, T.P.M.; van Santen R.A.; Gieskes, W.W.C. *J. Biotechnol.* **1999**, *70*, 39-51.

[6] a) Simpson, T. L. & Volcani, B. E. Silicon and Siliceous Structures in Biological Systems (Springer, New York, 1981). b) Kroeger, N.; Lehmann, G.; Rachel, R.; Sumper, M. *Eur. J. Biochem.* **1997**, *250*, 99-105. c) Vrieling, E.G.; Beelen, T.P.M.; van Santen, R.A.; Gieskes,W.W.C. *J. Biotechnol.* 1999, *70*, 39-51. d) Morse, D.E.; *Trends Biotechnol.***1999**, *17*, 230-232.

[7] http://commons.wikimedia.org/wiki/Image:Haeckel_Diatomea.jpg.

[8] http://de.wikipedia.org/wiki/Aerogel; http://stardust.jpl.nasa.gov/photo/aerogel.html.

[9] McKelvey, C.A.; Kaler, E.W.; Zasadzinski, J.A.; Coldren, B.; Jung, H.A.T. *Langmuir* **2000**, *16*(22), 8285-8290.

[10] Cooper, E.R.; Andrews, C.D.; Wheatley, P.S.; Webb, P.B.; Wormald, P.; Morris, R.E. *Nature* **2004**, *430*(7003), 1012-1016.

[11] Zhou, Y.; Schattka, J.H.; Antonietti, M. *Nano Letters* **2004**, *4*(3), 477-481.

[12] Chen, Z.; Zhan, P.; Wang, Z.L.; Zhang, J.H.; Zhang, W.Y.; Ming, N.B.; Chan, C.T.; *Adv. Mater.***2004**, *16*(5), 417.

[13] Schroden, R.C.; Al-Daous, M.; Blanford, C.F.; Stein, A. *Chem. Mater.***2002**, *14*(8), 3305-3315.

[14] Bhatia, R.B.; Brinker, C.J.; Gupta, A.K.; Singh A.K. *Chem. Mater.***2000**, *12*, 2434-2441.

[15] Ferrer, M.L.; Monte, F.; Levy, D. *Chem. Mater.***2002**, *14*, 3619.

[16] Carn, F.; Saadaoui, H.; Masse, P.; Ravaine, S.; Julian-Lopez, B.; Sanchez, C.; Deleuze, H.; Talham, D.R.; Backov, R. *Langmuir* **2006**, *22*(12), 5469-5475.

[17] Tiemann, M. *Chem. Mater.* **2008**, *20*(3), 961-971.

[18] Lu, A.H.; Schüth, F. *Adv. Mater.***2006**, *18*(14), 1793-1805.

[19] Tiemann, M. *Chem. Eur. J.* **2007**, *13*(30), 8376.

[20] Kline, T.R.; Tian, M.L.; Wang, J.G.; Sen, A.; Chan, M.W.H.; Mallouk, T.E. *Inorganic Chem.* **2006**, *45*(19), 7555-7565.

[21] Kresge, C.T.; Leonowicz, M.E.; Roth, M.E.; Vartulli, J.C.; Beck, J.S. *Nature* **1992**, *359*, 710-712.

[22] Thomas, A.; Goettmann, F.; Antonietti, M. *Chem. Mater.***2008**, *20*(3), 738-755.

[23] Imhof, A,; Pine, D.J. *Nature* **1997**, *389*, 948-951.

[24] Zhao D.; Feng J.; Huo Q.; Melosh, N.; Fredrickson, G.H.; Chmelka, B.F. *Science* **1998**, *279*, 548-552.

[25] Wijnhoven, J.E.G.J.; Bechger, L.; Vos, W.L. *Chem. Mater.* **2001**, *13*, 4486-4499.

[26] Ciesla, U.; Fröba, M.; Stucky, G.; Schüth, F. *Chem. Mater.* **1999**, *11*, 227-234.

[27] Li, A.P.; Müller, F.; Birner, A.; Nielsch, K.; Gösele U. *J. Appl. Phys.* **1998**, *84*(11), 6023-6026.

[28] Gonzalez-Pena,V.; Marquez-Alvarez, C.; Sastre, E.; Perez-Pariente, J. *Studies in Surface Science and Catalysis* **2002**, *142*, 1283-1290.

[29] Vaudry, F.; Khodabandeh, S.; Davis, M.E. *Chem. Mat.* **1996**, *8*(7), 1451-1464.

[30] Sallard, S.; Brezesinski, T.; Smarsly, B.M. *J. Phys. Chem. C* **2007**, *111*(19), 7200-7206.

[31] Lian, S.Y.; Wang, E.; Kang, Z.H.; Bai, Y.P.; Gao, L.; Jiang, M.; Hu, C.W.; Xu, L. *Solid State Commun.* **2004**, *129*(8), 485-490.

[32] Hüsing, N.; Schubert, U. *Angew. Chem. Int. Ed.* **1998**, *37*(1-2), 23-45.

[33] Hüsing, N.; Schubert, U. *Angew. Chem.* **1998**, *110*, 22.

[34] Schäfer, D. *Science* **1989**, *243*, 1023.

[35] K. D. Keefer, D. W. Schaefer, *Phys. Rev. Lett*. **1986**, *56*, 2376

[36] Cerveau, G.; Corriu, R.J.P.; Framery, E. *J. Mat. Chem.* **2001**, *11*(3), 713-717.

[37] Tan, B.; Rankin, S.E. *J. Phys. Chem. B* **2006**, *110*, 22353-22364.

[38] Holderich, W.; Hesse, M.; Naumann, F. *Angew. Chem. Int. Ed.* **1988**, *27*(2), 226-246.

[39] Davis, M.E.; Lobo, R.F. *Chem. Mater.***1992**, *4*(4) 756-768.

[40] Huo, Q.; Margolese, D.I.; Stuc, G.D. *Chem. Mater.* **1996**, *8*, 1147-1160.

[41] Smarsly, B.; Polarz, S.; Antonietti, M. *J. Phys. Chem. B* **2001**, *105*(43), 10473-10483.

[42] Attard, G.S.; Glyde, J.C.; Göltner, C.G. Nature 1995, 378, 366-368.

[43] Attard, G.S.; Göltner, C.G; Corker, J.M.; Henek, S.; Templer, R.H. *Angew. Chem. Int. Ed.* **1997**, *36*, 1315-1317.

[44] Thomas, A. Dissertation **2003** „Poröse Silikate durch nanocasting: Von chiralen Templaten zu neuer Chemie“

[45] Chevalier, P.; Corriu, R. J. P.; Delord, P.; Moreau, J. J. E.; Man, M. W. C. *New J. Chem.* **1998**, *22*, 423.

[46] Hatton, B.; Landskron, K.; Whitnall, W.; Perovic, D.; Ozin, G. A. *Acc. Chem. Res.* **2005**, *38*, 305.

[47] Hoffmann, F.; Cornelius, M.; Morell, J.; Froba, M., J. *Nanosci. Nanotechnol.* **2006**, *6*, 265.

[48] Shea, K. J.; Loy, D. A., *Chem. Mater.* **2001**, *13*, 3306.

[49] Brown, J.F.; Vogt, L.H.; Prescott, P.I. *J. Am. Chem. Soc.* **1964**, *86*(6), 1120-1125.

[50] Burkett, S.L.; Sims, S.D.; Mann, S. *Chem. Commun.* **1996**, 1367 – 1368.

[51] Mercier, L.; Pinnavaia, T.J. *Chem. Mater.* **2000**, *12*, 188 – 196.

[52] Fowler, C.E.; Burkett, S.L.; Mann, S. *Chem. Commun.* **1997**, 1769 – 1770.

[53] Richer, R.; Mercier, L., *Chem. Commun.* **1998**, 1775 – 1776.

[54] Walcarius, A.; Delacte, C. *Chem. Mater.* **2003**, *15*, 4181 – 4192.

[55] Yokoi, T.; Yoshitake, H.; Tatsumi, T. *J. Mater. Chem.* **2004**, *14*, 951 – 957.

[56] Macquarrie, D.J. *Chem. Commun.* **1996**, 1961 – 1962.

[57] Chong, A.S.M.; Zhao, X.S. *J. Phys. Chem. B* **2003**, *107*, 12 650 – 12657.

[58] Huh, S.; Wiench, J.W.; Yoo, J.-C.; Pruski, M.; Lin, V.S.-Y. *Chem. Mater.* **2003**, *15*, 4247 – 4256.

[59] Macquarrie, D.J.; Jackson, D.B.; Mdoe, J.E.G.; Clark, J.H. *New J. Chem.* **1999**, *23*, 539 – 544.

[60] Yokoi, T.; Yoshitake, H.; Tatsumi, T. *Chem. Mater.* **2003**, *15*, 4536 – 4538.

[61] Macquarrie, D.J. *Chem. Commun.* **1996**, 1961 – 1962.

[62] Cagnol, F.; Grosso, D.; Sanchez, C. *Chem. Commun.* **2004**, 1742 – 1743.

[63] Lim, M.H.; Blanford, C.F.; Stein, A. *J. Am. Chem. Soc.* **1997**, *119*, 4090 – 4091.

[64] Hall, S.R.; Fowler, C.E.; Lebeau, B.; Mann, S. *Chem. Commun.* **1999**, 201 – 202.

[65] Lim, M.H.; Stein, A. *Chem. Mater.* **1999**, *11*, 3285 – 3295.

[66] Corriu, R.J.P.; Hoarau, C.; Mehdi, A.; Reyl, C. *Chem. Commun.* **2000**, 71 – 72.

[67] Bambrough, C.M.; Slade, R.C.T.; Williams, R.T. *J. Mater. Chem.* **1998**, *8*, 569 – 571.

[68] Slade, R.C.T.; Bambrough, C.M.; Williams, R.T. *Phys. Chem.* **2002**, *4*, 5394 – 5399.

[69] Hoffmann, F.; Cornelius, M.; Morell, J.; Fröba, M. *Angew. Chem. Int. Ed.* **2006**, *45*, 3216 – 3251.

[70] MacLachlan, M.J.; Asefa, T.; Ozin, G.A. *Chem.-A European J.* **2000**, *6*(14), 2507-2511.

[71] Clark, J.H.; Macquarrie, D.J. *Chem. Commun.* **1998**, 853-860.

[72] Loy, D.A.; Shea, K.J. *Chem. Rev.* **1995**, *95*, 1431-1442.

[73] Loy, D.A.; Shea, K.J. *Chem. Mater.***2001**, *13*(10), 3306-3319.

[74] Corriu, R.J.P.; Moureau, J.J.E.; Theopot, P.; Man, M.W.C. *Chem. Mater.***1992**, *4*(6), 1217-1224.

[75] Asefa, T.; Yoshina-Ishii, C.; MacLachlan, M. J.; Ozin, G. A. *J. Mater. Chem.* **2000**, *10*, 1751.

[76] Yoshina-Ishii, C.; Asefa, T.; Coombs, N.; MacLachlan, M. J.; Ozin, G. A. *Chem. Commun.* **1999**, 2539.

[77] Inagaki, S.; Guan, S.; Ohsuna, T.; Terasaki, O. *Nature* **2002**, *416*, 304-307.

[78] Asefa, T.; Kruk, M.; MacLachlan, M. J.; Coombs, N.; Grondey, H.; Jaroniec, M.; Ozin, G. A. *J. Am. Chem. Soc.* **2001**, *123*, 8520.

[79] Melde, B.J.; Holland, B.T.; Blanford, C.F.; Stein, A. *Chem. Mater.* **1999**, *11*, 3302-3308.

[80] Price, P.M.; Clark, J.H.; Macquarrie, D.J *J. Chem. Soc.- Dalton Trans.* **2000**, 101–110.

[81] Clark, J.H.; Macquarrie, D.J. *Chem. Commun.* **1998**, 853-860.

[82] Wight, A.P.; Davis, M.E. *Chem. Rev.* **2002**, *102*, 3589-3614.

[83] Chisem, I.C.; Rafelt, J.; Shieh, M.T.; Chisem, J.; Clark, J.H.; Jachuck, R.; Macquarrie, D.J.; Ramshaw, C.; Scott, K. *Chem. Commun.* **1998**, 1949.

[84] Enomoto, N.; Furukawa, S.; Ogasawara, Y.; Akano, H.; Kawamura, Y.; Yashima, E.; Okamoto, Y. *Anal. Chem.* **1996**, *68*, 2798-2804.

[85] Angeletti, E.; Canepa, C.; Martinetti, G.; Venturello, P. *Tetrahedron Lett.* **1988**, *29*, 2261;

[86] Macquarrie, D. J.; Clark, J. H.; Lambert, A.; Mdoe, J. E. G.; Priest, A. *React. Funct. Polym.* **1997**, *35*, 153.

[87] Bigi, F.; Carloni, S.; Maggi, R.; Mazzacani, A.; Sartori, G. *Stud. Surf. Sci. Catal.* **2000**, *130*, 3501.

[88] Utting, K.A.; Macquarrie, D.J. *New J. Chem.* **2000**, *24*, 591.

[89] Subba Rao, Y.V.; De Vos, D.; Jacobs, P.A. *Angew. Chem. Int. Ed.* **1997**, *36*, 2661.

[90] Brown, H.C.; Rao, B.C.S. *J. Am. Chem. Soc.* **1959**, *81*(24), 6428-6434.

[91] Brown, H.C.; Rao, B.C.S. *J. Org. Chem.* **1957**, *22*(9), 1136-1137.

[92] Brown, H.C. *J. Org. Chem.* **1989**, *54*, 6085-6096.

[93] Pasto, D.J.; Lepeska, B.; Cheng, T.C. *J. Am. Chem. Soc.* **1972**, *94*, 608.

[94] Jones, P.R. *J. Org. Chem.* **1972**, *37*, 1886.

[95] Dhillon, R.S. "Hydroboration and Organic Synthesis" *Springer* **2007**.

[96] Brown, H.C.; Ramachandran, P.V. *J. Organomet. Chem.* **1995,** *500*, 1-19.

[97] Voss, R.; Thomas, A.; Antonietti, M.; Ozin, G. A., *J. Mater. Chem.* **2005,** *15*, 4010.

[98] Voss R. Dissertation **2005** „Mesoporous organosilica materials with amine functions: surface characteristics and chirality"

[99] Boury, B.; Chevalier, P.; Corriu, R. J. P.; Delord, P.; Moreau, J. J. E.; Chiman, M. W. *Chem. Mater.* **1999,** *11*, 281.

[100] Shea, K. J.; Loy, D. A.; Webster, O., *J. Am. Chem. Soc.* **1992,** *114*, 6700.

[101] Boury, B.; Corriu, R. J. P.; Le Strat, V., *Chem. Mater.* **1999,** *11*, 2796.

[102] Boury, B.; Corriu, R. J. P., *Adv. Mater.* **2000,** *12*, 989.

[103] Chong, A. S. M.; Zhao, X. S., *J. Phys. Chem. B* **2003,** *107*, 12650.

[104] Corriu, R. J. P.; Mehdi, A.; Reye, C.; Thieuleux, C., *Chem. Commun.* **2002**, 1382.

[105] Wahab, M. A.; Imae, I.; Kawakami, Y.; Ha, C. S., *Chem. Mater.* **2005,** *17*, 2165.

[106] Wahab, M. A.; Kim, I.; Ha, C. S., *J. Solid State Chem.* **2004,** *177*, 3439.

[107] Sing, K. S. W.; Everett, D. H.; Haul, R. A. W.; Moscou, L.; Pierotti, R. A.; Rouquerol, J.; Siemieniewska, T. *Pure Appl. Chem.* **1985**, *57*, 603.

[108] Ryoo, R.; Park, I.-S.; Jun, S.; Lee, C. W.; Kruk, M.; Jaroniec, M. *J. Am. Chem. Soc.* **2001**, *123*, 1650.

[109] Kruk, M.; Jaroniec, M. *Chem. Mater.* **2000**, *12*, 222.

[110] Ravikovitch, P.I.; Neimark, A.V. *Langmuir* **2002**, *18*, 1550-1560.

[111] Broeckhoff, J.C.P.; Boer J.H. *J. Catal.* **1967**, *9*, 8.

[112] Cole, M.W.; Saam, W.F., *Phys. Rev. Lett.* **1974**, *32*, 985.

[113] Evans, R.J. *Phys. Condens. Mater.* **1990**, *2*, 8989.

[114] Celstini, F. *Phys. Lett. A* **1997**, *228*, 84.

[115] Barrett, E.P.; Joyner, L.G.; Halenda, P.P. *J. Am. Chem. Soc.* **1951**, *73*, 373.

[116] Ravikovitch, P.I.; ODomhnaill, S.C.; Neimark, A.V.; Schuth, F.; Unger, K.K. *Langmuir* **1995**, *11*(12), 4765-4772.

[117] Snurr, R.Q.; Bell, A.T.; Theodorou, D.N. *J. Phys. Chem.* **1993**, *9* (51), 13742-13752.

[118] Maddox, M.W.; Olivier, J.P.; Gubbins, K.E. *Langmuir* **1997**, *13*(6), 1737-1745.

[119] Beck, J.S.; Vartulli, J.C.; Roth, W.J.; Leonowitz, M.E.; Kresge, C.T.; Schmitt, K.D.; Chu, C.T.W.; Oloson, D.H.; Sheppard, E.W.; Mccullen, S.B.; Higgins, J.B.; Schlenker, J.L. *J. Am. Chem. Soc.* **1992**, *114*(27): 10834-10843.

[120] Beck, J.S.; Vartulijc J.C.; Roth W.J. *J. Am. Chem. Soc.* **1992**, *114*(27), 10834-10843.

[121] Kresge, C.T.; Leonowicz, M.E.; Roth, W.J. *Nature* **1992**, *359*(6397), 710-712.

[122] Feng, P.Y.; Bu, X.H.; Pine, D.J. *Langmuir* **2000**, *16*(12): 5304-5310.

[123] Khushalani D.; Kuperman A.; Ozin G.A. *Adv. Mater.* **1995**, *7*, 842.

[124] Zhao, D.Y.; Feng, J.L.; Huo, Q.S. *Science* **1998**, *279*(5350), 548-552.

[125] Thomas, A.; Schlaad, H.; Smarsly, B.; Antonietti, M. *Langmuir* **2003**, *19*, 4455-4459.

[126] Brown, H.C.; Kramer, G.W.; Levy, A.B.; Midland, M.M. Organic Synthesis via Boranes; Wiley-Interscience: New York, **1975**.

[127] Schwier, J.R.; Brown, H.C. *J. of Organic Chem.* **1993**, *58*, 1546-1552.

[128] Kolb, H.C.; Finn, M.G.; Sharpless, K.B. *Angew. Chem. Int. Ed.* **2001**, *40*, 2004.

[129] Weber, J.; Su, O.; Antonietti, M.; Thomas, A. *Macromolecular Rapid Commun.* **2007**, *28*(18-19), 1871-1876.

[130] Chen, S.Y.; Cheng, S. *Chem. Mater.* **2007**, *19*, 3041-3051.

[131] Doshi, D.A.; Gibaud, A.; Goletto, O.V.; Lu, M.; Gerung, H.; Ocko, B.; Han, S.M.; Brinker, C.J. *J. Am. Chem. Soc.* **2003**, *125*, 11646-11655.

[132] Binder, K. „Glassy materials and disordered solids : an introduction to their statistical mechanics“ **2005**, New Jersey: World Scientific.

[133] Chistovskaya, I.; Janowski, F. *React. Kinet. Catal. Lett.* **1991**, *43*(2), 277-282.

[134] Zhou, Y.; Antonietti, M. *Adv. Mater.***2003**, *15*, 1452-1455.

[135] Zhou, Y.; Antonietti, M. *Chem. Mater.***2004**, *16*, 544-550.

[136] Ruland, W. J. *Appl. Cryst.* **1971**, *4*, 70.

[137] Ayral, A.; Phalippou, J.; Woignier, T.J. *Mat. Science* **1992**, *27*, 1166-1170.

[138] Fowler, C.E.; Burkett, S.L.; Mann S. *Chem. Commun.* **1997**, 1769.

[139] Burleigh, M.C.; Markowitz, M.A.; Spector, M.S.; Gaber, B.P. *J. Phys. Chem. B* **2001**, *105*, 9935-9942.

[140] Burleigh, M.C.; Markowitz, M.A.; Spector, M.S.; Gaber, B.P. *Chem. Mater.* **2001**, *13*, 4760-4766.

[141] Chiron, N.; Guilet, R.; Deydier, E. *Water Resarch* **2003**, 3079-3086.

[142] Mahmoud, M.E.; El-EssBaughmanawi, M.M.; Kholeif, S.A.; Fathalla, E.M.I. *Analytica Chimica Acta* **2004**, *525*, 123-132.

[143] Mahmoud, M.E.; Soayed, A.A.; Hafez, O.F. *Microchimica Acta* **2003**, *143*(1), 65-70.

[144] Yantasee, W.; Lin, Y.H.; Fryxell, G.E.; Alford, K.L.; Busche, B.J.; Johnson, C.D. *Industrial & Engineering Chem. Research* **2004**, *43*(11), 2759-2764.

[145] Boden, V.; Winzerling, J.J.; Vijayalakshmi, M.; Porath, J. *J. Immunol. Methods* **1995**, *181*(2), 225-232.

[146] Klonkowski, A. M.; Grobelna, B.; Widernik, T.; Jankowska-Frydel, A. *Langmuir* **1999**, *15*, 5814.

[147] Harris, D.C. “Quantitative Chemical Analysis”, 2nd ed., W.H. Freeman, New York **1987**.

[148] Bois, L.; Bonhomme, A.; Ribes, A.; Pais, B.; Raffin, G.; Tessier, F. *Colloids and Surfaces A: Physicochem. Eng. Aspects* **2003**, *221*, 221-230.

[149] Walcariusa, A.; Lüthi, N.; Blinc, J.-L.; Suc, B.-L.; Lamberts, L. *Electrochimica Acta* **1999**, *44*, 4601-4610.

[150] Dai, S.; Burleigh, M.C.; Shin, Y.; Morrow, C.C.; Barnes, C.E.; Xue, Z. *Angew. Chem. Int. Ed.* **1999**, *38*(9), 1235-1239.

[151] Soliman, E.M. *Analytical Letters* **1997**, *30*(9), 1739-1751.

[152] Mahmoud, M.E.; El-Essawi, M.M.; Kholeif, S.A.; Fathalla, E.M.I. *Analytica Chemica Acta* **2004**, *525*, 123-132.

[153] Putlitz, B.; Landfester, K.; Fischer, H.; Antonietti, M. *Adv. Mater.* **2001**, *13*, 500 – 503.

[154] Bamnolker, H.; Nitzan, B.; Gura, S.; Margel, S. *J. Mater. Sci. Lett.* **1997**, *16*, 1412 – 1415.

[155] Bommel, K.J.C.; Jung, J.H.; Shinkai, S. *Adv. Mater.* **2001**, *13*, 1472 – 1476.

[156] Thomas, A.; Antonietti, M. *Advanced Functional Materials* **2003**, *13*(10), 763-766.

[157] Zhao, D.Y.; Huo, Q.S.; Feng, J.L.; Chmelka, B.F.; Stucky, G.D. *J. Am. Chem. Soc.* **1998**, *120*(24), 6024-6036.

[158] Bates, F.S. *Science* **1991**, *251*(4996), 898-905.

[159] Alberius, P.C.A.; Frindell, K.L.; Hayward, R.C. *Chem. Mater.* **2002**, *14*, 3284-3294.

[160] Hentze, H. P.; Krämer, E.; Berton, B.; Förster, S.; Antonietti, M. *Macromolecules* **1999**, *32*, 5803-5809.

[161] Göltner, C. G.; Berton, B.; Krämer, E.; Antonietti, M. *Adv. Mater.* **1999**, *11*, 395-398.

[162] Göltner, C. G.; Berton, B.; Krämer, E.; Antonietti, M. *Chem. Commun.* **1998**, 2287-2288.

[163] Förster, S.; Berton, B.; Hentze, H. P.; Krämer, E.; Antonietti, M.; Lindner, P. *Macromolecules* **2001**, *34*, 4610-4623.

[164] Göltner, C. G.; Henke, S.; Weiaenberger, M. C.; Antonietti, M. *Angew. Chem.* **1998**, *110*, 633-636.

[165] Thomas, A.; Schlaad, H.; Smarsly, B.; Antonietti M. *Langmuir* **2003**, *19*, 4455-4459.

[166] Göltner, C.G.; Berton, B.; Krämer, E.; Antonietti, M. *Adv. Mater*. **1999**, *11*(5), 395-398.

[167] Hentze, H.P.; Krämer, E.; Berton, B.; Förster, S.; Antonietti, M. *Macromolecules* **1999**, *32*, 5803-5809.

[168 Cowie, J.M.G. „Polymers: Chem. & Physics of Modern Materials“ Blackie Academic & Professional **1991**

[169] Chukin, G.D.; Malevich, V.I. translated from *Zhurnal Prikladnoi Spektroskopii* **1989**, *50*(4), 639–646.

[170] Borner, H.G.; Beers, K.; Matyjaszewski, K.; Sheiko, S.S.; Moller, M. *Macromolecules* **2001**, *34*(13), 4375-4383.

[171] Borner, H.G.; Duran, D.; Matyjaszewski, K.; da Silva, M.; Sheiko, S.S. *Macromolecules* **2002**, *35*(9), 3387-3394.

[172] Wilhelm, M.; Zhao, C.L.; Wang, Y.C.; Xu, R.L.; Winnik, M.A.; Mura, J.L.; Riess, G.; Croucher, M.D. *Macromeloecules* **1991**, *24*(5), 1033-1040.

[173] Lammerhofer, M.; Lindner, W. *J. of Chromatography A* **1996**, *741* (1), 33-48.

[174] Caude, M.; Tambute, A.; Siret, L *J. of Chromatography* **1991**, *550*(1-2), 357-382.

[175] Benitez, M.; Bringmann, G.; Dreyer, M.; Garcia, H.; Ihmels, H.; Waidelich, M.; Wissel, K. *J. Org. Chem.* **2005,** *70*, 2315.

[176] Alvaro, M.; Benitez, M.; Das, D.; Ferrer, B.; Garcia, H. *Chem. Mater.* **2004,** *16*, 2222.

[177] Baleizao, C.; Gigante, B.; Das, D.; Alvaro, M.; Garcia, H.; Corma, A. *Chem. Commun.* **2003**, 1860.

[178] Jiang, D.M.; Yang, Q.H.; Wang, H.; Zhu, G. R.; Yang, J.; Li, C. *J. Catal.* **2006,** *239*, 65.

[179] Brethon, A.; Hesemann, P.; Rejaud, L.; Moreau, J. J. E.; Man, M.W.C. *J. Organomet. Chem.* **2001**, *627*, 239.

[180] Moreau, J.J.E.; Vellutini, L.; Man, M.W.C.; Bied, C. *J. Am. Chem. Soc.* **2001**, *123*, 1509.

[181] Polarz, S.; Kuschel, A. *Adv. Mater.* **2006,** *18*, 1206.

[182] Brown, H.C.; Ramachandran, P.V. *J. Organomet. Chem.* **1995,** *500*, 1-19.

[183] Hunnius, M.; Rufinska, A.; Maier, W. F. *Microporous Mesoporous Mater.* **1999,** *29*, 389.

[184] Thomas, A.; Polarz, S.; Antonietti. M. *J. Phys. Chem. B* **2003**, *107*, 5081.

[185] Kuroda, R.; Honma, T. *Chirality* **2000,** *12*, 269.

[186] Yang, Y. G.; Suzuki, M.; Fukui, H.; Shirai, H.; Hanabusa, K. *Chem. Mater.* **2006,** *18*, 1324.

[187] Tanaka, K.; Kato, M.; Toda, F. *Chirality* **2001,** *13*, 347.

[188] Rolison, D.R. *Science* **2003,** *299*, 1698.

[189] Muth, O.; Schellbach, C.; Froba, M. *Chem. Commun.* **2001**, 2032.

[190] Hunks, W.J.; Ozin G.A. *Adv. Funct. Mater.* **2005**, *15*, 259.

[191] Guo, W.P.; Li, X.; Zhao, X.S. *Microporous Mesoporous Mater.* **2006**, *93*, 285.

[192] Dotsevi, G. *J. Am. Chem. Soc.* **1975**, 97(5): 1259-1261.

[193] Cintas, P. *Angew. Chem.* **2007**, *119*, 4090 – 4099.

[194] Borman, S. *Chem. Eng. News* **1990**, *68*(28), 9.

[195] Wainer, I.W. Trends in analytical Chem. vol 6, no.5, **1987**.

[196] Pirkle, W.H.; Finn, J.M.; Schreiner, J.L. *J. Am. Chem. Soc.* **1981**, *103*(13), 3964-3966.

[197] Daniel W. Armstrong **1985** U.S.patent 4539399.

[198] Davankov ,V.A. *Advances in chromatography* Vol 18 Marcel Dekker NY 1980 139.

[199] Goettmann, F.; Sanchez, C.J. *Mat. Chem.* **2007**, *17*(1), 24-30.

[200] Zou, H.F.; Huang, X.D.; Ye M.L. *J. of Chromatography A* **2002**, *954*(1-2), 5-32.

[201] Claessens, H. A.; Straten, M. A. *J. of Chromatography A* **2004**, *1060*(1-2), 23-41.

[202] Stöber, W.; Fink, A. *J. of Colloid and Interface Sience* **1968**, *26*, 62-69.

[203] Nozawa, K.; Gailhanou, H.; Raison, L. Panizza, P. *Langmuir* **2005**, *21*, 1516-1523.

[204] Yang, H.; Vovk, G.; Coombs, N.; Sokolov, I., Ozin, G.A. *J. Mater. Chem.* **1998**, *8*(3), 743–750.

[205] Nakanishi, K.; Takahashi, R.; Nagakane, T.; Kitayama,K.; Koheiya, N.; Shikata, H.; Soga, N.; *J. of Sol-Gel Science and Technology* **2000**, *17*(3), 191-210.

[206] Svec, F.; Fréchet, J.M.J. *Anal. Chem.* **1992**, *64*, 820.

[207] Masamme, S.; Choy, W.; Petersen, J.S.; Sita, L.R. *Angew. Chem. Int. Ed.* **1985**, *24*, 1-30.

[208] Kantam, M.L.; Sreekanth, P. *Catal. Lett.* **2001**, *77*, 241.

[209] Macquarrie, D.J.; Jackson, D.B. *Chem. Commun.* **1997**, 1781-1782.

[210] Kubota, Y.; Nishizaki, Y.; Ikeya, H.; Saeki, M.; Hida, T.; Kawazu, S.; Yoshida, M.; Fujii, H.; Sugi, Y. *Microporous and Mesoporous Mater.* **2004**, *70*, 135-149.

[211] Tamami, B.; Fadavi, A. *Catalysis Commun.* **2005**, *6*, 747-751.

[212] Santaniello, E.; Ferraboschi, P.; Grisenti, P.; Manzocchi, A. *Chemical Reviews* **1992**, *92*(5), 1071-1140.

[213] Jaeger, K.E.; Liebeton, K.; Zonta, A.; Schimossek, K.; Reetz, M.T. *Appl Microbiol Biotechnol* **1996**, *46*, (99-105)

[214] Rakels, J.L.L.; Stranthof, A.J.J.; Heijnen, J.J. *Tetrahedron-Asymmetry* **1994**, *5*(1), 93-100.

[215] Marciniec, B.; Maciejewski, H.; Gulinski, J.; Rzejak, L., *J. Organomet. Chem.* **1989,** *362*, 273.

[216] Schlaad, H.; Kukula, H.; Rudloff, J.; Below, I. *Macromolecules* **2001**, *34*, 4302.

[217] Kukula, H.; Schlaad, H.; Falkenhage, J.; Krüger, R-P. *Macromolecules* **2002**, *35*, 7157.

Acknowledgment

Zu guter Letzt möchte ich allen danken, die zum Gelingen dieser Arbeit beigetragen haben und mich während meiner Zeit in Golm begleitet haben.

Zuerst möchte ich PROF. MARKUS ANTONIETTI danken, dass er es mir ermöglicht hat meine Doktorarbeit am MPI-KG durchzuführen zu können. Ein besonderer Dank gebührt dabei der ausgezeichneten Betreuung und der angenehmen Atmosphäre, die das Arbeiten sehr erleichtert haben.

Ein großes Dankeschön geht an meinen direkten Betreuer DR. ARNE THOMAS, der durch seine Anregungen, Ratschläge und die immer offene Bürotür wesentlich zum gelingen dieser Arbeit beigetragen hat.

PD DR. GUDRUN SCHOLZ von der Humboldt Universität zu Berlin möchte ich für die Festkörper NMR Messungen danken und dafür das sie immer ein offenes Ohr für alle Fragen hatte, die während der Arbeit aufgetreten sind.

Ebenso möchte ich mich bei DR. HEINZ BUKOWSKI und THERESA von der Universität Potsdam für die Atom Absorptions Messungen bedanken, besonders für ihre große Bereitschaft und die unkomplizierte Zusammenarbeit.

Für die Hilfe unserer LaborantInnen und TechnikerInnen bin ich ebenso dankbar, insbesondere REGINA ROTHE, INGRID ZENKE, INES BELOW, MARLIES GRÄWERT, OLAF NIEMEYER, RONA PITSCHKE, HEIKE RUNGE und SYLVIA PIROK.

Ganz besonderer Dank geht an ANNE, JONG und NICOLE die ihre Freizeit mit dem Korrekturlesen der Arbeit verbracht haben. Weiterhin MAGDA, die mir eine Einführung in die HPLC geben hat und mit wertvollen Tipps stets weitergeholfen hat.

Ganz besonders möchte ich meinen Freunden und Kollegen danken, mit denen ich in, während und auch außerhalb des Instituts viel Zeit verbracht habe. Ich hoffe, dass wir in Kontakt bleiben! Danke : FREDERIC, FARNOOSH, JULIA, CRISTINA, MICHAEL, ANNA, GEORG, JENS (small) & JENS (meso) & JENS (tall), JOHN, HELENA, PHILIPP, REZAN, CECILE, PIERRE, PHILIPPE, KIRSTIN, ERWAN, ELODIE, SILKE, NANCY, DENNIS, ANTONIO, SIMONE, ANTJE, JÖRG, YOUNG-SI, LAEM, ZOFIA, HARALD, STEFFI, THORSTEN, JOHANNES, FLORIAN, PANTEA, NICOLA, EMRE, JELENA, SEBASTIEN …….

Meinen Eltern, Großeltern und Moogli möchte ich ganz herzlich für Ihre Zuversicht und Unterstützung während der Entstehung dieser Arbeit danken. Danke auch dir SUSI, dass du mich begleitet hast und mir mit vielen schönen Dingen die Zeit unglaublich erleichtert hast!